Beat Noise and Related Phenomena in Optical Networks

A thesis submitted for the degree of
Doctor of Philosophy
in Electronic and Electrical Engineering

2000

John Edward Mitchell

Department of Electrical and Electronic Engineering
University College London

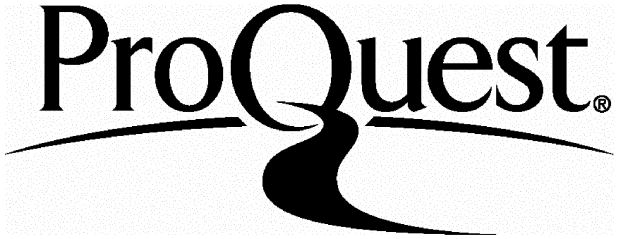

Acknowledgements

I wish to express my thanks to my supervisor Professor John J. O'Reilly for his advice, guidance and support during the course of this study.

I would also like to thank Dr Phil Lane and all the members of the Telecommunications Research Group who have offered valuable advice and discussion on the work in this thesis, and those at the Marconi Research Centre, Great Baddow, who provide the opportunity to conduct the optical measurements.

I would like to thank my family and friends for their support and encouragement.

Financial support was provided by the U.K. Engineering and Physical Sciences Research Council (EPSRC) and the Marconi Research Centre, Chelmsford, for which I am very grateful.

To the memory of my father.

Abstract

This thesis is concerned with the characterisation and modelling of spurious signals created in wavelength division multiplexed optical networks. The main focus of this work considers interferometric noise in various optical network scenarios. Simulation tools and analytic techniques are described and developed to produce performance metrics for the systems involved. Interferometric noise has been recognised as a significant limitation in many forms of network, yet primarily only simplistic studies have been performed. A theoretical analysis of interferometric beat noise is presented which uses an accurate statistical characterisation to evaluate system performance. This allows comparison with published results and techniques and enables system factors such as extinction ratio and crosstalk-crosstalk beating to be included which have previously either been ignored or approximated. It is shown that accepted approximations can lead to erroneous results and the prediction of counter intuitive network trends. The results are supported by simulation using the Signal Processing Worksystem (SPW) which exploits custom written blocks to model optical devices.

The study of interferometric noise is extended to systems transporting signals with modulation formats other than intensity modulation. Quadrature amplitude modulation is selected for detailed consideration as it is the preferred format for many hybrid fibre radio systems. Results are presented concerning the tolerable crosstalk levels using this scheme for optical generation of millimetre waves using a heterodyne mixing technique as employed in the MODAL system. The tools and techniques described are used to explore two specific illustrative network examples.

1. The use of incoherent light in a technique called spectrum slicing is investigated for the transport of analogue signals

2. The potential effects of interferometric noise in optical beamforming networks are identified, with the main parameters shown to be source wavelength separation and receiver filter order.

System performance metrics are presented demonstrating the component characteristics required for acceptable operation.

Contents

1 Introduction **14**
- 1.1 Thesis Organisation . . . 15
- 1.2 Contributions . . . 16

2 Optical WDM Networks **19**
- 2.1 Introduction . . . 19
- 2.2 Review of current WDM technology. . . . 19
  - 2.2.1 DFB lasers . . . 20
  - 2.2.2 Incoherent Light Sources . . . 22
  - 2.2.3 Fibre Amplifiers . . . 23
  - 2.2.4 Mach-Zehnder Modulators . . . 24
  - 2.2.5 Optical Receivers . . . 26
  - 2.2.6 Optical Filtering . . . 27
  - 2.2.7 Fibre Bragg Gratings . . . 28
  - 2.2.8 WDM Network devices . . . 28
  - 2.2.9 Interferometric Noise . . . 30
- 2.3 Simulation of WDM networks . . . 31
  - 2.3.1 The Signal Processing Worksystem . . . 31
- 2.4 Summary . . . 33

3 Optical delivery of mm-wave signals **35**
- 3.1 Introduction . . . 35
- 3.2 Review of mm-wave delivery . . . 36
- 3.3 Hybrid fibre radio systems . . . 37
  - 3.3.1 Millimetre wave generation . . . 38
  - 3.3.2 Generation of mm-wave signals by frequency doubling . . . 40
  - 3.3.3 QAM modulation . . . 42
- 3.4 Beamforming Networks . . . 43
- 3.5 Simulation of RF delivery networks . . . 45
- 3.6 Summary . . . 46

4 Interferometric Beat Noise **47**
- 4.1 Introduction . . . 47
- 4.2 Formation of Interferometric Noise . . . 49
- 4.3 Terms affecting IN . . . 51
  - 4.3.1 Polarisation . . . 51
  - 4.3.2 In-band Noise . . . 52

4.3.3 Coherent and Incoherent Noise . . . 53
4.3.4 Probability Density Function of IN . . . 53
4.4 Evaluation Methods . . . 54
4.4.1 Methods Using 'Partial' statistics . . . 56
4.4.2 Formulation of the Gaussian Approximation . . . 59
4.4.3 Methods Using 'Full' Statistics . . . 61
4.4.4 Formulation of the MGF . . . 65
4.4.5 Comparison of MGF based Methods . . . 67
4.5 Results and Observations . . . 70
4.5.1 System Performance . . . 70
4.5.2 Crosstalk-Crosstalk beating . . . 72
4.5.3 Finite Extinction Ratio . . . 75
4.5.4 Interferers of unequal power . . . 78
4.6 An Optical Network Example . . . 82
4.7 Quadrature Amplitude Modulation. . . . 87
4.7.1 Formulation of QAM . . . 87
4.7.2 QAM in HFR systems . . . 90
4.7.3 Formulation of MGF . . . 95
4.7.4 Coding of a QAM signal . . . 97
4.7.5 Symbol Conditioning . . . 100
4.7.6 Results . . . 102
4.8 Summary . . . 103

5 Optical Beamforming Networks 105
5.1 Introduction . . . 105
5.2 Details of system operation . . . 106
5.3 Carrier Suppression . . . 109
5.3.1 Mach-Zehnder Modulator . . . 110
5.3.2 Carrier Suppression Experiment . . . 113
5.3.3 Carrier Suppression with Saturated Amplification . . . 115
5.4 Multiple Wavelength Mixing . . . 118
5.4.1 Analytic Formulation . . . 120
5.4.2 Simulation Model . . . 123
5.4.3 Experimental Evaluation . . . 124
5.4.4 Results . . . 127
5.5 System Issues . . . 131
5.6 Summary . . . 134

6 Spectrum Slicing in RF delivery Systems 136
6.1 Introduction . . . 136
6.2 Review of Spectrum Slicing . . . 137
6.3 Analytic Characterisation . . . 139
6.4 Experimental Evaluation . . . 145
6.5 Application of Spectrum Slicing . . . 149
6.6 Summary . . . 153

7 Conclusion **154**
7.1 Thesis Summary 154
7.2 Main Contributions of this thesis 155
7.3 Suggestions for further work 157

A SPW Blocks **159**
A.1 Optical Coupler 159
A.2 Optical Circulator 161
A.3 Fiber Bragg Grating 163
A.4 Mach-Zehnder Modulator 164
A.5 Photo Diode 165
A.6 Time to frequency domain conversion 166
A.7 Non-linear amplifier 167
A.8 Optical Fiber 168
A.9 DFB laser 169

List of Figures

2.1 Basic structure of a Mach-Zehnder modulator. 25
2.2 Mach-Zehnder Modulator Response 26
2.3 An example of an add drop multiplexer 29
2.4 Illustrative 'windows' for the signal processing worksystem 32
2.5 Composition of transmitted vector to process multiple wavelengths . . 33

3.1 Schematic of a mm-wave generation system 42
3.2 Four level (16 symbol) QAM constellation 43
3.3 A linear array of dipole elements 44

4.1 An example of how imperfect isolation at an ADM causes in-band crosstalk 48
4.2 The Arc Sinusoidal distribution 54
4.3 The schematic of a system to simulate beat noise 64
4.4 Comparison of Bit Error Rate results from MCB (solid) and SPA (dashed) 68
4.5 Comparison of floating point operations required for MCB (solid) and SPA (dashed) 69
4.6 BER against crosstalk isolation given by Gaussian approximation, MCB and simulation 71
4.7 Power penalty against crosstalk isolation given by Gaussian approximation, MCB and simulation 72
4.8 Power penalty for an increasing number of interferers with constant total power. GA, MCB 73
4.9 Comparison of noise variance for signal-crosstalk and crosstalk-crosstalk beating 73
4.10 Ratio of bit error rate, with/without crosstalk-crosstalk beating, calculated by the MCB 75
4.11 Power Penalty against crosstalk isolation calculated using a Gaussian approximation and the modified Chernoff bound. 77
4.12 Crosstalk isolation required for a 1dB power penalty vs extinction ratio, calculated used the MCB (top) and Gaussian Approximation (bottom). 78
4.13 The transition of the PDF as Gaussian Noise becomes dominant, with (right) the relative interferer strengths 80
4.14 Relative interfering power for k=0,5,10 80
4.15 Total crosstalk power required for a 1dB power penalty with relation to number of interfering terms and the distribution of interferer power. 81

4.16 Intermediate MWTN node 84
4.17 Variation of power penalty with crosstalk isolation. Annotation denotes number of first order interferers, and number of second order interferers bracketed 85
4.18 Variation of power penalty with crosstalk isolation. 3 crosstalk terms due to the DeMUX and 3 due to the space switch 85
4.19 Variation of power penalty with crosstalk isolation. 2 crosstalk terms due to the DeMUX and 3 due to the space switch 86
4.20 Evolution of power penalty with number of nodes passed 86
4.21 Explanation of the convolution of random variables $\phi_d(t)$ and θ . . . 97
4.22 Four level (16 symbol) QAM constellation with Gray coding 98
4.23 Crosstalk isolation against Bit Error Rate for 16QAM transmission . 103

5.1 Multiple Fixed Beam Optical Fiber TTD Beamforming 107
5.2 Bragg fiber grating Multiple Fixed Beam TTD Beamforming 108
5.3 Experimental setup for carrier suppression 114
5.4 Optical Power vs modulator bias 116
5.5 Experimental setup for carrier suppression with EDFA 116
5.6 Performance of carrier suppression. 117
5.7 Laser power spectral density 124
5.8 Power spectral density of the modulated laser field 124
5.9 SPW block diagram of the experiment to beat two laser sources. . . . 126
5.10 Experimental setup 126
5.11 Histogram of interferometric beating 126
5.12 Analytic and experimental results of frequency separation against SNR for a 4GHz signal, 2-6GHz filter band. 128
5.13 Experimental results of frequency separation against SNR for 4GHz signal, 2-6GHz filter band. Adjusted analytically for various electrical filter orders 129
5.14 Frequency Separation against SNR for a 4GHz signal, filter band 2-6 GHz, with 3 sources. 130
5.15 Frequency separation against SNR for a 4GHz signal, filter band 2-6 GHz, with 5 sources. 130
5.16 Power spectral density of the beat spectra of two laser sources separated by 0.032nm (4GHz). 131
5.17 Frequency Separation against SNR for a 4GHz signal, filter band 2-6 GHz. 132
5.18 Frequency Separation against SNR, filter band 8-12.4 GHz, 8GHz signal 132
5.19 Frequency separation against Power for Signal, beating and noise. . . 133
5.20 Frequency separation against Power for Signal, beating and noise. (Expanded vertical power) 133
5.21 Relative power of beating terms 134

6.1 Schematic of a spectrum sliced WDM transmitter 137
6.2 Example of noise spectra in spectrum sliced system with RF modulation 143
6.3 Experimental setup for spectrum slicing of incoherent light. 145
6.4 Amplified ASE spectrum. 146

6.5 Spectrum sliced ASE 146
6.6 Probability Density of ASE noise. 147
6.7 Noise floor due to excess and thermal noise. 148
6.8 Experimental setup for transmission of RF using incoherent light. . . 148
6.9 Noise floor and RF signal. 149
6.10 Optical power received against SNR for 3.65nm slice. 149
6.11 Optical Bandwidth against SNR for spectrum sliced systems 151
6.12 SNR against bandwidth measured at 7.5GHz 152

List of Tables

2.1 Illustrative filter crosstalk levels 27

4.1 Summary of Interferometric noise evaluation methods 55
4.2 Noise Variance and MGFs of interferometric noise with finite extinction ratio 76
4.3 Number of first and second order interfering terms created per node. . 83

5.1 Evaluation parameters: Analytic 123
5.2 Evaluation parameters: Simulation 125

6.1 Comparison of spectrum slicing systems 138

Glossary of Terms

Glossary of Abbreviations and Acronyms

ACTS	Advanced Communications Technologies and Services
ADM	Add-drop multiplexer
ADSL	Asynchronous Digital Subscriber Line
AM	Amplitude Modulation
AON	All optical network
ASE	Amplified spontaneous emission
ATM	Asynchronous transfer mode
BER	Bit error rate
BT	British Telecommunications PLC
CB	Chernoff Bound
CW	Continuous Wave
DeMUX	Demultiplexer
DFB	Distributed FeedBack
DSF	Dispersion Shifted Fibre
DSL	Digital Subscriber Line
DSP	Digital Signal Processing
DWDM	Dense Wavelength Division Multiplexing
EDFA	Erbium-doped fiber amplifier
EDFL	Erbium-doped fiber laser
EELED	Edge Emitting Light Emitting Diode
FBG	Fibre Bragg Grating
FDMA	Frequency Division Multiple Access
FFT	Fast Fourier Transform
FRANS	Fiber Radio ATM Networks and Services
FTTC	Fibre to the Curb
FTTH	Fibre to the Home
GA	Gaussian Approximation
GaAs	Gallium Arsenide
GSM	Global System for Mobile communications
GVD	Group Velocity Dispersion
HDTV	High Definition Television
HFR	Hybrid Fibre Radio
IIR	Infinite Impulse Response
IM-DD	Intensity Modulated -Direct detection
IN	Interferometric Noise
ISDN	Integrated Services Digital Network

ITU-T	International Telecommunications Union-Telecommunication Standardisation Sector
InP	Indium Phosphide
LAN	Local Area Network
LED	Light Emitting Diode
LiNbO	Lithium Niobate
LSB	Least Significant Bit
MCB	Modified Chernoff Bound
MGF	Moment Generating Function
MSB	Most Significant Bit
MQW	Multi-Quantum Well
MUX	Multiplexer
MWTN	Multi-Wavelength Transport Network
MZI	Mach-Zehnder Interferometer
mm-wave	Millimetre Wave
OOK	On-Off keying
OXC	Optical Cross-Connect
PDF	Probability Density Function
PSD	Power Spectral Density
QAM	Quadrature Amplitude Modulation
QoS	Quality of Service
RF	Radio Frequency
RIN	Relative Intensity Noise
RV	Random Variable
SLD	Super Luminescent diode
SNR	Signal to noise ratio.
SOA	Semiconductor Optical Amplifier
SoP	State of Polarisation
SPA	Saddle Point Approximation
SPW	Signal Processing Worksystem
SRS	Stimulated Raman Scattering
TTD	True Time Delay
UHF	Ultra High Frequency
UMTS	Universal Mobile Telecommunications System
WDM	Wavelength Division Multiplexing
WDMA	Wavelength Division Multiple Access
XPM	Cross phase modulation

Chapter 1

Introduction

Although optical fibre is now the dominant transport technology for point to point transmission in the core of the telecommunications network, many of the unique advantages it offers are yet to be fully utilised. WDM for example offers much, much more than simply capacity increase. It also allows routing and control functions to be performed in the optical domain. We are also seeing the emergence of optical fibre networks for the transport of microwave and millimetre-wave signals as an answer to the loss associated with electrical distribution of high frequency signals.

The low loss distribution of mm-wave signals is a vital component to realising broadband wireless access networks to customer premises that are seen to be necessary to cope with the envisaged growth in traffic. This may be only consider to be a relatively short term solution as some forecast that fibre to the home will soon be essential to provide for the demand in bandwidth, but, history shows that even the greatest minds do not always make the most accurate predictions. Alexander Graham Bell was said to have made this remark soon after he had invented the

telephone: "I do not think I am exaggerating the possibilities of this invention when I tell you that it is my firm belief that one day there will be a telephone in every major town in America".

1.1 Thesis Organisation

Following this introductory chapter a common structure is used throughout this thesis. Each chapter opens with an introduction detailing the aims and contents of the chapter, and is concluded with a summary of the main contributions of the chapter. The organisation of this thesis is as follows;

Chapter 2 reviews a number of the component and network technologies that are considered vital to the future WDM networks. We discuss the attributes of these devices that give rise to the noise effects studied in later chapters. Consideration is given to the choice of software package used to simulate these WDM components in optical networks.

Chapter 3 reviews some of the networks and applications that have driven research into the transport of high frequency analogue signals over optical fibre, including L band radar delivery systems and mm-wave access networks. We investigate some of the technologies and issues involved in the study of these networks.

Chapter 4 investigates the phenomenon of interferometric noise, which is considered to be a major limiting factor in WDM networks. We discuss and compare a number of evaluation methods, illustrating the limitations of approximate methods and extending the current application of rigorous techniques. These methods are applied to two network examples, the first being a multi-wavelength switching node

and the second a network transporting QAM data for mm-wave broadcast.

Chapter 5 provides an evaluation of the performance of a specific beamforming network architecture, demonstrating the effect of performing true time delay in the optical domain using fibre Bragg gratings. We also investigate a solution to the optical power issues that will be encountered in such networks. Included in this chapter are experimental results for validation.

Chapter 6 studies the technique of spectrum slicing for which the inherent noise mechanism is spontaneous-spontaneous beating between the incoherent components that form the source light. We discuss the application of this technique to high frequency transmission networks by various methods, presenting an extension to the present approximate analysis together with experimental work.

Chapter 7 concludes the thesis, summarising the main contributions and suggesting further lines of enquiry. Appendix A includes software documentation for the modules used in the simulations described in chapter 5.

1.2 Contributions

The main contributions made by this research may be summarised as:

- Comparative assessments have been made between performance evaluation techniques used to study interferometric noise.
- Rigorous statistical models for interferometric noise have been extended to include network factors such as finite extinction ratio and crosstalk-crosstalk beating. These were then extended to consider the effect on modulation schemes such as QAM.

- The applicability of spectrum slicing for high frequency analogue transport networks has been investigated, including an extension to the basic SNR formulation, with an evaluation of the limits of this technique for RF delivery systems.

- The effects of multiple wavelength mixing in optical beamforming networks have been characterised both analytically and using simulation, with validation presented from experimental results.

The following research papers were published as a result of this work:

- J. E. Mitchell, P. M. Lane and J. J. O'Reilly. "Investigation of Interferometric Beat Noise in Optical Networks" In *Proc. TRS'97 (University College London Telecommunications Research Symposium)*, London, 21-22 July 1997.

- J. E. Mitchell, P. M. Lane and J. J. O'Reilly. "Statistical Characterization of Interferometric Noise in Optical Networks" In *Proc. OFC'98 The Optical Fiber Communications Conference*, San Jose, Ca. USA 22-28 Feb. 1998 paper WD3.

- J. E. Mitchell, P. M. Lane and J. J. O'Reilly. "Comparative Assessment of Methods for the Evaluation of Interferometric Noise" In *Proc. TRS'98 (University College London Telecommunications Research Symposium)*, London, 27-28 July 1998.

- J. E. Mitchell, P. M. Lane and J. J. O'Reilly. "Evaluation of Extinction Ratio Induced Performance Penalty due to Interferometric Noise" *IEE Electronics Letters* Vol.35 No.12, pp.964-965, 10th July 1999.

- J. E. Mitchell, P. M. Lane and J. J. O'Reilly. "Investigations of the effects of interference terms of un-equal power in systems corrupted with interferometric noise" in *Proc LCS'99 London Communications Symposium*, London July 26-27. 1999.

- J. E. Mitchell, M. Nawaz and C. Pescod. "Evaluation of multiple wavelength mixing effects in optical beamforming networks" in *proc. LCS'99 London Communications Symposium*, London July 26-27, 1999.

- J. E. Mitchell, P. M. Lane and J. J. O'Reilly. "Performance of radio-over-fibre broadband access in the presence of interferometric noise" accepted for presentation at IEEE/LEOS Summer Topical Meetings on Broadband Optical Networks, July 2000 paper ThC2.

- J. E. Mitchell, P. M. Lane and J. J. O'Reilly. "Comparative Assessment of Rigorous Methods to Evaluate Interferometric Noise in Optical Networks" accepted for presentation at ISITA2000 International Symposium on Information Theory and Its Applications. Nov 2000.

Chapter 2

Optical WDM Networks

2.1 Introduction

This chapter reviews the current devices and technologies influencing the work in this thesis. The research is centred around interference issues in a number of WDM optical network types, designed to deliver a variety of services. Section 2.2 discusses the optical components that are the building blocks of envisaged future network architectures, considering their role and some of the inherent characteristics that we must model if we are to form valid performance evaluations. Section 2.3 presents some of the simulation tools that are available to us to aid the evaluation process. A summary of the contributions of this chapter will be given in section 2.4.

2.2 Review of current WDM technology.

Optical fibre communications offers as a degree of freedom, the ability to use the "colour of light". This technique of wavelength division multiplexing (WDM) opens

many new avenues of interest for optical communications. At the basic level it may be used to increase capacity on a point to point link; in 1996 the Tbit/s over a single fibre barrier was broken, today research labs are reporting 3 Tbit/s transmission [1] and commercial systems operating at bit rates greater than 6 Tbit/s are already in the pipeline. This increase in capacity represents only the 'tip of the iceberg' of the advantages that WDM can bring. It is possible for routing, switching and control functions to be governed by the wavelengths used, allowing processing of signals to be kept entirely in the optical domain.

To facilitate these new network transport and routing mechanisms a number of new and novel components and component architectures have been required. To provide multiple wavelength networks, stable laser diodes with relatively small linewidths centred at various wavelengths are needed. To aid even further advance, tunable laser diodes are required that can rapidly lock on any desired wavelength over a wide spectral range. The use of multiple wavelengths demands wavelength selective devices to allow the separation of the channels. These generic components form the basis of network nodes that will route channels according to wavelength and allow channels to be dropped and replaced at will to provide dynamic routing. In the following sections we discuss these and other optical components.

2.2.1 DFB lasers

Distributed Feedback (DFB) lasers are the industry standard optical source for telecommunications networks using single mode fibre. Designed to oscillate in just one longitudinal (and transverse) mode they offer a near monochromatic coherent light source. Typically DFBs supply output powers of the order of tens of mW and

linewidths in the range of kHz. There are a number of techniques used to model semiconductor laser diodes. Detailed models involve the solution of the laser non-linear rate equations for the carrier and photon populations in the device, although, on occasions simplistic models will suffice. For most of the models used in this work only the characteristics relevant to the investigation are required.

We consider the parasitic effects witnessed in laser diodes to form a model of the important noise contributions produced. The starting point is to define the ideal output from a laser diode as;

$$E = \alpha \cos(\omega t + \phi) \tag{2.1}$$

where α is the field amplitude, ω is the laser frequency, and ϕ is the laser phase. Ideally all these parameters are constants and time independent. However, in a real laser both the amplitude and phase are random with respect to time. The random fluctuations of the amplitude lead to *relative intensity noise* (RIN). More important for most of our investigations is the phase noise characteristic of the laser. The spontaneous emission process in the cavity causes small variations of random magnitude in the phase of the output electric field. This can be viewed as the phase exhibiting a random walk in time, which is described as a Wiener-Lévy random process, and produces the effect of linewidth broadening. The instantaneous phase is given by:

$$\theta(t) = 2\pi \int_{-\infty}^{t} f(t')dt' \tag{2.2}$$

where $f(t')$ is the frequency noise, characterised by a Gaussian distribution. The variance of which is given by [2]:

$$\sigma_{laser} = \frac{2\pi\Delta v}{f_s} \tag{2.3}$$

where Δv and f_s are the laser linewidth and frequency. This leads to a Lorentzian linewidth shape of the laser output spectrum. It is this phase noise that is inherent to the process of interferometric noise which will be described in more detail in chapter 4.

2.2.2 Incoherent Light Sources

Although the DFB laser is the obvious and accepted choice for most WDM networks, there has been renewed research interest in the broadband incoherent sources that were used in some of the first simple optical links. A light emitting diode (LED) emits light due to the spontaneous emission of photons from the conduction band which is populated by a forward current applied to the junction. This therefore produces a wide bandwidth incoherent optical source, which can be modelled approximately as a large number of spectral lines each of random phase.

There is interest in such a broadband source because of the idea of slicing the wide output spectrum into many channels to create, in effect, an array of WDM sources from a single low cost unit. However, as we will show the inherent noise in an incoherent source creates a number of new problems not encountered in coherent laser sources. Although the viability of this technique was demonstrated with an LED, the low power available, reduced by the filtering to create separate channels,

limited the usefulness. The advances seen since the introduction of high power sources such as the super luminescence diode and ASE from Erbium doped fibre amplifiers will be discuss in chapter 6.

2.2.3 Fibre Amplifiers

Arguably the most important WDM enabling technology is the fibre amplifier, specifically the Erbium doped fibre amplifier (EDFA) which although only first reported in 1987 has revolutionised optical networks. Before the advent of the EDFA the possibility of long haul WDM networks of more than a few channels seemed remote due to the need for a repeater per wavelength. The EDFA faithfully amplifies multi-wavelength optical signals without the need for conversion into the electrical domain. Such was the advance that the EDFA offered that in 1995 the first undersea system to use optical amplification was installed.

In a fibre doped with Erbium a pump light promotes the Er ions into an excited state, where the optical signal propagating through the fibre induces stimulated emission, thereby giving amplification. Inescapably the process of stimulated emission is accompanied by spontaneous emission of photons which will also be amplified within the fibre to give a noise contribution known as amplified spontaneous emission (ASE). This noise is often characterised as white noise of approximately flat power spectral density across the bandwidth of the optical amplifier, given by:

$$P_{ASE} = n_{sp} h\upsilon_s (G - 1) \tag{2.4}$$

where n_{sp} is the spontaneous emission factor, $h\upsilon_s$ is the photon energy and G the

amplifier gain.

The standard design of EDFA at present offers optical gain over a bandwidth of approximately 35nm, still somewhat short of the 100nm available in the optical fibre low loss window around 1550nm, which due to advances in fibre design is growing all the time. Research is currently underway to produce either fibre doped with Erbium and a co-dopant or entirely new doping schemes that will stretch the width of this gain region further than presently realised. Three main approaches exist to produce broadband amplification. The first extends the current bandwidth by co-doping with elements such as Fluoride or Tellurite. The second involves the parallel use of EDFAs in the 1550nm (C-band) region with those shifted to the 1580nm (L-band) region. This method has demonstrated bandwidths of more than 70nm. However, the third option involves the use of Raman amplification technology, which can produce total gain bandwidths of more than 130nm [3].

2.2.4 Mach-Zehnder Modulators

An optical modulator is a fundamental device to impose information onto the lightwave passed through it. A number of physical effects can be used (electro-optic, acousto-optic, magneto-optic) in conjunction with a number of different materials (GaAs, InP, $LiNbO_3$) to produce waveguide devices. However, in this thesis we focus on a particular electro-optic device, the Mach-Zehnder interferometric intensity modulator. In certain materials on application of an electric field the electro-optic effect is exhibited, causing a localised change in the refractive index proportional to the applied voltage. This change in refractive index, Δn, leads to an induced phase

change, $\Delta\phi$, which is related to the interaction length,L, by:

$$\Delta\phi = \left(\frac{2\pi}{\lambda}\right)\Delta nL \tag{2.5}$$

where λ is the optical wavelength. This phase modulation technique can be used to realise intensity modulators such as the Mach-Zehnder interferometer (MZI) modulator shown in figure 2.1. The basic principle is thus: the input optical wave is split into two equal components into the two arms of the modulator. In each arm the phase modulator either advances or retards the phase of each signal, with the amount of change governed by the applied voltage. When the paths are recombined the total optical signal power is dependent on the relative phases of the two paths. If on recombination the two signals are in phase then they will interfere constructively, while if they are of opposite phase they will interfere destructively and cancel. It is therefore theoretically possible to produce any output state varying from no light, to full input power. It can be shown [4] that the transfer function of a balanced

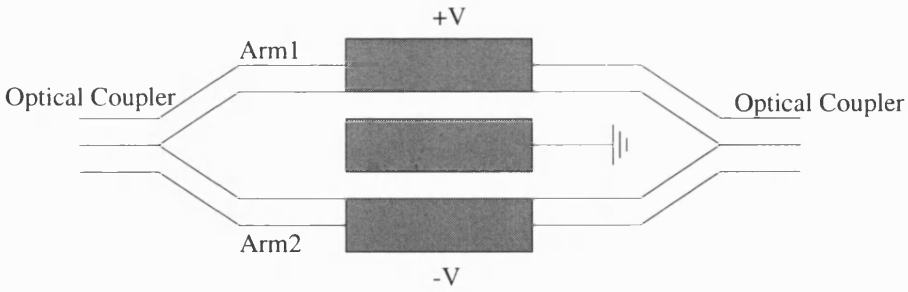

Figure 2.1: Basic structure of a Mach-Zehnder modulator.

modulator is given by:

$$\frac{E_{out}}{E_{in}} = \cos\left(\frac{\pi}{2}.\frac{V}{V_\pi}\right) \tag{2.6}$$

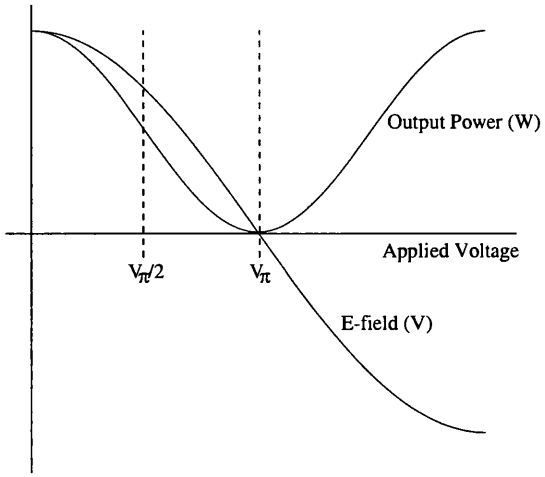

Figure 2.2: Mach-Zehnder Modulator Response

where V is the applied voltage and V_π is the applied voltage required to induce a relative phase shift of π between the two signals. In terms of the output optical power this is:

$$\frac{P_{out}}{P_{in}} = \cos^2\left(\frac{\pi}{2}.\frac{V}{V_\pi}\right) \tag{2.7}$$

This shows that both the E-field and the power response are non-linear as shown in figure 2.2. It is therefore usual for intensity modulation applications to bias the modulator at $V_\pi/2$.

2.2.5 Optical Receivers

The rapid increases in bit rates that have been seen in optical systems have only been possible due to advances in photodetector technology. This increase also effects analogue transmission, with commercially available photodetectors capable of recognising modulated signals >60GHz, well into the millimetre wave region. The basic

principle of an optical photodiode is the production of a photocurrent proportional to the incident optical power. It is this square law effect that is responsible for the production of beat terms if more than one signal is present. This interferometric beating is detailed in section 4.2.

2.2.6 Optical Filtering

One of the most important types of device in determining the performance of optical systems are the optical filters that provide the wavelength selectivity required in WDM networks. An ideal filter would allow the selected wavelength to pass, while completely blocking all other channels. One of the most common practical filter types is the Fabry Perot etalon filter, although many different filter arrangements and fabrication techniques are available, such as fibre Bragg gratings, interferometers etc.

There are a number of critical characteristics for filters employed in WDM systems, perhaps the most vital of which is the crosstalk isolation. All real filter realisations will have a given roll-off slope which may create crosstalk giving rise to interference at the photodiode. In a system of many nodes the cascade of multiplexers and demultiplexers will effect the overall end-to-end bandwidth response of an individual wavelength path.

Fabrication	Isolation	Ref.
Planar SiO_2	$\approx 25dB$	[5]
$LiNbO_3$	$\approx 30dB$	[6]
Micromachined switches	$\approx 60dB$	[7]

Table 2.1: Illustrative filter crosstalk levels

2.2.7 Fibre Bragg Gratings

Fibre Bragg Gratings (FBG) have been suggested for numerous applications in WDM networks due to their unique filtering properties [8], which have already been highlighted in section 2.2.6. Another application which we discuss here is to form optical fibre delay lines that are polarisation insensitive, inherently fibre compatible, relatively easy to produce and low loss [9].

Fibre gratings are produced by etching a periodic perturbation of the refractive index in the core of a fibre by exposure to an intense optical interference pattern. This forms a high dispersive reflector whose response is strongly dependent on optical wavelength. Therefore a series of gratings can be 'written' into a fibre that produce a variable time delay controllable by wavelength selection. Further to this it is possible to form 'chirped' gratings that allow continuously variable delay [10].

These devices have been suggested for the realisation of true-time delay elements of the optical beamforming networks discussed in section 3.4. Detailed descriptions of the grating characteristics are provided by Zhao et al [11].

2.2.8 WDM Network devices

The dominant drive in today's optical network research is to move as much control and routing as possible from the electrical domain into the optical domain. Any attempt to mesh point to point links using traditional electrical methods will soon encounter bottlenecks due to electronic processing speeds. The predominant architecture for network interconnects is based on the idea of an optical add drop multiplex (ADM), as shown in figure 2.3. Many variants of this exist, however here

we will examine the design suggested by Hill et al [12].

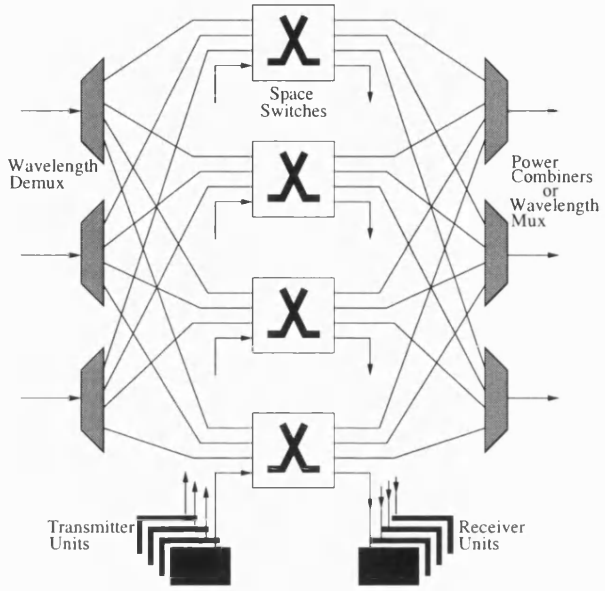

Figure 2.3: An example of an add drop multiplexer

This network node acts as a optical cross-connect (OXC) for many fibres each carrying multiple wavelengths. The principle of operation is as follows. As each fibre enters the node optical demultiplexers separate the various wavelength components carried on that fibre. These are then switched using optical space switches, which may either direct the optical channels to output fibres or may direct selected channels to a local receiver where the signal enters the electrical switching domain. The switches also allow for locally generated channels to be added into the traffic leaving the node.

The flexibility of the node is almost entirely determined by the wavelength tuneability of the components in the local transmitter and receiver units. For example, the simplest node structure would allow only a designated wavelength to be added and dropped at a specific node, which does not require tunable components in the

receiver. In this way information is 'addressed' by the wavelength it is transmitted on, but wideband tunable sources are required so that information may be sent to any other node. This scheme and similar fixed wavelength schemes run into a number of scalability problems, whereby to increase the number of nodes in the network, an upgrade is required to all of the other nodes in the mesh. Other problems exist, such as wavelength contention and signal blocking, which due to the lack of practical optical buffering, is not an easy problem to over come.

It is now seen that the most adaptive node must have both tunable receivers and transmitters, while the use of wavelength conversion techniques to eradicate blocking is of considerable interest.

2.2.9 Interferometric Noise

Now that we are envisaging networks where wavelengths on multiple fibres are split, routed and reordered at a network node, some consideration must be given to the effect of the crosstalk inevitably produced within these nodes. As discussed earlier in this chapter optical filters do not give perfect isolation, allowing many spurious signals to build up on each main channel. When this composite signal comes to its final receiver point, spurious signals of different wavelengths can be easily removed by filtering, whereas any spurious signals that are at nominally the same wavelength cannot be removed in this way and will degrade the system performance.

This inband crosstalk power will not only create a photocurrent, it will also form a beat noise component, termed interferometric beat noise, due to the square law response of the photodiode. The investigation of this and other related phenomena form the main drive of this thesis. A detailed description of the formation of this

noise component is given in chapter 4.

2.3 Simulation of WDM networks

Today a number of commercial packages are available to simulate optical WDM networks, with the choice of which to use conditioned by the exact nature of the simulations required. The simulation package discussed here, the Signal Processing Worksystem (SPW)[1], was chosen for work requiring physical layer modelling as it provides a well structured front end for both standard and custom coded blocks. Although originally designed for DSP applications SPW lends itself well to communication system modelling as complex mathematical functions can easily be combined with random functions to produce component models.

2.3.1 The Signal Processing Worksystem

SPW is a graphically driven simulation package which facilitates the formation of complex mathematical functions to model communications systems. It provides a hierarchical structure allowing standard network functions to be design and reused in the system. The built-in functions include standard mathematical functions, vector functions, fast Fourier transforms, as well as some ready-built radar, RF and communications blocks. Custom coded blocks are created by compiling C code, which is embedded within a user defined block.

[1] Alta Systems, Cadence Group.

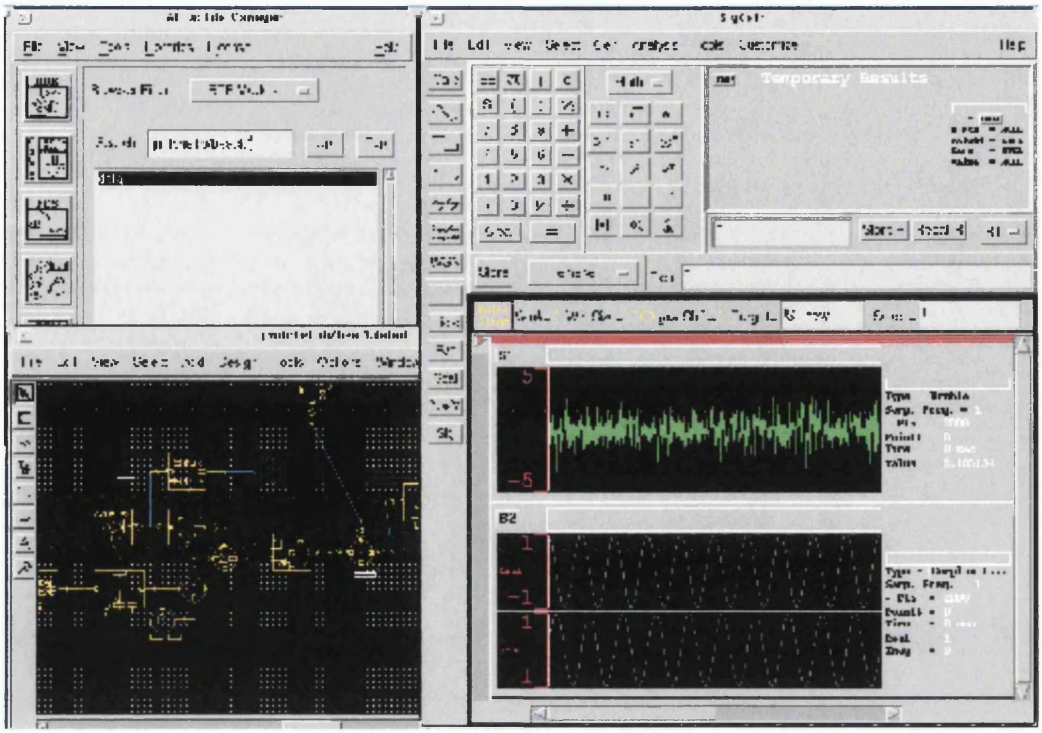

Figure 2.4: Illustrative 'windows' for the signal processing worksystem

Handling Multiple Wavelengths

Prior to undertaking any simulation work, the first priority was to devise a standard way to handle the multiple wavelength signals within the model. Factors considered include: computation time; development time; frequency, time, or mixed domain simulation; and the potential to use blocks from previous experiment. In keeping with previous work it makes sense to operate a mixed domain simulation [13], with the source and modulation modelled in the time domain, before FFT conversion to the frequency domain for the main frequency dependent processing involved in modelling the fibre and mixing effects. The signals are then converted back to the time domain after the receiver model for error calculation. Previous experiments have considered and used different methods of processing multiple wavelength sig-

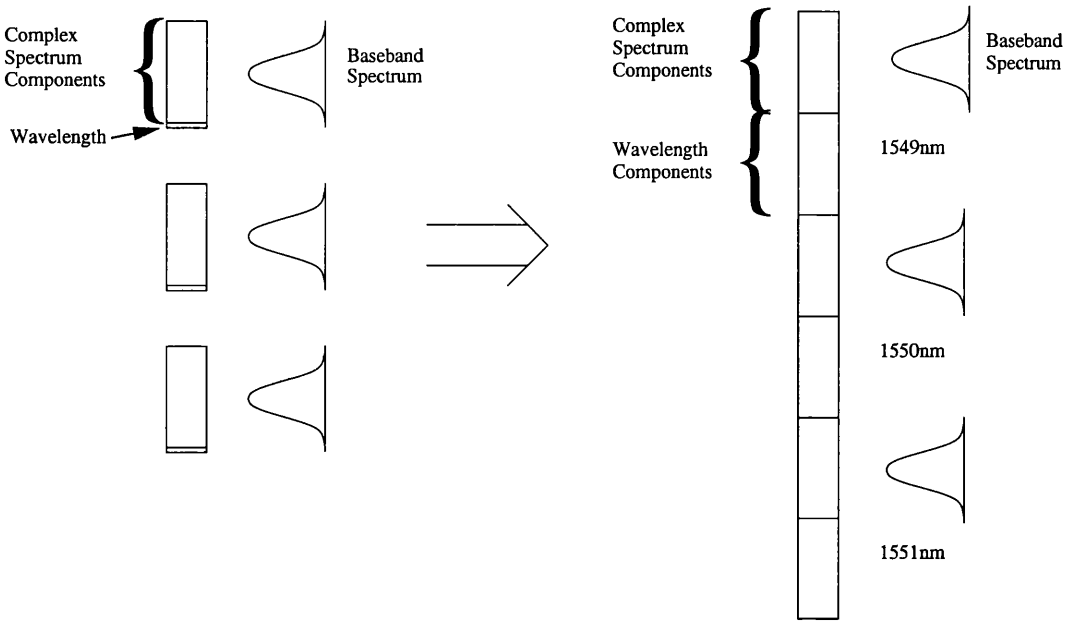

Figure 2.5: Composition of transmitted vector to process multiple wavelengths

nals; however due to the disparity between signal rates ($\approx 10^9 Hz$) and the optical carrier frequency ($\approx 10^{14} Hz$), all have considered just the complex envelope. Using this equivalent baseband representation we consider a method of differentiating between signals of different wavelength. The method found most convenient is to 'butt' together the vector of FFT amplitude and phase information with a vector containing a wavelength value for each FFT point. This creates a longer vector than some previous methods but improves computation speeds within processing blocks by removing the need to continually calculate the wavelength of the data.

2.4 Summary

In this chapter we have reviewed some of the devices and network technologies that are important to the study of WDM networks. The characteristics of the

devices discussed here will be used in the following chapters to evaluate network performance. Techniques and packages used to simulate the performance of WDM systems and networks have also been discussed focusing on the package SPW, which will be used for the simulation work contained within this thesis.

Chapter 3

Optical delivery of mm-wave signals

3.1 Introduction

The transport of high frequency analogue signals over optical fibre is at present receiving enormous research interest for a number of applications, including mobile radio communications and radar applications. After a review of this area in section 3.2 we review two specific application areas, for which we will investigate the contribution of beat noise in later chapters of this thesis.

In section 3.3 we consider the production and delivery of millimetre wave (mm-wave) signals over fibre optical cables for hybrid fibre radio systems, before turning our attention in section 3.4 to the optical beamforming networks that have been suggested for future phased array antenna designs. Section 3.5 then considers the problems encountered when simulating such networks, with section 3.6 summarising the contributions of this chapter.

3.2 Review of mm-wave delivery

The unprecedented growth in mobile communications in recent years has renewed research interest in radio systems, with the envisaged demand for broadband services forcing a migration from UHF and microwave frequencies towards millimetre wave technologies. However, with the use of mm-wave transmission, defined nominally as the region between 30GHz and 300GHz, comes increased engineering difficulties. Primarily the generation and distribution of mm-wave signals can be both technically difficult and potentially expensive. Distribution over any reasonable distance in the electrical domain is impracticable due to the high loss of co-axial cable and the high cost and rigidity of mm-wave waveguides.

These constraints have fuelled interest in optical delivery of high frequency signals using a technique known as hybrid fibre radio (HFR). In this approach optical fibre carry the mm-wave signals allowing simple and low cost antenna units to be used at the base transceiver station. This technique has been suggested for a number of applications:

- Cellular Radio links from the central office to base transceiver stations for systems such as GSM and UMTS.
- Wireless Local Area Networks (LANs) to provide mobile network facilities for computers in an office environment.
- Wireless High Definition TV (HDTV) distribution offering similar services to satellite or cable systems to specific cells.
- Wireless local loop delivery of broadband services to homes and businesses.

- Traffic information systems.

3.3 Hybrid fibre radio systems

The use of hybrid fibre radio to provide a final drop for broadband multimedia services to subscriber premises has gained a great deal of momentum since its study in the FRANS project of ACTS. At the time, the project envisaged the majority of traffic to be ATM, supplying services such as video on demand. Although these are no longer 'flavour of the month' this technique is even more relevant with the demand for high capacity data links to supply consumers hungry for internet bandwidth.

The principle of this system is that optical fibre will provide transport of many channels to a local distribution point serving a cell of customers, in an arrangement known as *fibre to the curb* (FTTC). The information content is carried in such a form that the mast head antenna unit need only consist of a photoreceiver, and any required electrical amplification to allow transmission. Methods of achieving this are discussed in section 3.3.1. Each subscriber is then equipped with a simple antenna and downconverter similar to satellite TV systems.

With the recent explosion of internet traffic and its proliferation into the home, the demand for high capacity links has grown at an exponential rate which is only just being addressed. In recent years private customers have had limited access choices, such as 56Kbit/s modem on a standard twisted pair copper line or the expense of installing and subscribing to an ISDN line which offers less than a three fold capacity benefit. Advances are being in made: in the UK asynchronous digital subscriber line (ADSL) technology is now offered and cable modem systems have

been trialled in many parts of the country.

These systems still offer insignificant capacity benefits compared to the capacity requirements envisaged in only a few years time. Also the ideology of a single fixed bandwidth link to each customer is undoubtedly a major stumbling block to the uptake of serious home internet use.

The ultimate 'Utopia' is fibre to the home (FTTH), offering a comparatively enormous increase in bandwidth even for simple installations with the advantage of almost infinite upgradability for future requirements (>1 Tbit/s). Although the cost of optical fibre is relatively cheap, the cost of installing new cable to each home is huge, with BT estimating that there is approximately 15 million miles of twisted pair copper in the UK alone (1995) [14], compared to the worlds production of around 4 million miles of optical fibre per year.

The fibre to the curb method described above offers increased bandwidth with only a small increase in fibre outreach. As has been demonstrated with satellite TV systems the cost of receiver equipment can be reduced by mass production to very affordable levels. Due to the broadcast nature of HFR systems the capacity assigned to each customer is not fixed, as it is with fixed lines. Therefore the implementation of dynamic bandwidth allocation schemes is possible to allow full use of the capacity available.

3.3.1 Millimetre wave generation

We now consider the problem of mm-wave generation for transport to the base station. Several methods have been suggested for the transmission of mm-wave signals over an optical fibre.

- *Direct modulation:* This is theoretically the simplest method available, in which the mm-wave signal is formed in the electrical domain and then modulated onto the optical carrier. This may be achieved using either direct modulation or external modulation of the laser source. The main limitation is the maximum modulation frequency afforded by this technique, MQW lasers have been produced that allow direct modulation rates up to 15GHz, and although expensive, MZ modulators that operate at 60GHz are available.

- *Coherent Mixing:* This method generates the mm-wave by the coherent mixing at the photodetector of two optical carriers displaced by the required frequency. The overriding requirement for the successful operation of this technique is reliable generation of two stable, coherent optical carriers for which a number of techniques have been suggested. The two best known are the use of optical locking circuits, and the use of frequency doubling.

  - *Optical locking circuits* use feedback from the output of a master laser to drive a control circuit for a slave laser. Frequency locking [15] is simplest to achieve but has no control over the phase deviation of the sources which leads to large electrical linewidth, while phase locking [16] requires much more complex circuitry yet produces phase correlation between the sources, reducing linewidths.

  - *Frequency doubling* [17] has received the most attention due to its novel solution to the problem of source correlation. A single optical source is used, with the two carriers produced by a Mach-Zehnder modulator biased to suppress the central optical carrier term. This produces two

perfectly correlated optical carriers separated by twice the MZ modulation frequency.

3.3.2 Generation of mm-wave signals by frequency doubling

Here, a brief analytical description of the generic method of mm-wave generation by coherent mixing is presented followed by specific details of the method of frequency doubling.

We consider two optical fields of frequency ω_1 and ω_2 described by:

$$E_1(t) = E_1 \cos(\omega_1 t) \tag{3.1}$$

$$E_2(t) = E_2 \cos(\omega_2 t) \tag{3.2}$$

If the two fields are both incident on a photodiode the resultant photocurrent will be described by the following:

$$i_t(t) = [E_1 \cos(\omega_1 t) + E_2 \cos(\omega_2 t)]^2 \tag{3.3}$$

$$= \frac{1}{2}\Big[E_1^2 + E_2^2 + E_1^2 \cos(2\omega_1 t) + E_2^2 \cos(2\omega_2 t) + E_1 E_2 \left[\cos(\omega_2 - \omega_1) + \cos(\omega_1 + \omega_2)\right]\Big] \tag{3.4}$$

Of these terms only one is of interest, the term at $\omega_2 - \omega_1$ which can be controlled to be the millimetre wave frequency f_{mm}:

$$f_{mm} = \frac{(\omega_2 - \omega_1)}{2\pi} \tag{3.5}$$

As discussed previously these two correlated carriers can be produced by a single source and an appropriately biased Mach-Zehnder modulator. The characteristic of such a modulator is shown in section 2.2.4 which can be described for our purposes as:

$$E_{out}(t) = \cos\left\{\frac{\pi}{2}\left[(1+\varepsilon) + \alpha\cos(\omega t)\right]\right\}\cos(\omega_o t) \tag{3.6}$$

assuming biasing at V_π, where ε and α are the normalised bias point and normalised drive voltage amplitude respectively and ω_o is the optical carrier frequency. The first two terms of the Bessel function expansion of this expression are:

$$\begin{aligned} E_{out}(t) = {} & \frac{1}{2}J_0\left(\alpha\frac{\pi}{2}\right)\cos\left[\frac{\pi}{2}(1+\varepsilon)\right]\cos(\omega_o t) \\ & - J_1\left(\alpha\frac{\pi}{2}\right)\sin\left[\frac{\pi}{2}(1+\varepsilon)\right]\cos(\omega_o t \pm \omega t) \end{aligned} \tag{3.7}$$

Equation (3.7) clearly shows a centre optical term with two components separated by 2ω which can be up to twice the bandwidth of the MZ modulator. We see that if the modulator is biased very close to V_π ($\varepsilon \approx 0$) then the centre term will be suppressed. The schematic of how this frequency doubling technique is used in a delivery system is shown in figure 3.1, where a single laser source is externally modulated with a RF signal at half the required mm-wave frequency. The two coherent optical carriers produced are split and one is modulated with data, after which they are combined and transmitted over the fibre link to the base transceiver stations for distribution to the cells.

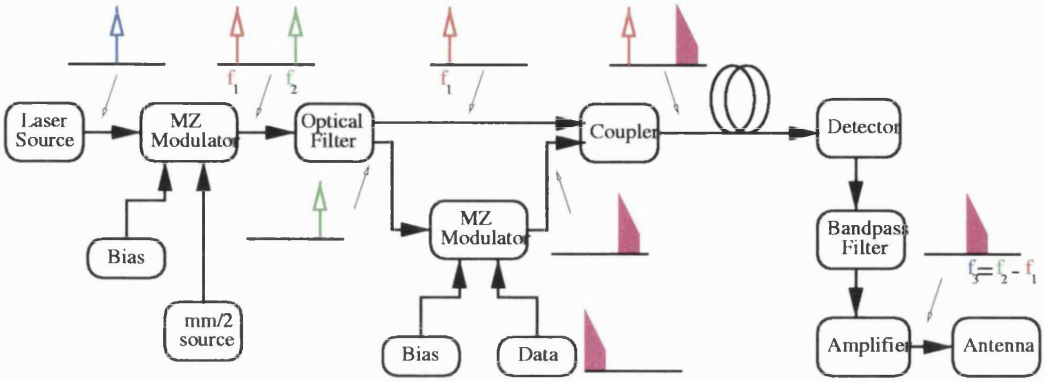

Figure 3.1: Schematic of a mm-wave generation system

3.3.3 QAM modulation

Quadrature Amplitude Modulation (QAM) is a well known technique to achieve bandwidth reduction by utilising both phase and amplitude modulation, with multi-level signalling. Using such a signalling scheme with M symbols and two carriers at quadrature allows $\log_2 M$ bits to be transmitted during each symbol period. The message signal is separated into two data streams, which are each multi-level coded, and used to modulate carriers that differ in phase by 90^o. Because sine and cosine functions are orthogonal, the two amplitude modulated waves can occupy the same transmission bandwidth. For 16 QAM this produces the constellation shown in figure 3.2, formed by sine and cosine carriers and 4 level signalling. Note that all points are equi-distant from each of the neighbouring points.

QAM has been of great interest in a number of fields due to the bandwidth reduction available, most notably for cable television applications where 256-QAM has been used [18]. QAM has also been adopted for use in mobile radio applications and satellite channels, and is used in digital subscriber line (DSL) techniques to provide high speed data access over twisted pair copper connections.

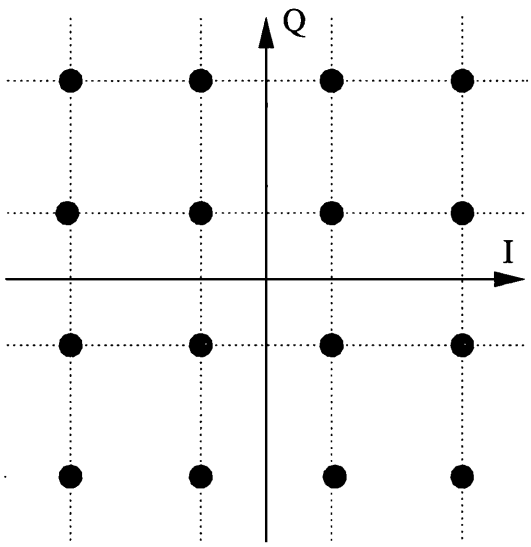

Figure 3.2: Four level (16 symbol) QAM constellation

3.4 Beamforming Networks

Phased array antennas have for a number of years been used for many high performance radar and communications applications. They have the advantage of a large virtual aperture and electronically controllable beam direction. As the theory of phased arrays has been well documented only a brief overview is presented here for completeness.

We consider a simple linear (one-dimensional) array with n elements, spaced by a distance d. If all elements transmit in phase, then the wavefront is radiated broadside to the array. If, however, there is a phase deviation between successive elements of Φ, then the wavefront will radiate at angle θ:

$$\theta = \sin^{-1}\left(\frac{\lambda\Phi}{2\pi d}\right) \tag{3.8}$$

where λ is the signal wavelength. Creating the required phase shifts is a relatively

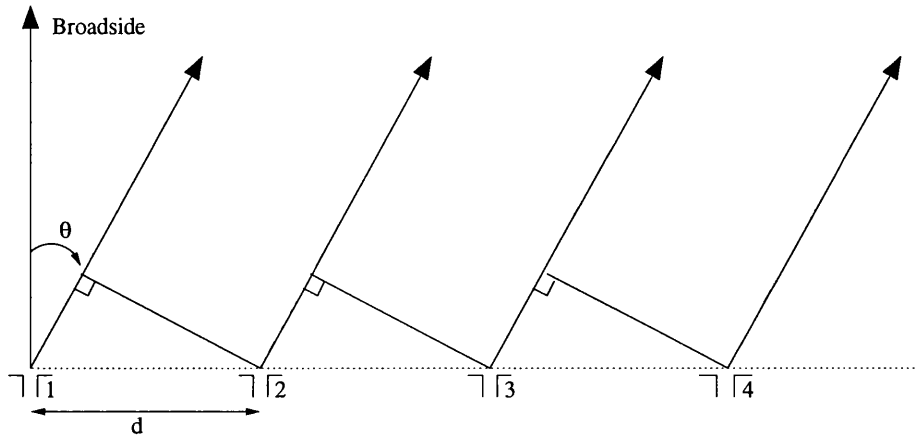

Figure 3.3: A linear array of dipole elements

simple process if the signal can be considered to be monochromatic, i.e. of a single frequency. This is unlikely in many applications, for example in radar applications a pulse of energy is usual, resulting in a wide signal spectrum. For such wide band signals, the result of performing phase shifting will be 'beam squinting' i.e. components of different frequency will be radiated in different directions [19]. The solution is to perform time delay rather than phase shift, creating what are know as true-time delay beamforming networks.

As mentioned in section 2.2.7 fibre Bragg gratings have been suggested to perform this delay function in the optical domain. In the electrical domain the production of a variable time delay is a relatively simple task, however the benefits of being able to perform this function optically are significant due to the losses and bulk of electrical options. Fibre gratings can be written that give a time delay dependent on the wavelength of the optical signal. This allows two modes of operation:

1. The simplest approach is to transmit each signal on a different wavelength, all coupled into a signal fibre and then applied via an optical circulator to a

series of gratings. Each series of gratings must be specially written for each beam angle to produce the correct delay. The formation requires each beam to have an optical circulator and a custom written set of gratings. In applications such as listening systems, and smart antennas this arrangement fulfils the vital criterion of being able to 'look' in all directions at once.

2. Recently it has been suggested that for scanning systems it would be possible to make use of a chirped fibre Bragg grating where instead of having a fixed flat response within the grating the wavelength response is continuous throughout the device length. If such a grating was used in conjunction with tunable wavelength laser sources it would be possible to create a sweeping motion by tuning each of the lasers at a different rate according to its position in the array.

The work in chapter 5 considers networks based upon the first principle.

3.5 Simulation of RF delivery networks

Previous studies using SPW have mainly been performed for digital systems and have largely been in the time domain [20], stemming from the original design of SPW for DSP applications. Radar systems, begin analogue in nature, present a number of problems for simulations of this kind, with the main inherent problem being that of accuracy. Considering the 4GHz band and allowing for the inclusion of only the first two harmonic terms formed by nonlinear processes, we can show that a sample frequency of >20GHz must be used. At this frequency a fast Fourier transform (FFT) length of 2^{25} is required if a resolution of greater than 1kHz is required in

the frequency domain. A single transform requires $N \log_2 N$ calculations, where N is the FFT length. Therefore over 838 million calculations are needed per FFT, of which there may be more than 100 in a multi-wavelength simulation run. Clearly this is impractical not only in terms of computation time but also due to memory requirements (>4Gb RAM/swap).

It would therefore be advantageous to consider schemes that reduce the simulation complexity, such as split step simulation. However, these are difficult to implement in SPW without having to radically recode large portions of the simulation, which remove the value of SPW as a tool. Certain simpler schemes have been implemented to reduce the computation burden to an acceptable level, the results of which can be seen in chapter 5.

3.6 Summary

In this chapter we have reviewed hybrid fibre radio networks, considering both the generation of the mm-wave signals in the optical domain, and the applications and modulation schemes suggested. Consideration has also been given to the possible applications of optical beamforming networks for phased array antennas, and the network structures required for beamsteering in the optical domain.

Chapter 4

Interferometric Beat Noise

4.1 Introduction

This chapter is concerned with the analysis and simulation of interferometric noise in optical systems. As discussed in chapter 2, it is envisaged that future WDM networks will use optical cross connects and add drop multiplexers to perform all optical routing within network nodes. These devices all produce crosstalk which accumulates on the optical channels as they traverse the network. Crosstalk can be defined as either in-band or intra-band crosstalk dependent on its position in wavelength relative to the channel concerned. In-band crosstalk arises due to the inadequate suppression of channels that are either of the same, or an almost identical wavelength and is of most significance, as once formed it cannot be removed by subsequent filtering. An example of how crosstalk accumulates due to imperfect isolation in an add drop multiplexer is shown in figure 4.1.

After a review of the formation of interferometric noise in optical networks in section 4.2, definition and description of the terms that effect IN are given in section

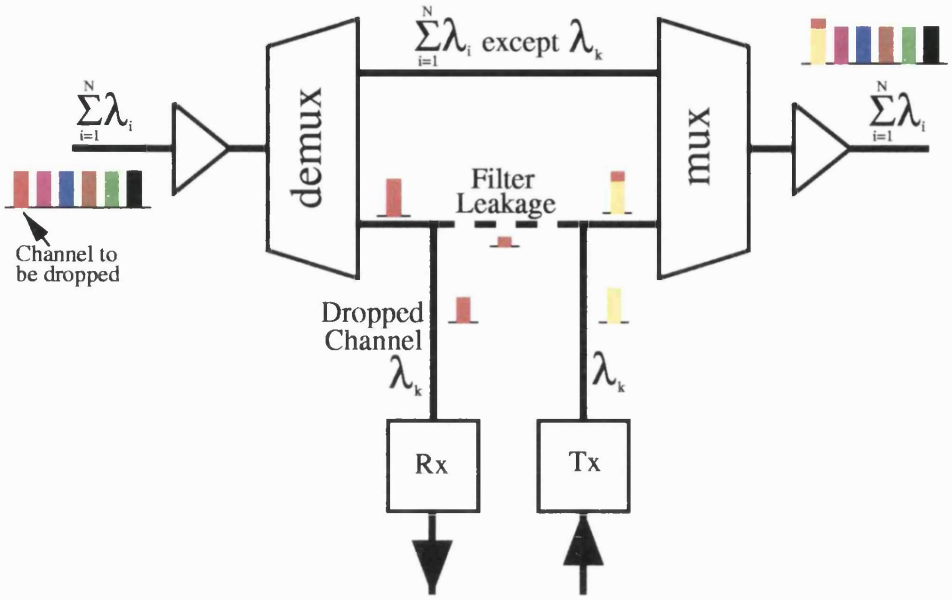

Figure 4.1: An example of how imperfect isolation at an ADM causes in-band crosstalk

4.3. This is followed in section 4.4 by details of many of the methods used to evaluate IN, including a derivation of the moment generating functions that will be used in the investigations of section 4.5. This section looks at detailed descriptions of performance evaluation in a number of scenarios encountered in optical networks, including evaluations of extinction ratio, crosstalk-crosstalk beating and the effect of interferers with unequal powers. The methods and metrics described are then used to examine a real optical network node in section 4.6.

Section 4.7 considers IN in a different context, that of hybrid fibre radio systems, examining the effect of interferometric beating in systems transporting QAM data. The chapter is summarised in section 4.8.

4.2 Formation of Interferometric Noise

Interferometric noise (IN) is formed when multiple signals of nominally the same wavelength fall upon a photodiode [21]. The square law relationship of electric field to photo-current displayed by a photodiode causes the various components to beat with one another resulting in what is now widely termed *interferometric beat noise* (also termed *phase induced intensity noise* [22], *homodyne beat noise* [23], *optical beat interference* [24]). In this section we present a unified description of IN and define a number of terms and assumptions that are often used in this field.

Let us consider how we describe an optical signal of power P emanating from a DFB laser, the electric field is given by:

$$E(t) = \vec{\rho}\sqrt{P}\exp j[\omega t + \phi(t)] \tag{4.1}$$

where $\vec{\rho}$ expresses the state of polarization, ω is the optical frequency and $\phi(t)$ the optical phase. Now taking the general case of a signal corrupted by N interfering terms, the total field incident on the photo-detector will be :

$$E_{tot}(t) = \vec{\rho_s}\sqrt{P_s m_s(t)}\exp j[\omega_s t + \phi_s(t)] + \sum_{k=1}^{N} \vec{\rho_k}\sqrt{\epsilon_k P_s m_k(t)}\exp j[\omega_k t + \phi_k(t)] \tag{4.2}$$

where ϵ_k is the relative power of the kth crosstalk term ($\epsilon_k = P_k/P_s$) with the subscript s denoting the desired signal and $m(t)$ representing the binary symbols forming the OOK message: $m(t) \in \{r, 1\}(0 < r < 1)$ with r accounting for the extinction ratio factor. Taking the semi classical approach of optical detection,

we define the instantaneous optical power as being proportional to the squared magnitude of the electro-magnetic field, allowing us to describe the field received at the photo-detector as :

$$i_t = \frac{\eta e}{h\nu}|E_{Tot}|^2 \tag{4.3}$$

where η is the quantum efficiency of the photodiode, e is the electron charge, h is Planck's constant and ν is the frequency of the lightwave. This is normalised without loss of generality by making $\frac{\eta e}{h\nu} = 1$. Using (4.2) and (4.3) we see that the received signal can be described by :

$$\begin{aligned} i_t =& P_s \Bigg[m_s(t) + \sum_{k=1}^{N} m_k(t)\epsilon_k \\ &+ 2\sum_{k=1}^{N} \vec{\rho_s}\vec{\rho_k}\sqrt{\epsilon_k}\sqrt{m_s(t)m_k(t)}\cos[(\omega_s - \omega_k)t + \phi_s(t) - \phi_k(t)] \\ &+ 2\sum_{k=1}^{N-1}\sum_{j=k+1}^{N} \vec{\rho_k}\vec{\rho_j}\sqrt{\epsilon_k\epsilon_j}\sqrt{m_k(t)m_j(t)}\cos[(\omega_k - \omega_j)t + \phi_k(t) - \phi_j(t)] \Bigg] \end{aligned} \tag{4.4}$$

This equation combines the signal plus three distinct noise effects. The first noise term is linear crosstalk, which simply alters the position of the lower and upper signal trajectories in the eye diagram by a factor proportional to the crosstalk power. The second noise term is the beating effect between the signal and the interfering terms, which is termed interferometric noise. The last term, referred to as crosstalk-crosstalk beating, is discussed in section 4.5.2. This is often assumed negligible and dismissed by assertion, until now with minimal proof.

If we examine the interferometric noise term further we find that the expression

involves a number of different contributions. The first contribution is of the relative polarisations $\vec{\rho_s}\vec{\rho_k}$, the effect of which is reviewed in section 4.3.1. The term $\sqrt{\epsilon_k}$ determines the relative power, while $\sqrt{m_s(t)m_k(t)}$ takes account of the symbol states of the channels. Within the cosine function, $(\omega_k - \omega_j)$ defines the relative positions in frequency of the signal which is discussed in section 4.3.2. The final part of the cosine term are the relative phases of the carriers which form the basis of the interferometric nature of the beat noise; these are covered in detail in section 4.3.3.

4.3 Terms affecting IN

In the sections that follow we consider the effect of the various terms that contribute to IN, detailing how others authors have treated them and justifying how we treat them.

4.3.1 Polarisation

In the above formulation the term $\vec{\rho}$ is included to define the state of polarisation. Many assessments choose to ignore this, citing the findings of [25] that the average result is skewed towards the worst case. Some authors however, have considered the statistics of the state of polarisation (SoP), as in [26] which views the probability function as the doubled non-negative part of an arc-sine distribution, giving the PDF of a single interferer as the convolution of the statistics of the phase and the polarisation. There is a potential limitation with this approaches due to the comparative time scales of phase and polarisation variation. The coherence time of a laser is typically of the order of nanoseconds while the rate of change of the

SoP is usually at least eight orders of magnitude greater, so simply combining these by convolution of PDFs and neglecting the widely differing time scales can easily be misleading. This has led some authors to treat slow polarisation fluctuations in a manner analogous to fading in radio systems and consider 'outage' time [27]. However, for most network planning and engineering purposes 'outage time' is inappropriate; what is required is very high certainty that the network will perform adequately, better than some given performance limit, providing for 'quality of service' (QoS) guarantees. With slow polarisation fluctuation the worst case can persist for considerable lengths of time so it is necessary to formulate a worst case analysis based on polarisation aligned signal and interferers rather that to statistically average over all states of polarisation.

4.3.2 In-band Noise

The level of IN experienced is dependent in part on the proportion of the beating products that fall within the bandwidth of the receiver. This is conditioned by two factors: the difference in optical frequency between the interferer and the signal, Δf, and the linewidths of the sources B_L. The former depends on the origin of the crosstalk and the method of, or requirement for, close wavelength correlation within the system. The later is not usually of importance as the linewidth of modern sources is generally very small ($\sim MHz$) compared to the bandwidths of high capacity networks ($\sim GHz$) and necessarily so for dense WDM (DWDM) systems and networks. These two factors have different effects on the received spectrum. As B_L increases the beat spectrum becomes broader, while Δf determines how far from baseband the beat spectrum is centred. If either the linewidth or wavelength

separation are comparable with the receiver bandwidth, the filtering imposed on the spectrum of the beating will affect the noise statistics and reduce the effect of the IN. In this work both these variables are set so that any beat terms produced fall in-band; this represents a 'worst case' in general.

4.3.3 Coherent and Incoherent Noise

The level of phase correlation between the signal and the interfering terms defines whether the interference should be regarded as coherent or incoherent. Due to phase noise in laser sources, discussed in 2.2.1, a laser can only be thought of as a continuous wave source for intervals shorter than the coherence time. Therefore, if the interferer originates from a different source or from the same source but delayed by greater than the laser's coherence time, τ_c, then the interference is incoherent. In this work we consider only incoherent interferers.

4.3.4 Probability Density Function of IN

Considering the formulation of interferometric noise in (4.4), and assuming in-band crosstalk as detailed in 4.3.2, the interferometric noise is described by a term of the form:

$$\alpha \cos(\theta) \tag{4.5}$$

where α is the symbol conditioned interfering power, and θ is a random variable describing the relationship between the phases. To describe the distribution of this term we consider that the phase of the desired signal is fixed and known. The phase

of the interferer being incoherent to the desired signal will at any point in time fall randomly within the interval $\pm\pi$, with all states equally likely. Therefore the difference between the two phases θ is uniformly distributed in the interval $\pm\pi$. This knowledge of θ allows us to define the probability density function as:

$$p_i(x) = \frac{1}{\pi\alpha\sqrt{1-\left(\frac{x}{\alpha}^2\right)}} \tag{4.6}$$

which is the well known arc-sinusoidal function [28]

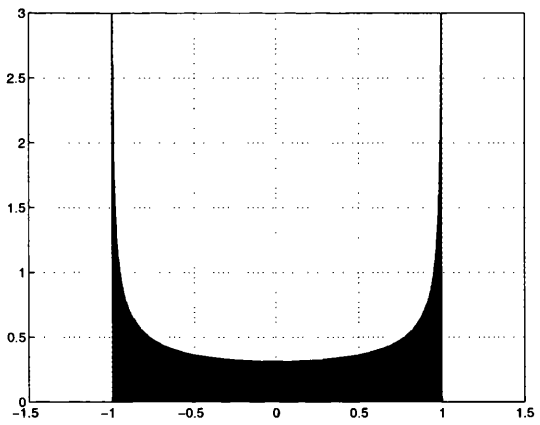

Figure 4.2: The Arc Sinusoidal distribution

4.4 Evaluation Methods

With the complexity, size and cost of modern telecommunications links it is not acceptable to build prototype systems without 99% certainty that these systems will function as expected. To aid system design, performance metrics evaluated using analytic methods have become the stock in trade for network designers, whether they are calculations for individual links or expressions embedded within complex

network simulation software.

TECHNIQUE	COMMENT	VARIABLES	REF
Gaussian Approximation	By central limit theorem appropriate for a large number of terms. However, questionable when N is small	Variance	[25] [29] [30] [31]
Inner eye (Distribution free) bound	Determine the worst case eye closure. Straight forward but often overly pessimistic	Mean, range and variance of the beating statistics	[23]
Chernoff Bound	Simple general bound, not exceptionally tight in all situations	Moment generating function of the random variable	[32]
Modified Chernoff Bound	Uses knowledge of presence of Gaussian component to improve the CB. Compact and accurate.	Moment generating function	[33]
Saddlepoint Approximation.	Approximates the cumulative probability distribution by finding the saddlepoint of the integrand of the MGF in the complex plane. Complex formulation due to the requirement for a second differential term	Moment generating function	[26]
Numerical Calculations	A number of different numerical methods have been demonstrated. Most are too complex to be of value, other than for a single interferer	PDF and boundary conditions to allow convolution	[34] [35]
Hermitian Polynomials	Used recently to produce a closed form bit error rate formula. Care must be taken with truncation to insure accuracy.	Limited set of moments	[36] [37]
Simulation	Generate a corrupted data stream. BER calculated using a quasi-analytic method. Heavy computational burden, very accurate with detailed models	Characteristic of all major network elements	[38]

Table 4.1: Summary of Interferometric noise evaluation methods

The most common measure of system performance in digital communications at the physical layer is the bit error rate, determined from the probability that a data bit is received in error. The receiver circuit integrates the energy over a bit period and the resulting signal is compared to a given level, termed the decision threshold,

to determine whether the received bit is a '0' or '1' symbol. However, random noise with the signal may result in errors in the output if noise on the signal causes it to cross the decision threshold.

Bit error rate evaluation is in principle relatively simple, if we know certain characteristics of the system. Firstly we define the probability of error:

$$P_e = p_0 \cdot \Pr\{N > \alpha|0\} + p_1 \cdot \Pr\{N \leq \alpha|1\} \tag{4.7}$$

So if we know the probability of each symbol being transmitted, p_0 and p_1, then all we need to find to calculated the probability of error is the likelihood of a '0' being detected when a '1' is transmitted ($\Pr\{N > \alpha|0\}$) and the likelihood of a '1' being detected when a '0' is transmitted ($\Pr\{N \leq \alpha|1\}$). The reason for mis-detection of symbols is noise on each symbol level that may cause the symbol energy to cross the decision threshold.

To calculate the probability of error for the noise distribution, the evaluation of infinite integrals is almost always required. The result is the bit error rate, although often a more useful metric which can be derived from it is the power penalty. This is a measurement of the additional power required to maintain a given bit error rate or signal to noise ratio, when a certain noise contribution is considered. This section details a number of the evaluation methods that are applicable to these calculations.

4.4.1 Methods Using 'Partial' statistics

To calculate the exact nature of the noise distribution at the optical receiver can be extremely difficult, and for certain noise types even if the distributions are

known, direct error probability calculation is not always forthcoming. Therefore a number of techniques have been devised that consider the use of elementary statistical measures, such as the mean and the variance, to facilitate the calculation of approximate performance values. Two such measures are outlined here.

Eye Opening

A simple yet effective comparative technique for performance evaluation is to consider the effect that the noise power will have on the eye opening at the receiver. If we consider the maximum values of the noise we can form a qualitative measure of the worst case degradation. This method was demonstrated in [32] for the evaluation of interferometric noise. As an example, we see from equation (4.4) that the amplitude of the interferometric noise is bounded by $\pm 2\sqrt{\epsilon}$. Thus when both data levels are one, the worst case situation, the upper eye closure will be $P_s + P_i - 2\sqrt{\epsilon}$ for a single interferer. Assuming perfect extinction the lower eye opening is only effected by the contribution of an interfering data '1', giving the worst case lower eye opening as P_i. Thus the worst case minimum eye opening is:

$$\begin{aligned} P_{eye} &= P_s + P_i - 2\sqrt{\epsilon} - P_i \\ &= P_s - 2\sqrt{\epsilon} \end{aligned} \tag{4.8}$$

Giving the total eye closure as $2\sqrt{\epsilon}$.

The Gaussian Approximation

Although the basic statistical nature of optical detection is the Poisson process it has been common practice for a Gaussian probability density to used to approximate the error probability. A Gaussian approximation (GA) involves treating the impairment as if it were characterised by a Gaussian PDF which is defined as:

$$P_g(s) = \frac{1}{\sqrt{2\pi}} e^{-s^2/2} \tag{4.9}$$

Therefore to calculate the error probability, as shown in section 4.4, it is required that we measure the area of the PDF that crosses the decision threshold x.

$$Q'(x) = \frac{1}{\sqrt{2\pi}} \int_x^\infty e^{-s^2/2} ds \tag{4.10}$$

Notice that $Q'(x)$ is the probability of exceeding value x, and is therefore the complementary cumulative density function of the Gaussian distribution. This integral can not be evaluated in closed analytic form so usually it is approximated using the first term of its Taylor expansion which is termed the 'Q' function:

$$Q'(x) \approx Q(x) = \frac{1}{x\sqrt{2\pi}} \exp(-x^2/2) \tag{4.11}$$

This function is related to the mathematical function *erfc* (complementary error function) as follows:

$$\mathrm{erfc}(x) = \frac{2}{\sqrt{\pi}} \int_x^\infty e^{-s^2} ds \approx \frac{e^{-x^2}}{x\sqrt{\pi}} \tag{4.12}$$

$$Q(x) = \frac{1}{2}\mathrm{erfc}\left(\frac{x}{\sqrt{2}}\right) \tag{4.13}$$

This approximation is frequently adopted in view of its simplicity: it makes use of only the minimum of statistical information about the noise and interference, the variance, to obtain a standard approximation of the tail integral. In its simplest form, again assuming perfect extinction, it can be given as:

$$BER \approx \frac{1}{2}\left(Q\left[\frac{P_s - D}{\sigma_1}\right] + Q\left[\frac{D}{\sigma_0}\right]\right) \tag{4.14}$$

In section 4.4.2 we describe how this approximation is formulated for the study of interferometric noise.

4.4.2 Formulation of the Gaussian Approximation

The variance of the beat noise can be shown to be $\sigma_{IN}^2 = 2N\epsilon P_s$ for N interferers each of relative strength ϵ [23], whence:

$$BER \approx \frac{1}{2}\left(Q\left[\frac{P_s - D}{\sqrt{\sigma_n^2 + \sigma_{IN}^2}}\right] + Q\left[\frac{D}{\sigma_n}\right]\right) \tag{4.15}$$

Previous studies have formulated a power penalty from this by adjusting P_s to equate the quality factors (argument of $Q[\bullet]$) of a signal with and without beating [30]. However, in doing this two important implicit assumptions are involved.

First, that the noise on signal 0's may be neglected. Second, that equating the quality factors of corrupted and uncorrupted signals, which simply scales the $Q[\bullet]$ function without changing its form, is a reasonable approximation for the strictly non-Gaussian composite noise plus interference distribution . Both of these may be broadly acceptable for the simplistic case involving small interference signals, however for analysis of more complex systems their validity cannot be taken for granted.

As a refinement, rather than simply using the average value of σ_{IN}^2 we may weight this approximation by means of a binomial expansion to consider all possible signal conditioned combinations of beating terms.

This leads us to the expression:

$$BER \approx \left(\frac{1}{2}\right)^{N+1} . \sum_{k=0}^{N} C_k^N . Q\left[\frac{P_s - D}{\sqrt{\sigma_n^2 + \sigma_{IN_k}^2}}\right] + \left(\frac{1}{2}\right) Q\left[\frac{D}{\sigma_n}\right] \tag{4.16}$$

with D representing the decision threshold

From central limit theorem arguments one would expect that for a large number of independent terms this will provide a good approximation, and as we shall see this is ultimately the case. However, if the constituent PDFs are markedly different from Gaussian the convergence under the central limit theorem can be very slow indeed [39]. Here the PDF of a single incoherent interferer corresponds to an arc-sinusoidal distribution [23, 31, 40]. As this is strictly bounded the Gaussian approximation will be a poor descriptor for this PDF. Even with several such interferers, convergence will be slow, especially in the tails of the distribution - of critical importance for BER considerations [39]. Due to the simple formulation of the GA it is a convenient tool

for a first approximate assessment and can be applied more generally to instances when the central limit theorem can be relied upon. However, as will be shown in section 4.5.1, it has been found to produce inaccurate results in many instances and predicts erroneous trends. Accordingly it should be applied with care, recognising the wisdom and implicit caution in the observation "The central limit theorem is more commonly applied by incantation than by proof!"

The simplest form of the GA used to evaluate the power penalty may be modified for finite extinction ratio, as demonstrated in [41]. The nature of this modification will be discussed further in section 4.5.3

4.4.3 Methods Using 'Full' Statistics

If we require more accurate evaluation of bit error rates than those demonstrated in section 4.4.1, then we need to consider the exact statistics of the signal and noise components, the stochastic element being the sum of the random variables (RV) involved. The summation of independent random variables corresponds to the convolution of the probability density functions of the RVs, which for many of the distributions encountered is a non-trivial operation. A number of papers have demonstrated results formed from the numerical convolution of the PDFs [34, 35] but this has proved to be a computationally time consuming task.

Another solution is to consider the moments of the PDF, which can be utilised in a number of different ways. The simplest form is in reality an extension of the Gaussian approximation as the mean and variance are the first and second moments of the PDF. A number of series expansions have been used, including Gram-Charlier series [42] and Hermitian polynomials [37], which although more detailed still rep-

resent a truncated set of moments. To use the entire set of moments it is possible to take advantage of the properties of the moment generating function (MGF). The most useful property to note is that although the summation of independent RV's is equivalent to the convolution of PDFs, it is equivalent to the multiplication of MGFs [39](p15), which is a much simpler mathematical operation. Evaluation methods making use of the moment generating function e.g. [43, 44] can overcome many of the shortcomings of approximate methods based on limited statistics, albeit sometimes at the expense of increased complexity. The MGF for interferometric noise based on multiple incoherent interferers is readily obtained as demonstrated in section 4.4.4

Moment Generating Functions

Here we introduce the definition of the moment generating function of random variable X as :

$$\psi_X(s) = E[e^{sX}] \tag{4.17}$$

where $E[\bullet]$ denotes the statistical expectation. Care must be taken not to confuse the moment generation function with the characteristic function which is similar in definition [45] but complex.

$$\Phi(\theta) = E[e^{j\theta X}] \tag{4.18}$$

Modified Chernoff Bound

The Modified Chernoff Bound (MCB) may be defined [33] as:

$$P_e \leq \text{MCB} = \frac{M_G(s)}{2s\sigma_n\sqrt{2\pi}}\left[M_{Itot(0)}(s)e^{(-sD)} + M_{Itot(1)}(s)e^{-s(V-D)}\right] \quad ; s > 0 \quad (4.19)$$

This method originally proposed by Prabhu [46] extends the well known Chernoff bound to exploit directly the presence of an additive Gaussian noise component. Equation (4.19) may be minimised, yielding the tightest form of the bound by selecting s appropriately, either as a common s_{opt}, or separately as s_1,s_0 for data 1's and 0's respectively.

Saddlepoint Approximation

The saddlepoint approximation(SPA), defined in [47], adjusted to the study of IN has the form:

$$P_e \approx \frac{1}{2}\left[\frac{\exp[\psi_0(s_0)]}{\sqrt{2\pi\psi_0''(s_0)}} + \frac{\exp[\psi_1(s_1)]}{\sqrt{2\pi\psi_1''(s_1)}}\right] \quad (4.20)$$

$$\text{where} \quad \psi_0(s_0) = \ln[M_G(s_0)M_{Itot(0)}(s_0)] - s_0D - \ln|s_0| \quad (4.21)$$

$$\psi_1(s_1) = \ln[M_G(s_1)M_{Itot(1)}(s_1)] - s_1D - \ln|s_1| \quad (4.22)$$

where D is the normalised decision threshold and s_0, s_1 are determined by the positive and negative roots of $\psi_i'(s) = 0, (i = 0, 1)$ respectively. The error probability is determined by finding the saddlepoint of the contour integral of the complex MGF. The terms given in equation (4.20) are second order terms from the respective Taylor series expansion; greater accuracy can be obtained if higher order terms are included.

Simulation

With the increase of computing power in recent years the use of computer simulation to produce detailed analyses of optical systems is now common. Detailed models of sources, fibre and detectors are used to simulate the received electrical signal. An example of a system constructed in SPW to simulate the effect of beat noise is shown in figure 4.3 . This system models the interferometric beat signal as a

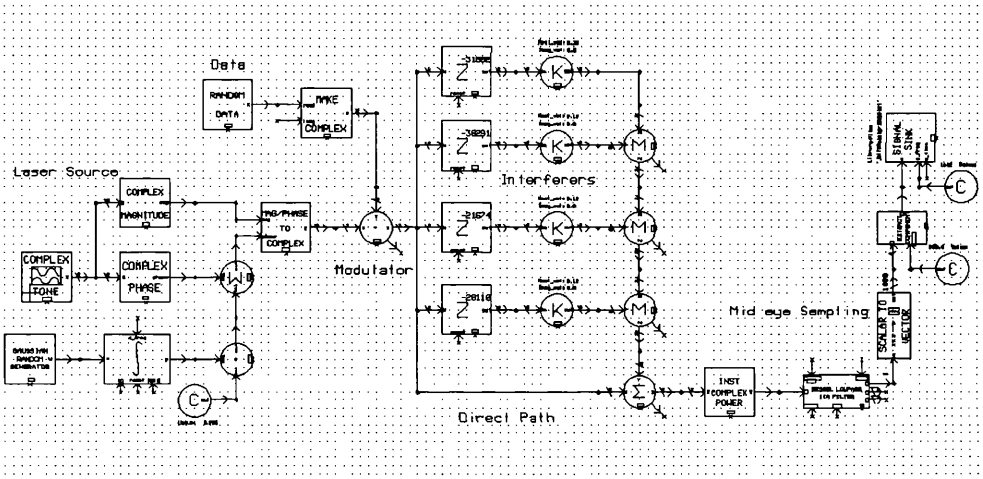

Figure 4.3: The schematic of a system to simulate beat noise

delayed attenuated replica of the original transmitted signal from an optical source with phase noise modelled as a Weiner Levy process. From the data representing the received signal the statistics of the mid-eye level can be sampled, allowing calculation of the system bit error rate, using a quasi-analytic method.

In these simulation models, care must be taken in the selection of the system parameters so that the results are from the same regime as that assumed in the analytic assessment. The linewidth of the laser source is set so that all beat noise terms will fall within the receiver bandwidth, and the delay used to form the interfering terms is significantly greater than the coherence time of the laser.

4.4.4 Formulation of the MGF

To formulate the MGF we consider first a single interferer. We see from equation (4.4) that the beat term is of the form $\alpha \cos \phi$, where ϕ will be uniformly distributed within the region $\pm\pi$. The probability density function for the beat random variable is thus of arc-sine form as shown in section 4.3.4 and the corresponding MGF from (4.17) is given by:

$$M_I(s) = I_0(\alpha s) \tag{4.23}$$

where $I_0(\bullet)$ is the modified Bessel function, first kind zero order and s is the transform variable.

For N independent interferers and substituting $\alpha = 2\sqrt{\epsilon_i}P_s$ the MGF is:

$$M_{IN}(s) = \prod_{i=1}^{N} I_0(2s\sqrt{\epsilon_i}P_s) \tag{4.24}$$

If all interferers are of equal strength (ϵP_s), previously identified as the worst case for a given total interference power [23], then this becomes:

$$M_{IN}(s) = [I_0(2s\sqrt{\epsilon}P_s)]^N \tag{4.25}$$

In order to accommodate additive noise in the receiver we note also that the MGF for a zero mean Gaussian random variable with variance σ_n^2 is given by:

$$M_G(s) = \exp \frac{(s\sigma_n)^2}{2} \tag{4.26}$$

From these terms we can form the MGF for both transmitted 1s and 0s, by taking the product of all contributing MGFs, including if we wish any symbol conditioning. In this context it is appropriate to note that for the case of a single interferer with perfect extinction, beating only occurs when two 1s are present.

Symbol Conditioning of the MGF

We have stated previously that beat noise is symbol conditioned, so an accurate model must include a statistical representation of this occurrence. The beat term is only non-zero when $m_s(t)$ and $m_k(t)$ are both non-zero so we must consider the conditional MGF, averaged over all possible combinations. This involves a binomial expansion and assuming that each term is a '1' half the time (equal *a priori* probabilities for 1s and 0s) we obtain:

$$M_{Itot(1)}(s_1) = \left(\frac{1}{2}\right)^N \sum_{k=0}^{N} C_k^N I_0(2s\sqrt{\epsilon_i}P_s)^k \tag{4.27}$$

The effect of finite extinction ratio is present to some extent in every real system due to constraints in laser diodes and optical modulators. For instance, to obtain high speed operation in directly modulated systems the laser is typically biased just above the threshold level, resulting in the transmission of data '0' not being characterised by a complete absence of light. If the source/modulator has a finite extinction ratio then all combinations of bits will cause a beating component, as data '0' is no longer of zero power. With extinction ratio r we then obtain:

For data '1'

$$M_{Itot(1)}(s) = \left[\frac{I_0(s2\sqrt{r\epsilon}P_s) + I_0(s2\sqrt{\epsilon}P_s)}{2}\right]^N \tag{4.28}$$

For data '0'

$$M_{Itot(0)}(s) = \left[\frac{I_0(sr2\sqrt{\epsilon}P_s) + I_0(s2\sqrt{r\epsilon}P_s)}{2}\right]^N \tag{4.29}$$

4.4.5 Comparison of MGF based Methods

Here we will consider two particular BER assessment techniques making use of the MGF: the saddlepoint approximation [47] and the modified Chernoff bound [33]. The close relationship between these has been shown previously [48]. Section 4.4.3 described these two MGF based evaluation methods which offer increased rigour compared with Gaussian approximation based methods, which are applied here to interferometric noise. To illustrate this let us consider just the simple case of a single interfering term with symbol conditioning and perfect extinction. The full formulation of both the SPA and the MCB are shown in equations (4.30) and (4.31) respectively. There is considerable difference between these in terms of the level of complexity involved in their application.

$$\text{BER} \approx \frac{1}{2}\left[\frac{\frac{\exp[\frac{(s\sigma_n)^2}{2}-sD]}{|s|}}{\sqrt{2\pi\left(\sigma_n^2+\frac{1}{s^2}\right)}}\right.$$
$$\left.+\frac{\frac{\exp[\frac{(s\sigma_n)^2}{2}I_0(2s\sqrt{\epsilon_i}P_s)-sD]}{|s|}}{\sqrt{2\pi\left[4\epsilon P_s^2\left[\frac{I_0(s2\sqrt{\epsilon_i}P_s)+I_2(s2\sqrt{\epsilon_i}P_s)}{2(1+I_0(s2\sqrt{\epsilon_i}P_s))}-\frac{(I_1(s2\sqrt{\epsilon_i}P_s))^2}{(1+I_0(s2\sqrt{\epsilon_i}P_s))^2}\right]\right]+\sigma_n^2+\frac{1}{s^2}}}\right] \quad (4.30)$$

$$P_e \leq \text{MCB} = \frac{\exp\frac{(s\sigma_n)^2}{2}}{2s\sigma_n\sqrt{2\pi}}\left[e^{(-sD)}+\left(\frac{1+I_0(2s\sqrt{\epsilon_i}P_s)}{2}\right)e^{-s(V-D)}\right] \quad ;s>0 \quad (4.31)$$

Firstly we note that the initial formulation of the MCB is easier and much more

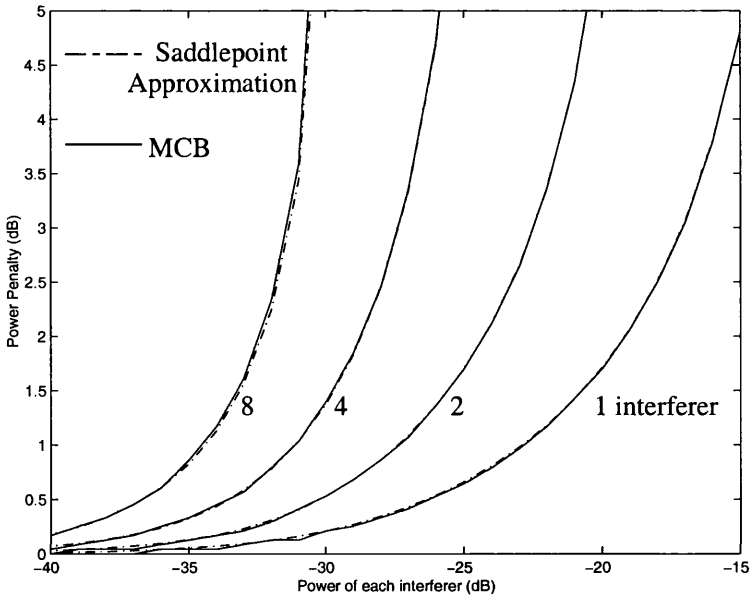

Figure 4.4: Comparison of Bit Error Rate results from MCB (solid) and SPA (dashed)

compact than that of the SPA. Further we note that equation (4.30) for the SPA is very involved compared with equation (4.31) for the MCB considering the relatively simple form of the MGFs being evaluated. The optimising process (selection of 'best'

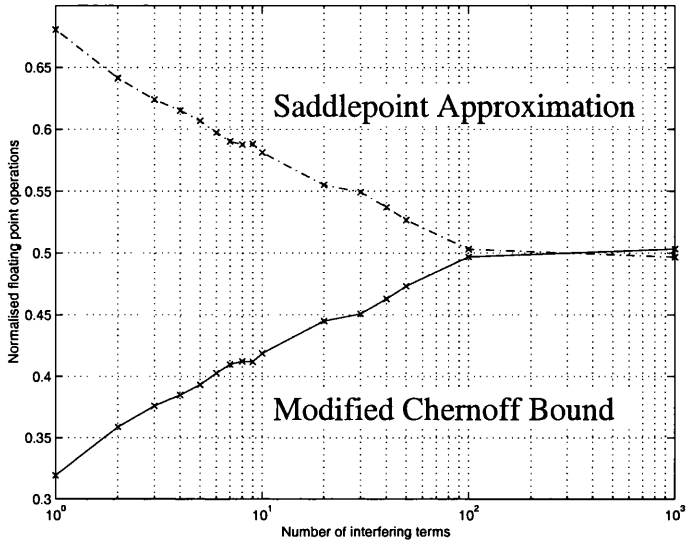

Figure 4.5: Comparison of floating point operations required for MCB (solid) and SPA (dashed)

s value) for both is similar but again the size of the SPA complicates this. Since the formulation of the SPA involves the second differential of (4.21) and (4.22), it is clear that once the full expressions for the moment generating functions are included the result is an expansive, complicated final formulation compared with the simple application of the MCB.

Figure 4.4 shows the results given by each of these techniques for 1,2,4 and 8 interferers. We note that both these MGF-based methods generate virtually identical results. Figure 4.5 clearly shows that in the region of application where the number of significant interferers is such that a rigorous approach is necessary, the MCB significantly out performs the SPA computationally. This consideration, while of only slight impact for a single evaluation, assumes considerable significance in the context of a large scale iterative design. We conclude that the MCB, practically indistinguishable from the SPA, offers markedly the best performance/complexity

trade-off.

4.5 Results and Observations

We now compare performance predictions obtained using three different methods: the Gaussian approximation, the modified Chernoff bound and direct simulation. For these studies we assume a system with a receiver sensitivity such that in the absence of IN the BER is 10^{-9}. From the results provided in figure 4.6 we see that simulation as described in section 4.4.3 indicates a degree of isolation needed for a given bit error rate that agrees closely with the value produced by the MCB. In contrast the Gaussian approximation severely overestimates the required isolation - by as much as 5dB - unless a large number of interferers are contributing. Figure 4.7 shows that the MCB agrees with direct simulation to within $\pm$0.5dB when realistically acceptable and usable power penalties ($<$ 5dB) are considered. For very severe interference the simulation results diverge from the MCB, although this reflects as much on the uncertainty limits of the simulation results in this regime as on the loosening of the bound.

4.5.1 System Performance

In the previous section we confirmed, using simulation, the inadequacy of the Gaussian approximation for a small number of interferers and the applicability of the MCB to the problem of IN. However, it is not as obvious that the inherent inaccuracy in the Gaussian approximation leads to erroneous trends if we consider the effect of interferometric noise as the number of contributing terms in a network

grows. Figure 4.8 shows that for a given total interference power as the number of interferers increases the GA erroneously predicts -counter intuitively- that the power penalty improves [31]. However, a rigorous approach based on the MCB demonstrates that this counter intuitive prediction is incorrect. In actuality for low N the network has a markedly increased tolerance to interferometric noise compared with the GA predictions, but degrades as the number of contributing interferers increases for a given total interfering power. Such a result serves to underscore the deficiency of the GA for studying IN: whilst it does indeed have regions of validity and the advantage of simplicity, extreme care is required if a reliable performance estimate is to be obtained.

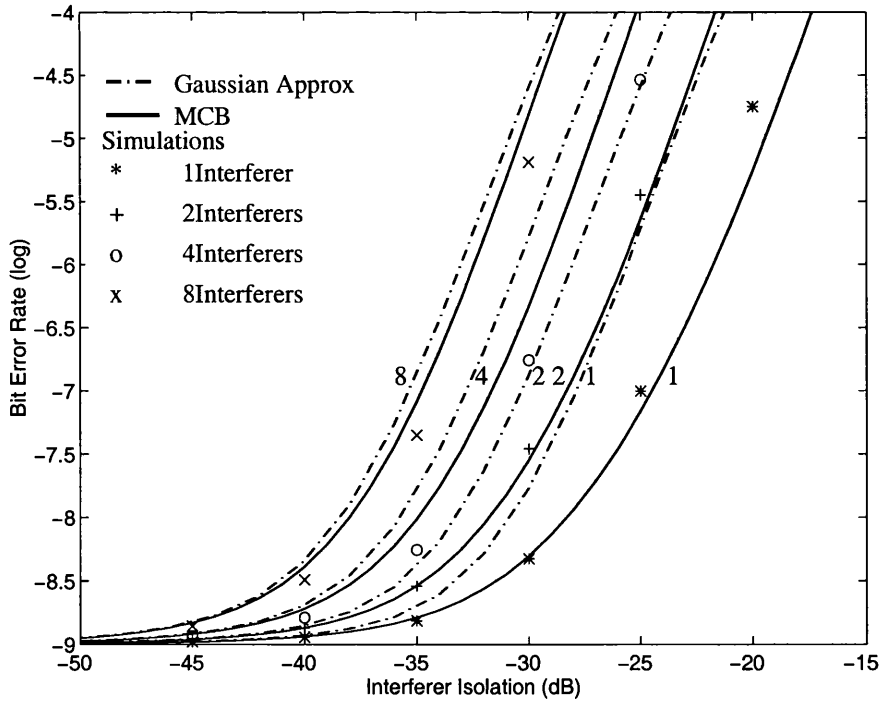

Figure 4.6: BER against crosstalk isolation given by Gaussian approximation, MCB and simulation

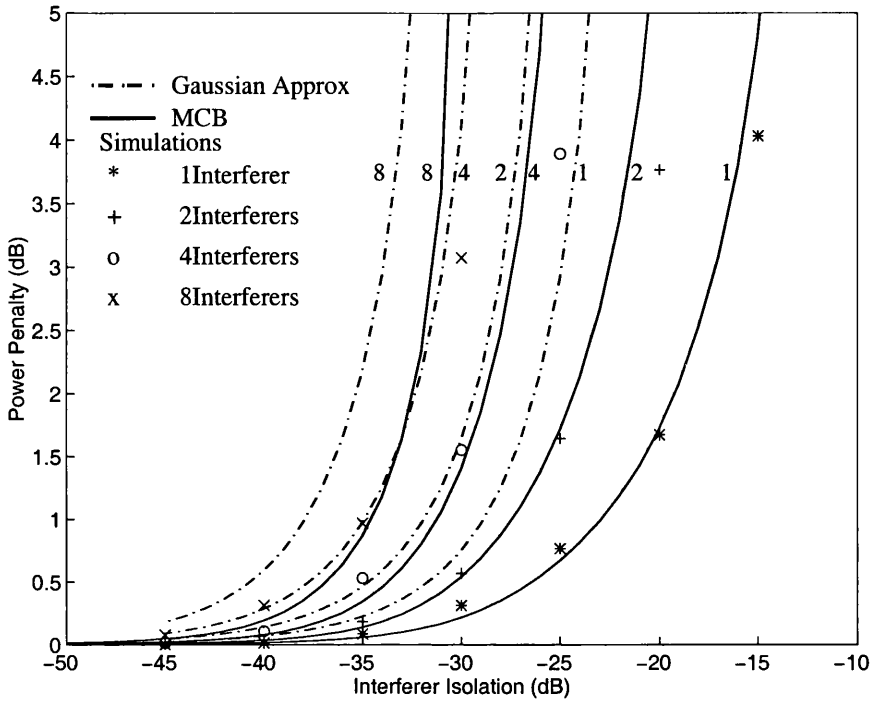

Figure 4.7: Power penalty against crosstalk isolation given by Gaussian approximation, MCB and simulation

4.5.2 Crosstalk-Crosstalk beating

Until this point we have restricted consideration to the terms formed by the beating between the 'wanted' signal and each interferering term. However, each interfering term will also beat with every other interfering term to create crosstalk-crosstalk beating. This is usually dismissed as likely to be negligible but given the limitations and deficiencies we have demonstrated for 'established' performance assessment techniques such as the GA, it is appropriate that we use our more accurate MCB technique to validate this assumption. From equation (4.4) it is noted that the crosstalk-crosstalk beating term can be considered to be of the same general form as the signal-crosstalk beating, i.e. $\alpha \cos\phi$, with $\alpha = 2\sqrt{\epsilon_k \epsilon_j}$ for the C.W. case.

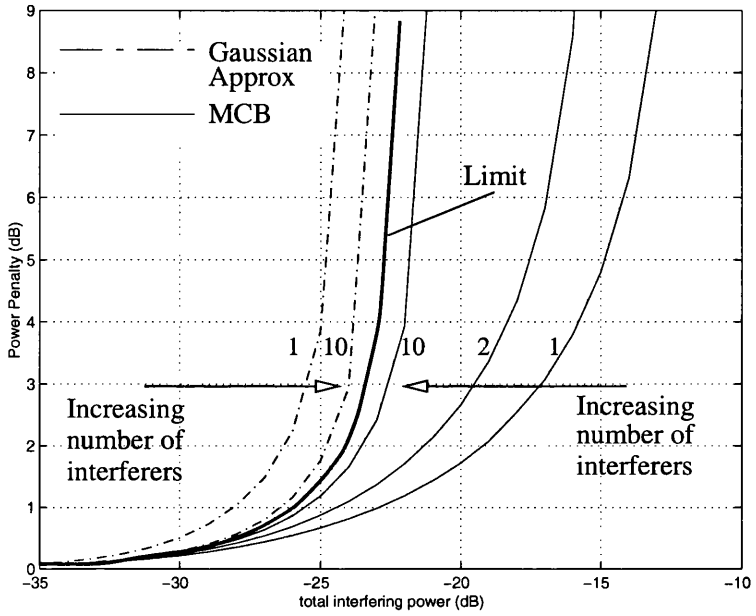

Figure 4.8: Power penalty for an increasing number of interferers with constant total power. GA, MCB

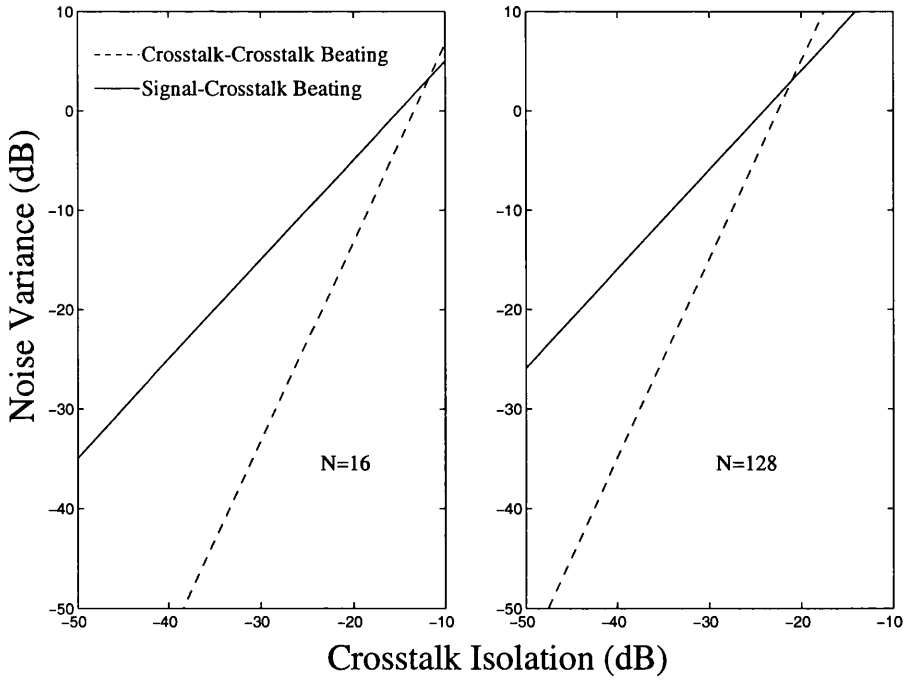

Figure 4.9: Comparison of noise variance for signal-crosstalk and crosstalk-crosstalk beating

The crosstalk-crosstalk variance is thus given by:

$$\sigma^2_{xxtot}(s) = \epsilon^2 P_s^2 N(N-1) \tag{4.32}$$

If we consider first just how the signal variance is affected by the inclusion of crosstalk-crosstalk beating, we produce using similar methods to [30] the results of figure 4.9, suggesting that as the number of interferers increases crosstalk-crosstalk beating may become dominant for high crosstalk levels. Let us now form the moment generating function. Again beating only occurs between data '1's and therefore symbol conditioning must be introduced. If all interfering terms are considered equal the MGF takes the form:

$$M_{xx}(s) = \left(\frac{1}{2}\right)^N \sum_{k=0}^{N} \mathrm{C}_k^N I_0(s2\epsilon P_s)^{\frac{k(k-1)}{2}} \tag{4.33}$$

However, as the presence of beat noise, which is highly non-Gaussian, has a strong impact on the operating point on the non-linear BER versus signal characteristic it is inappropriate simply to compare the noise level or variance of crosstalk-crosstalk beating with that of signal crosstalk beating as they will always occur simultaneously. Accordingly in this analysis we assess the bit error rate degradation induced due to the contribution of this form of crosstalk-crosstalk noise. We see from figure 4.10 that even though the overall effect of crosstalk-crosstalk beating increases with the number of interferers it is still negligible in terms of its impact on BER, the relevant system performance parameter. Even for 128 equal interfering terms the deviation from the BER without crosstalk-crosstalk beating is only 3% - even for the individual

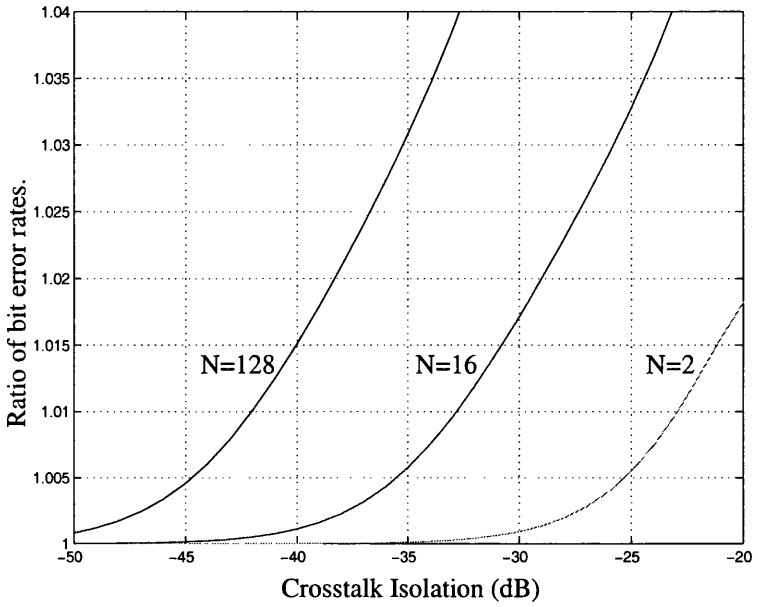

Figure 4.10: Ratio of bit error rate, with/without crosstalk-crosstalk beating, calculated by the MCB

crosstalk level of -35dB. This provides confirmation, based on a rigorous assessment model, that crosstalk-crosstalk beating at virtually all levels has negligible impact on system performance.

4.5.3 Finite Extinction Ratio

Laser biasing or modulator extinction constraints will inevitably cause a finite extinction ratio in practical optical systems. 'Traditional' evaluation methods consider this as a simple degradation of the eye opening by including a factor of $(1-r)/(1+r)$ in the Q value, while systems corrupted by IN will, in addition, have terms due to the signal-crosstalk beating. In a model with all components having perfect extinction it is assumed that a data '0' is symbolised by a complete absence of light, so therefore no beating will occur if either signal or crosstalk is data '0'. Now we must consider that data '0' is represented by a signal power of rP_s, allowing the beating

between the signal and each interferer to be governed by one of four possible RVs dependent on the symbol conditions. The variance and MGFs of the data components are given in table 4.2 We compare two evaluation methods, the first being

Signal	Interferer	Variance	MGF
1	1	$2P_s^2 k\epsilon_i$	$I_0(s2\sqrt{\epsilon_i}P_s)$
1	0	$2P_s^2 rk\epsilon_i$	$I_0(s2\sqrt{r\epsilon_i}P_s)$
0	1	$2P_s^2 rk\epsilon_i$	$I_0(s2\sqrt{r\epsilon_i}P_s)$
0	0	$2P_s^2 r^2 k\epsilon_i$	$I_0(sr2\sqrt{\epsilon_i}P_s)$

Table 4.2: Noise Variance and MGFs of interferometric noise with finite extinction ratio

the Gaussian approximation with non-optimised decision threshold extended from (4.16) to give:

$$BER \approx \frac{1}{2}Q\left[\frac{i_p - D}{\sqrt{\sigma_n^2 + \sigma_{IN1}^2}}\right] + \frac{1}{2}Q\left[\frac{D - ri_p}{\sqrt{\sigma_n^2 + \sigma_{IN0}^2}}\right] \tag{4.34}$$

and the modified Chernoff bound (MCB) defined in section 4.4.3:

$$P_e \leq \frac{M_G(s)}{2s\sigma_n\sqrt{2\pi}}\left[M_{I(0)}(s)e^{(-sD)} + M_{I(1)}(s)e^{-s(i_p - D)}\right] \quad ; s > 0 \tag{4.35}$$

where D represents the decision threshold, σ_n^2 is the thermal noise variance, with σ_{IN1}^2 and σ_{IN0}^2 being the beat noise variance for signal '1's and '0's respectively. The performance degradation is evaluated at various extinction ratios including $-8dB$ (ITU-T Recommendation G.957(7/95)). We investigate the claim of previous work using the GA with an optimised decision threshold that has suggested that the inclusion of a finite extinction ratio affects the maximum tolerable crosstalk level [49]. The calculation using the MCB, using an average power decision threshold, as shown

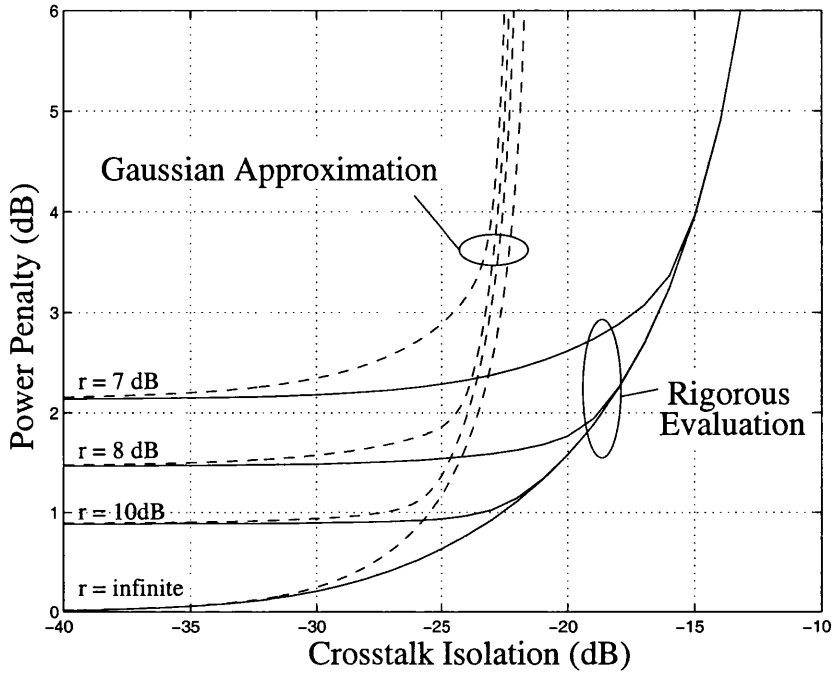

Figure 4.11: Power Penalty against crosstalk isolation calculated using a Gaussian approximation and the modified Chernoff bound.

in figure 4.11, demonstrates that finite extinction ratio inherently causes eye closure, as can be seen by the marked power penalty floor in keeping with established theory [50]. However, we find now that there is a single crosstalk limit regardless of extinction ratio. From this we deduce that even though additional beating terms are introduced by finite extinction ratio, the beating of the two data '1's still dominates in the tails, determining the error probability, while the GA again suggests, erroneously that crosstalk limits are dependent on extinction ratio. To illustrate this observation further, figure 4.12 demonstrates the crosstalk isolation required for a 1dB power penalty (above that inherently due to finite extinction), calculated using both the inadequate GA and the accurate MCB. The actual isolation required is shown by the MCB to be -22.9 dB, irrespective of extinction ratio, for all realistic extinction values. Assessment using the GA indicates a more severe requirement of

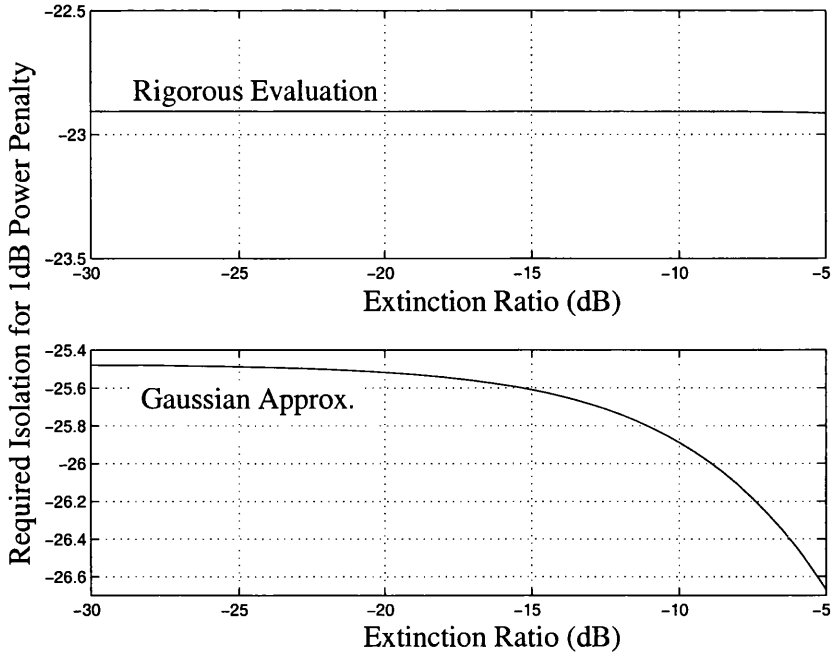

Figure 4.12: Crosstalk isolation required for a 1dB power penalty vs extinction ratio, calculated used the MCB (top) and Gaussian Approximation (bottom).

between -25.4dB and -26.7dB dependent on the extinction ratio. This establishes that the dependency on extinction ratio predicted by the GA is due to the inaccuracies of the model rather than any statistical phenomenon of interferometric beat noise.

4.5.4 Interferers of unequal power

In this section the impact on the level of interferometric beating witnessed in a system with unequal interfering power is studied. It has been stated that only a few crosstalk terms are necessary before the Gaussian approximation is good, although previously we have suggested that this may not be the case due the symbol conditioned nature of interferometric noise. Furthermore, we conjecture that if the interfering terms falling on the photodiode are not of equal power then the statistics

may be far from Gaussian even if a large number of interferers contribute. As the use of optical cross connects (OXC) and other optical routing components increases, it is probable that a large number of different components will contribute to the crosstalk in the signal path, making it unlikely that all interfering signals will be of comparable strength.

Let us consider what may be thought of when the central limit theorem is cited as justification of the Gaussian approximation.

> "If random variable x is in fact a linear sum of n statistically independent constituent variables ... then no matter what probability density functions the constituent variables may have, the probability density function (of the sum) .. will approach the normal form.. as n approaches infinity"
>
> p35 'Engineering Applications of Correlation and Spectral Analysis'
> J.S. Bendal and A.G. Piersol

Often this is taken as justification that if n is large (some have deemed this to start being valid at n=8) then the Gaussian approximation can be used with confidence. However, given the previously demonstrated limitations it is far from obvious that this is correct. Figure 4.13 shows the convolution of Gaussian and arc-sine PDFs, illustrating the transition witnessed as Gaussian noise becomes dominant. We investigate altering the relative strengths and number of interferers contributing to system noise. To effect this let us multiply the interfering power by a scaling factor:

$$\alpha(n) = \frac{n^k}{c} \quad ; \quad c = \sum_{n=1}^{N} n^k \tag{4.36}$$

where n is the number of the interferer $n = 1 \ldots N$, k controls the relative scaling

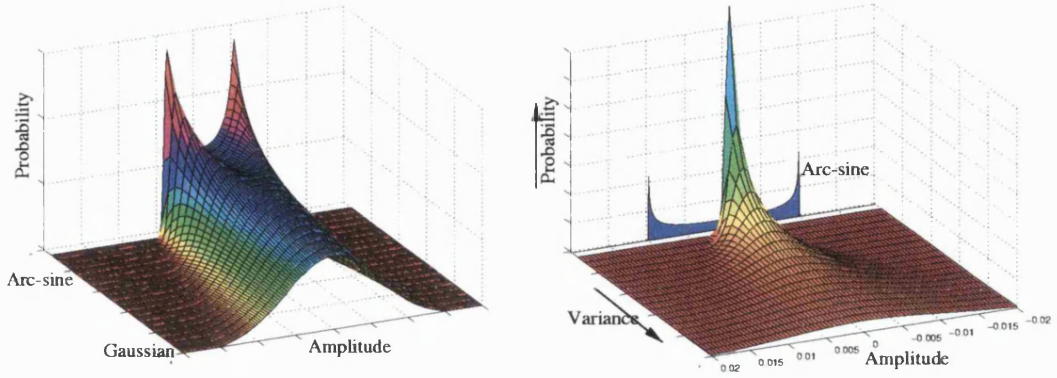

(a) PDF Transition (b) Relative Strengths

Figure 4.13: The transition of the PDF as Gaussian Noise becomes dominant, with (right) the relative interferer strengths

between interferers, and c is a factor to keep the total power constant. To illustrate

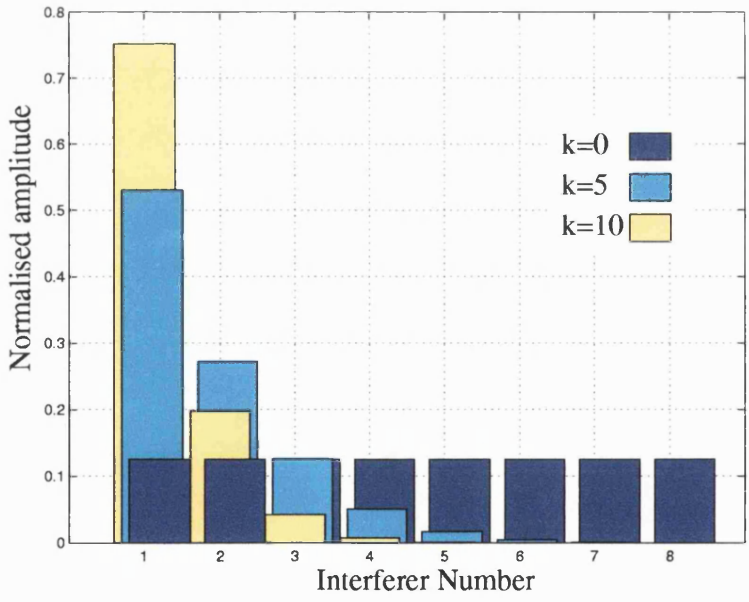

Figure 4.14: Relative interfering power for k=0,5,10

the function of this factor, figure 4.14 shows the relative strengths of 8 interferers for $k = 0$, $k = 5$ and $k = 10$, demonstrating that as the k factor increases the relative power level skews towards one interferer being dominant. To our knowledge all

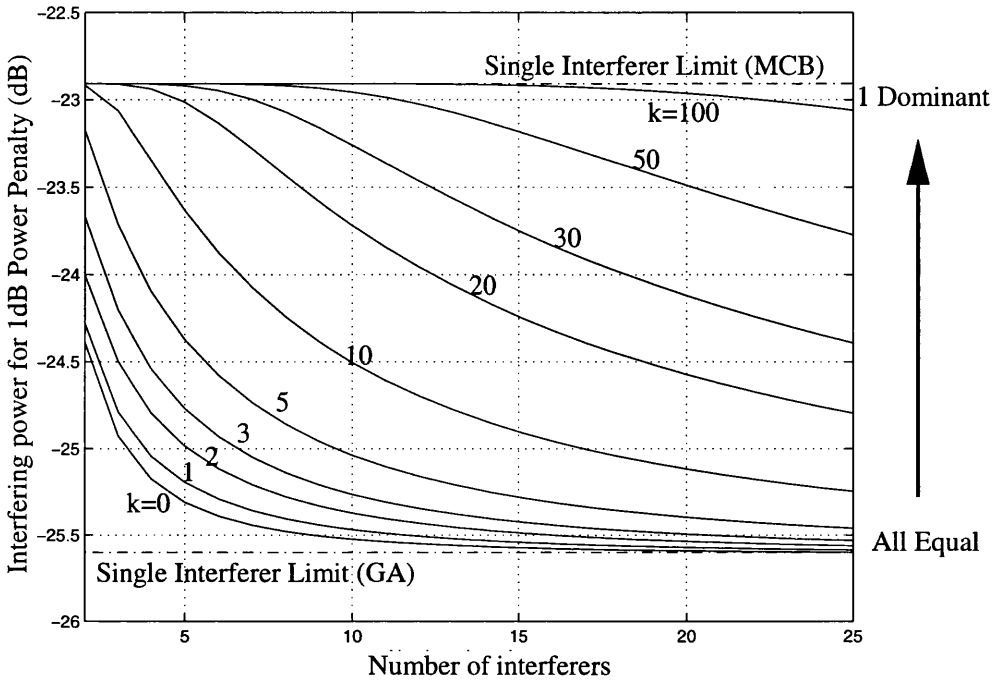

Figure 4.15: Total crosstalk power required for a 1dB power penalty with relation to number of interfering terms and the distribution of interferer power.

studies to date have only considered the situation corresponding to k=0, i.e. when all interferers are equal. We observe from figure 4.15 that the relative strengths of the interferers has a marked impact on the overall power penalty and is as important as the number of interfering terms in determining performance. From figure 4.15 we see that if the relative strengths of the contributing interferers varies markedly, even if a large number contribute to the overall system noise, then in contradiction to some assertions of the central limit theorem, Gaussian statistics may not be adequate. We see that regardless of how many interferers contribute, a system power penalty of $<$ 1dB is assured if the total power in all interferers is < -25.65dB below the signal power what ever the distribution. However, if only a small number of interferers dominate the statistics then it is possible that the system is afforded $\approx$ 3dB of extra crosstalk tolerance compared to that which a Gaussian model would predict.

This demonstrates theoretical limits of total crosstalk power between which a 1dB power penalty will occur regardless of the statistical nature of the contributing crosstalk, i.e. irrespective of the number of contributing interferers. In future all-optically switched networks, the number of contributing terms will depend greatly on the configuration of the network at a particular time instance. This work provides a sound basis for being able to predict the tolerance of such a system if appropriate control on the total interfering power can be enforced.

This leads us to conclude that for such situations perhaps a slightly different statement of the central limit theorem should noted:

> "If a large number n of independent random variables be added or averaged in such a way that the total variance is finite and non-zero, *with no one contribution dominating* than as n increases the sum distribution tends towards Gaussian form."
>
> p20 'Problems of Randomness in Communications
> K.W. Cattermole and J.J. O'Reilly

4.6 An Optical Network Example

In this section we illustrate the application of the model developed in the previous sections to a specific form of network node. The node type used is that proposed in the Multi-Wavelength Transport Network project (MWTN) [12] which considers a 4 wavelength node consisting of 4×4 InGaAs/InP switches as shown in figure 4.16. This form of network node has been widely accepted as a generic block for network design [51, 52].

It has been shown that the number of interferers per node is dependent on the exact node structure and the origins of the signal entering and leaving the node. We

examine here nodes with either power combiners or wavelength multiplexers at the output. Wavelength multiplexers have the advantage of filtering a greater number of crosstalk terms but at the expense of added complexity and potential cost. We consider signals that are sourced at the node, pass through the node and those terminated at the node, the number of contributing terms for each being as shown in table 4.3. It is assumed that all crosstalk terms are either from distinct sources or become incoherent due to differences in effective path length.

Two components in the node contribute to the total leakage, the wavelength demultiplexer (DeMUX) and the space switch. Previous studies have usually considered nodes in which both lossy components have equal crosstalk isolation, the results of which can be see in figure 4.17. Here, we believe for the first time, we also consider how unequal losses affect the system and our results take into account binary data modulated on both signal and interfering terms.

Output Type	Signal Type	1st Order	2nd Order
Power Combiners	Sourced	6	36
	Pass	5	27
	Terminate	3	10
Wavelength multiplexer	Sourced	3	11
	Pass	3	8
	Terminate	3	6

Table 4.3: Number of first and second order interfering terms created per node.

Figure 4.18 considers a node where the output signal examined emanates from that node, resulting in 3 crosstalk terms due to the switch and 3 due to the DeMUX. Clearly, with an equal number of terms a symmetrical plot results. There are a range of isolation values that will give equal performance allowing for more tolerance to one device or the other which may facilitate the use of a lower cost/sophistication

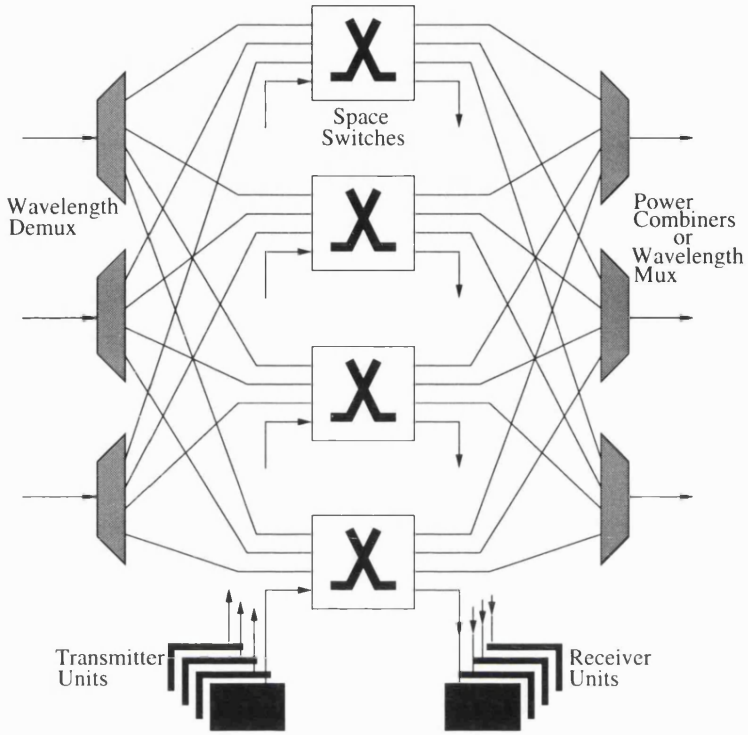

Figure 4.16: Intermediate MWTN node

technology for either the DeMUX or switches. The effect of differing interferer power is increasingly marked if switch and DeMUX create an unequal number of terms, as shown in figure 4.19. This considers a signal that is passed from input to output by the node thereby being corrupted by 3 terms due to the switch but only 2 due to the DeMUX. Once again we observe quite a wide range of tolerance. It is worth noting that at crosstalk levels less than 30dB the power of the dominant interferer controls the power penalty within a few tenths of a dB until the secondary interference level is within $\approx 5dB$. We may extend our consideration to a number of nodes: figure 4.20 illustrates how the power penalty evolves if the signal is passed through a chain of network nodes.

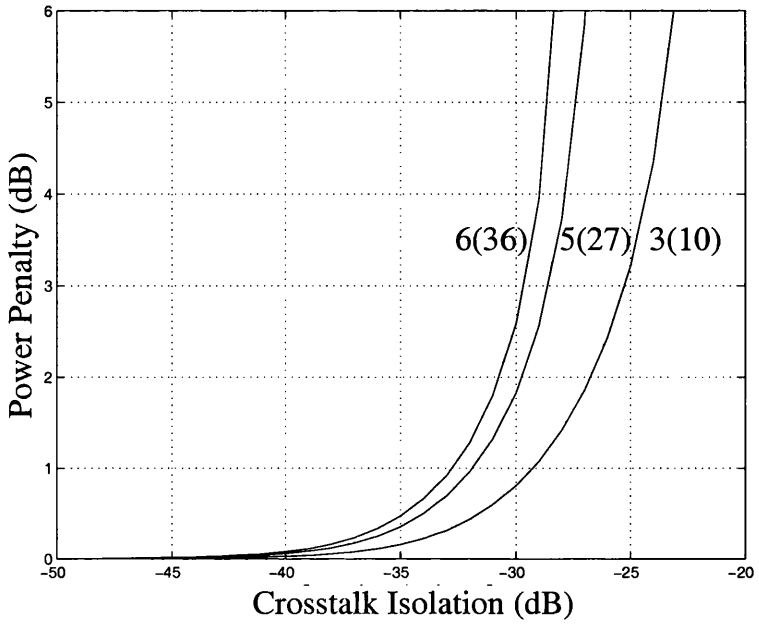

Figure 4.17: Variation of power penalty with crosstalk isolation. Annotation denotes number of first order interferers, and number of second order interferers bracketed

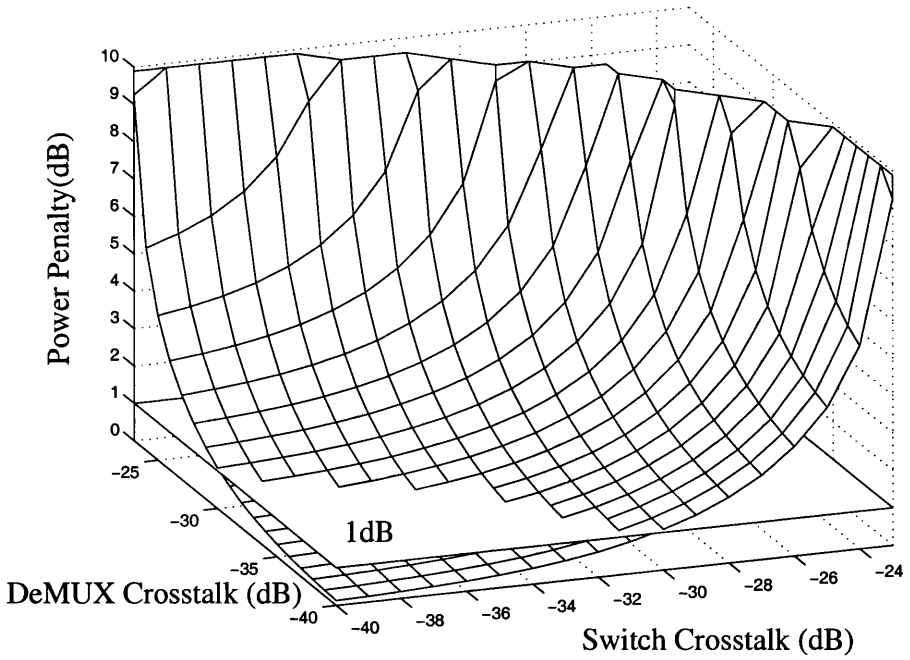

Figure 4.18: Variation of power penalty with crosstalk isolation. 3 crosstalk terms due to the DeMUX and 3 due to the space switch

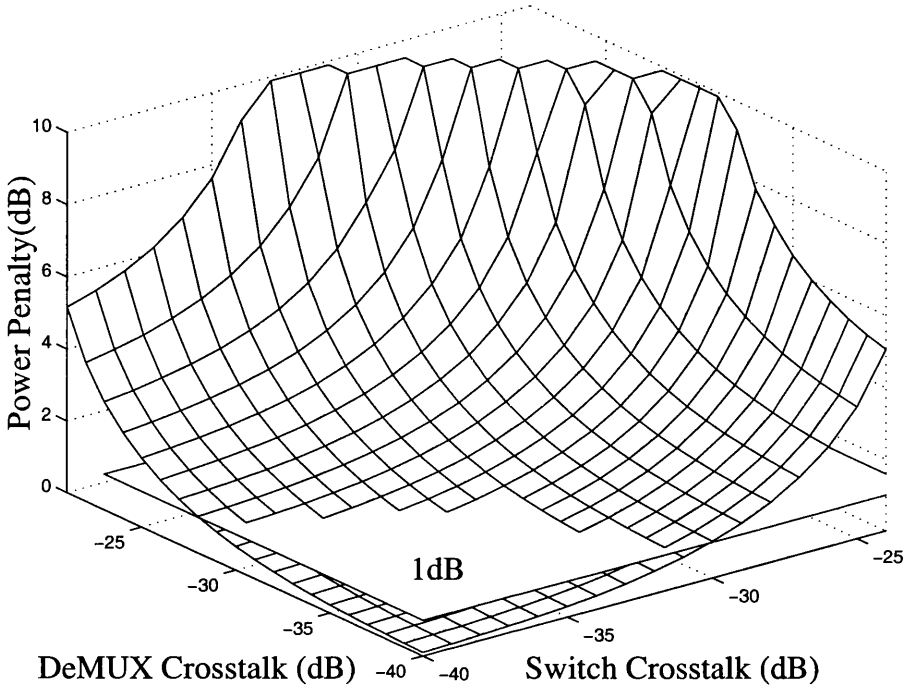

Figure 4.19: Variation of power penalty with crosstalk isolation. 2 crosstalk terms due to the DeMUX and 3 due to the space switch

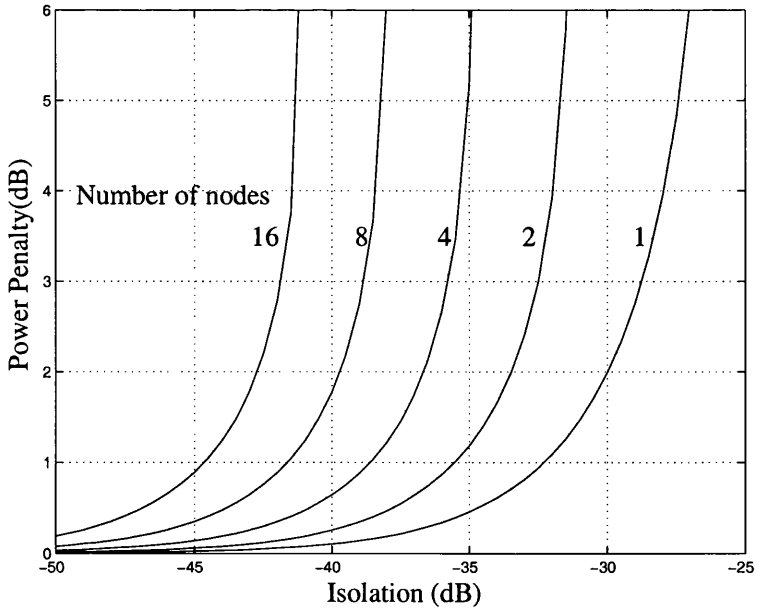

Figure 4.20: Evolution of power penalty with number of nodes passed

4.7 Quadrature Amplitude Modulation.

As discussed previously in section 3.3.3 QAM provides a method of signal bandwidth reduction which has been considered for applications in a number of different scenarios. In this section we first formulate the effect of interferometric crosstalk on optical carrier signals modulated with QAM data. This is then extended to consider the effect this crosstalk has on the hybrid fibre radio systems discussed in section 3.3, the analysis of which is complicated by the frequency doubling method of mm wave frequency generation employed.

4.7.1 Formulation of QAM

The QAM signal $m(t)$ used to modulate the optical carrier is defined as:

$$m(t) = E_r[a(t)\sin(\omega_{rf}t) + b(t)\cos(\omega_{rf}t)] \tag{4.37}$$

where E_r is the amplitude of the modulation signal, $a(t), b(t)$ are the two multi-level data streams, $a(t), b(t) \in \{-3, -1, 1, 3\}$ for 16 QAM. If m(t) modulates an optical carrier from a laser source described by:

$$E_L(t) = \sqrt{P_o}e^{j(\omega_o t + \phi_o(t))} \tag{4.38}$$

where P_o the optical power, ω_o and $\phi_o(t)$ are the optical frequency and phase respectively. The modulated optical field is:

$$E(t) = \sqrt{P_o}\big(1 + ma(t)\sin(\omega_{rf}) + mb(t)\cos(\omega_{rf})\big)e^{j(\omega_o t + \phi_o(t))} \tag{4.39}$$

If we now consider an interfering signal created by an identical transmitter, certain parameters will be equal, however the carrier phases and the transmitted data will be uncorrelated, giving:

$$E_i(t) = \mathbf{Re}\Big|\sqrt{P_i}\,[1 + ma_i(t)\sin(\omega_{rf}t + \theta) + mb_i(t)\cos(\omega_{rf}t + \theta)]\,e^{j(\omega_o t + \phi_i(t))}\Big| \tag{4.40}$$

where i denotes an interfering signal. Therefore at the photodiode the optical field is :

$$\begin{aligned} E(t) = \mathbf{Re}\Big|&\sqrt{P_o}\,[1 + ma(t)\sin(\omega_{rf}t) + mb(t)\cos(\omega_{rf}t)]\,e^{j(\omega_o t + \phi_o(t))} \\ &+\sqrt{P_i}\,[1 + ma_i(t)\sin(\omega_{rf}t + \theta) + mb_i(t)\cos(\omega_{rf}t + \theta)]\,e^{j(\omega_o t + \phi_i(t))}\Big| \end{aligned} \tag{4.41}$$

Photodetection by a square law photodiode produces the photocurrent:

$$\begin{aligned} i(t) &= E(t)E(t)^* \\ &= P_o[1 + ma(t)\sin(\omega_{rf}t) + mb(t)\cos(\omega_{rf}t)]^2 \\ &+ P_i[1 + ma_i(t)\sin(\omega_{rf}t + \theta) + mb_i(t)\cos(\omega_{rf}t + \theta)]^2 \\ &+ 2\sqrt{P_o P_i}\Big(1 + ma(t)\sin(\omega_{rf}t) + mb(t)\cos(\omega_{rf}t)\Big) \\ &\cdot \Big(1 + ma_i(t)\sin(\omega_{rf}t + \theta) + b_i(t)\cos(\omega_{rf}t + \theta)\Big).\cos[\phi_o(t) - \phi_i(t)] \end{aligned} \tag{4.42}$$

We define $\phi_d(t) = \phi_o(t) - \phi_i(t)$ and $\epsilon = P_i/P_o$. After bandpass filtering this gives:

$$\begin{aligned} i(t) = 2mP_o\Big[&a(t)\sin(\omega_{rf}t) + b(t)\cos(\omega_{rf}t) \\ &+ \epsilon\Big(a_i(t)\sin(\omega_{rf}t+\theta) + b_i(t)\cos(\omega_{rf}t+\theta)\Big) \\ &+ \sqrt{\epsilon}.\cos[\phi_d(t)][a(t)\sin(\omega_{rf}t) + b(t)\cos(\omega_{rf}t) \\ &+ a_i(t)\sin(\omega_{rf}t+\theta) + b_i(t)\cos(\omega_{rf}t+\theta)]\Big] \end{aligned} \tag{4.43}$$

The i and q channels are demodulated by applying sine and cosine signals - phase locked to the received signal. Assume that there is a given phase error of ψ, the demodulating signals are:

$$r_i(t) = V_r\cos(\omega_{rf}t + \psi) \tag{4.44}$$

$$r_q(t) = V_r\sin(\omega_{rf}t + \psi) \tag{4.45}$$

The i channel after low pass filtering is :

$$\begin{aligned} i_i(t) = P_o m V_r\Big[&a(t)\sin(\psi) + b(t)\cos(\psi) + \epsilon\big[a_i(t)\sin(\theta-\psi) + b_i(t)\cos(\theta-\psi)\big] \\ &+\sqrt{\epsilon}\cos(\phi_d(t))\big(a(t)\sin(\psi) + b(t)cos(\psi) + a_i(t)\sin(\theta-\psi) + b_i(t)\cos(\theta-\psi)\big)\Big] \end{aligned} \tag{4.46}$$

The q channel after low pass filtering is :

$$\begin{aligned} i_i(t) = P_o m V_r\Big[&a(t)\cos(\psi) + b(t)\sin(\psi) + \epsilon\big(a_i(t)\cos(\theta-\psi) + b_i(t)\sin(\theta-\psi)\big) \\ &+\sqrt{\epsilon}\sin(\phi_d(t))\big[a(t)\cos(\psi) + b(t)\sin(\psi) + a_i(t)\cos(\theta-\psi) + b_i(t)\sin(\theta-\psi)\big]\Big] \end{aligned} \tag{4.47}$$

Assuming perfect phase locking i.e. $\psi = 0$:

$$i_{signal} = mV_r P_o b(t) \tag{4.48}$$

$$q_{signal} = mV_r P_o a(t) \tag{4.49}$$

$$i_{noise} = mV_r P_o \Big[\epsilon\big(a_i(t)\sin(\theta) + b_i\cos(\theta)\big) + \sqrt{\epsilon}\cos[\phi_d(t)]\big[b(t) + a_i(t)\sin(\theta) + b_i(t)\cos(\theta)\big]\Big] \tag{4.50}$$

$$q_{noise} = mV_r P_o \Big[\epsilon\big(a_i(t)\cos(\theta) + b_i\sin(\theta)\big) + \sqrt{\epsilon}\cos[\phi_d(t)]\big[a(t) + a_i(t)\cos(\theta) + b_i(t)\sin(\theta)\big]\Big] \tag{4.51}$$

As with interferometric noise in ASK systems, the received noise component can again be seen to comprise of a linear contribution and a beat contribution.

We define the interferometric contribution for the i and q channels as:

$$i_{beat} = mV_r P_o \Big[\sqrt{\epsilon}\cos[\phi_d(t)]\big[b(t) + a_i(t)\sin(\theta) + b_i(t)\cos(\theta)\big]\Big] \tag{4.52}$$

$$q_{beat} = mV_r P_o \Big[\sqrt{\epsilon}\cos[\phi_d(t)]\big[a(t) + a_i(t)\cos(\theta) + b_i(t)\sin(\theta)\big]\Big] \tag{4.53}$$

These terms will be used to formulate the MGF in section 4.7.3

4.7.2 QAM in HFR systems

This section describes the analysis of IN generation in a system employing coherent mixing of two optical carriers to produce an intermediate carrier frequency to transport QAM signals. This coherent mixing method has been presented in section 3.3.1, where figure 3.1 is a schematic diagram of a mm-wave delivery system. We start this analysis by assuming that the optical field at the output of the laser diode

can be described as :

$$E_L(t) = \sqrt{P_o} e^{j(\omega_o t + \phi_o(t))} \tag{4.54}$$

where P_o is the optical power, and ω_o and ϕ_o are the optical frequency and phase respectively. As shown previously, a mm wave subcarrier is produced by the coherent mixing of two optical signals separated by the desired mm wave frequency. These carriers are created by driving a Mach-Zehnder modulator at $\omega_{mm}/2$, using 'off-quadrature' biasing to create carrier suppression. This creates an optical signal $E_{mm}(t)$ of:

$$E_{mm}(t) = \sqrt{P_o} e^{j(\omega_o \pm \frac{\omega_{mm}}{2} t + \phi_o(t))} \tag{4.55}$$

These two carriers are then separated using optical filtering and the modulation signal $m(t)$ is imposed upon one of them.

$$m(t) = E_r[a(t)\sin(\omega_{rf} t) + b(t)\cos(\omega_{rf} t)] \tag{4.56}$$

where $a(t), b(t)$ are the data streams defined as $a(t), b(t) \in \{\pm 1, \pm 3, ...\pm(2N-1)\}$ for $2N^2$ QAM, and ω_{rf} is the electrical carrier frequency. Defining m as the modulation depth $m = E_r/E_o$, the optical signal is described as:

$$\begin{aligned} E_s = & \sqrt{P_o} e^{j[(\omega_o - \frac{\omega_{mm}}{2})t + \phi_o(t)]} \\ & + \sqrt{P_o} m[1 + a(t)\sin(\omega_{rf} t) + b(t)\cos(\omega_{rf} t)] e^{j[(\omega_o + \frac{\omega_{mm}}{2})t + \phi_o(t)]} \end{aligned} \tag{4.57}$$

Assuming that an interfering signal is produced by an identical process the signal impinging on the photodetector is given by:

$$\begin{aligned} E_{total} &= \sqrt{P_o} e^{j[(\omega_o - \frac{\omega_{mm}}{2})t + \phi_o(t)]} \\ &+ \sqrt{P_o} m[1 + a(t)\sin(\omega_{rf}t) + b(t)\cos(\omega_{rf}t)] e^{j(\omega_o + \frac{\omega_{mm}}{2}t + \phi_o(t))} \\ &+ \sqrt{P_i} e^{j(\omega_o - \frac{\omega_{mm}}{2}t + \phi_i(t))} \\ &+ \sqrt{P_i} m[1 + a_i(t)\sin(\omega_{rf}t + \theta) + b_i(t)\cos(\omega_{rf}t + \theta)] e^{j[(\omega_o + \frac{\omega_{mm}}{2})t + \phi_i(t)]} \end{aligned} \quad (4.58)$$

where i as a subscript denotes the interfering signal. In equation (4.58) the first term is the unmodulated optical carrier, the second is the QAM modulated carrier. The third and fourth terms arise from the interfering signal, with the third term being the unmodulated interferer and the fourth being the modulated interferer. We assume that this signal falls upon an optical receiver with normalised responsivity, so that the photocurrent that results is the square of this signal

$$i(t) = |E_{total}(t)|^2 \equiv E_{total}(t).E_{total}(t)^* \quad (4.59)$$

where * denotes the complex conjugate. Expanding $i(t)$ gives the following signal and crosstalk terms:

1) dc terms.

$$\begin{aligned} i_{dc} = P_o[1 + \epsilon + \frac{m^2 a(t)}{2} + \frac{m^2 b(t)}{2} + \frac{\epsilon m^2 a_i(t)}{2} + \frac{m^2 b_i(t)}{2} \\ +2\sqrt{\epsilon}\cos(\phi_d) + m^2 a(t)a_i(t)\cos(\theta) + m^2 a(t)b_i(t)\sin(\theta) + m^2 b(t)a_i(t)\sin(\theta) \end{aligned} \quad (4.60)$$

2) Signal Terms

$$i_{sig} = P_o[2\cos(\omega_{mm}t)\big(1 + ma(t)\sin(\omega_{rf}t) + mb(t)\cos(\omega_{rf}t)\big)$$
$$+2\epsilon\cos(\omega_{mm}t)\big(1 + ma_i(t)\sin(\omega_{rf}t+\theta) + mb_i(t)\cos(\omega_{rf}t+\theta)\big)] \quad (4.61)$$

3) In-band Crosstalk terms

$$i_{xtalk} = P_o\Big[2\epsilon\cos(\omega_{mm}+\phi_d)\big[2 + ma(t)\sin(\omega_{rf}t) + mb(t)\cos(\omega_{rf}t)$$
$$+ma_i(t)\sin(\omega_{rf}t+\theta) + mb_i(t)\cos(\omega_{rf}t+\theta)\Big] \quad (4.62)$$

4) Out of band Crosstalk terms

$$\begin{aligned} i_{noise} = P_o\Big[&2ma_i(t)\sin(\omega_{rf}t+\theta) + 2mb_i(t)\cos(\omega_{rf}t+\theta) + 2ma(t)\sin(\omega_{rf}t) \\ &+ 2mb(t)\cos(\omega_{rf}t) + \Big(\frac{m^2a(t)}{2} + m^2a(t)b(t)\Big)\sin(2\omega_{rf}t) + \frac{m^2b(t)}{2}\cos(2\omega_{rf}t) \\ &+ \Big(\frac{\epsilon m^2a_i(t)}{2} + 2m^2a_i(t)b_i(t)\Big)\sin(2\omega_{rf}t+2\theta) + \frac{\epsilon m^2b_i(t)}{2}\cos(2\omega_{rf}t+2\theta) \\ &+ 2\sqrt{\epsilon}\cos(\phi_d)\Big[ma(t)\sin(\omega_{rf}t) + mb(t)\cos(\omega_{rf}t) + ma_i(t)\sin(\omega_{rf}t+\theta) \\ &+ mb_i(t)\cos(\omega_{rf}t+\theta) + \Big(m^2a(t)a_i(t) + m^2b(t)b_i(t)\Big)\cos(2\omega_{rf}t+\theta) \\ &+ \big(m^2a(t)b_i(t) + m^2b(t)a_i(t)\big)\sin(2\omega_{rf}+\theta)\Big] \end{aligned} \quad (4.63)$$

Therefore after bandpass filtering at ω_{mm} the remaining terms are:

$$\begin{aligned} i(t) = P_o \Big[& 2\cos(\omega_{mm}t)\Big(1 + ma(t)\sin(\omega_{rf}t) + mb(t)\cos(\omega_{rf}t)\Big) \\ & + 2\epsilon\cos(\omega_{mm}t)\Big(1 + ma_i(t)\sin(\omega_{rf}t+\theta) + mb_i(t)\cos(\omega_{rf}t+\theta)\Big) \\ & + \Big[2\sqrt{\epsilon}\cos(\omega_{mm}+\phi_d)\big[2 + ma(t)\sin(\omega_{rf}t) + mb(t)\cos(\omega_{rf}t) \\ & + ma_i(t)\sin(\omega_{rf}t+\theta) + mb_i(t)\cos(\omega_{rf}t+\theta)\big]\Big]\Big] \end{aligned} \tag{4.64}$$

The 'i' and 'q' channels are demodulated by applying sine and cosine signals whose phase is locked to that of the received signals. Assuming that there is a given phase error of ψ, the demodulating signals are:

$$r_i(t) = V_r\cos(\omega_{rf}t + \psi) \tag{4.65}$$

$$r_q(t) = V_r\sin(\omega_{rf}t + \psi) \tag{4.66}$$

The 'i' and 'q' channels after low pass filtering are

$$\begin{aligned} i_i(t) = P_o m V_r \Big[& a(t)\sin(\psi) + b(t)\cos(\psi) + \epsilon a_i(t)\sin(\theta-\psi) + \epsilon b_i(t)\cos(\theta-\psi) \\ & + \sqrt{\epsilon}\cos(\phi_d)\big[a(t)\sin(\psi) + b(t)\cos(\psi) + a_i(t)\sin(\theta-\psi) + b_i(t)\cos(\theta-\psi)\big]\Big] \end{aligned} \tag{4.67}$$

$$\begin{aligned} i_q(t) = P_o m V_r \Big[& a(t)\cos(\psi) + b(t)\sin(\psi) + \epsilon a_i(t)\cos(\theta-\psi) + \epsilon b_i(t)\sin(\theta-\psi) \\ & + \sqrt{\epsilon}\cos(\phi_d)\big[a(t)\cos(\psi) + b(t)\sin(\psi) + a_i(t)\cos(\theta-\psi) + b_i(t)\sin(\theta-\psi)\big]\Big] \end{aligned} \tag{4.68}$$

Assuming zero demodulation phase error, $\psi = 0$:

$$i_{isignal}(t) = P_o m V_r b(t) \tag{4.69}$$

$$i_{qsignal}(t) = P_o m V_r a(t) \tag{4.70}$$

$$\begin{aligned} i_{inoise}(t) = P_o m V_r \Big[& \epsilon a_i(t)\sin(\theta) + \epsilon b_i(t)\cos(\theta) \\ & + \sqrt{\epsilon}\cos(\phi_d)\big[b(t) + a_i(t)\sin(\theta) + b_i(t)\cos(\theta)\big]\Big] \end{aligned} \tag{4.71}$$

$$\begin{aligned} i_{qnoise}(t) = P_o m V_r \Big[& \epsilon a_i(t)\cos(\theta) + \epsilon b_i(t)\sin(\theta) \\ & + \sqrt{\epsilon}\cos(\phi_d)\big[a(t) + a_i(t)\cos(\theta) + b_i(t)\sin(\theta)\big]\Big] \end{aligned} \tag{4.72}$$

We note that the noise terms are of identical form to that given in (4.50) and (4.51) if we assume that the radio channel and mm-wave carrier recovery are noiseless and perfect.

4.7.3 Formulation of MGF

We have shown in section 4.4.3 how to form the MGF of a random variable. Again the random variable $\phi(t)$ is considered to be uniformly distributed in the region $\pm\pi$. We now consider how to form the MGF of the beat term. As both channels are identical we will consider the beat noise on the 'i' channel:

$$i_{noise} = P_r\sqrt{\epsilon}\cos(\phi_d(t))\Big[b(t) + a_i(t)\cos(\theta) + b_i(t)\sin(\theta)\Big] \tag{4.73}$$

where $P_r = mV_rP_o$. This equation can be viewed as the contribution of two terms.

$$i_{noise} = P_r\sqrt{\epsilon}\cos(\phi_d(t))b(t) + P_r\sqrt{\epsilon}\cos(\phi_d(t))\big[a_i(t)\cos(\theta) + b_i(t)\sin(\theta)\big] \tag{4.74}$$

Using our knowledge of the form of the QAM signal we can rearrange the second term of (4.74) to give:

$$i_{noise} = P_r\sqrt{\epsilon}\cos(\phi_d(t))b(t) + P_r\sqrt{\epsilon}\cos(\phi_d(t))\left[\sqrt{a_i^2(t)+b_i^2(t)}\cos[\phi_m+\theta]\right] \quad (4.75)$$

$$\text{where} \quad \phi_m = -\tan^{-1}\frac{b_i(t)}{a_i(t)}$$

We view both the optical and electrical phase difference, $\phi_d(t)$ and θ as random variables uniformly distributed in the interval $\pm\pi$. Expanding the second term we get:

$$i_{noise} = P_r\sqrt{\epsilon}\cos(\phi_d(t))b(t)$$
$$+\frac{1}{2}P_r\sqrt{\epsilon}\sqrt{a_i^2(t)+b_i^2(t)}\Big[\cos[\phi_d(t)-\phi_m-\theta]+\cos[\phi_d(t)+\phi_m+\theta]\Big] \quad (4.76)$$

which as ϕ_m is a constant added to two random variables described above, may be viewed as:

$$I_{noise} = P_r\sqrt{\epsilon}\cos(\phi_d(t))b(t) + P_r\sqrt{\epsilon}\sqrt{a_i^2(t)+b_i^2(t)}\cos[\phi_d(t)+\theta] \quad (4.77)$$

The cosine part of the second term of (4.77) is the addition of two random variables, therefore this can be rationalised to the convolution of their probability distributions. Figure 4.21 illustrates the formulation of the resultant distribution. We can define $\phi_d(t)+\theta = \varphi(t)$ giving:

$$I_{noise} = P_r\sqrt{\epsilon}\cos(\phi_d(t))b(t) + P_r\sqrt{\epsilon}\sqrt{a_i^2(t)+b_i^2(t)}\cos[\varphi(t)] \quad (4.78)$$

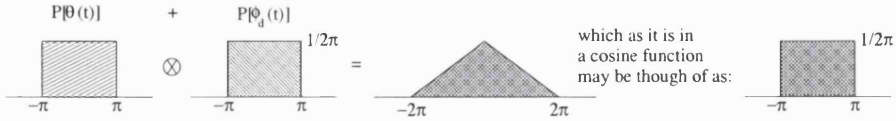

Figure 4.21: Explanation of the convolution of random variables $\phi_d(t)$ and θ

This again is the addition of two statistically independent random variables, however these are now in a form that can be directly transformed to moment generating functions. Using the procedure outlined in section 4.4.4:

$$\Psi(s) = I_0\Big(sP_r\sqrt{\epsilon}b(t)\Big) \cdot I_0\Big(sP_r\sqrt{\epsilon}\sqrt{a_i^2(t) + b_i^2(t)}\Big) \tag{4.79}$$

Equation (4.79) gives the basic moment generating function for QAM signals corrupted be interferometric noise. However as before, symbol conditioning must be taken into account. For QAM this is even more important since, as we will see, not only is the amplitude of the noise symbol dependent but as multilevel gray coded signals are used, so is the decision variable.

4.7.4 Coding of a QAM signal

So far in this section we have formulated the additive noise produced by crosstalk for each channel. We must now discuss the coding method used for QAM transmission to allow us to perform error evaluation. Because we are using a multi-level scheme we are afforded the luxury of being able to map the binary bit stream onto the constellation in an optimal manner. Considering the constellation in figure 3.2 it is clear that the most likely errors involve with neighbouring point, and in this event we would like the number of bits corrupted to be minimised. This suggests

that a coding scheme such as Gray coding should be employed. With this coding arrangement, shown in figure 4.22, the neighbouring points differ by only 1 bit, thus reducing the overall error probability [53].

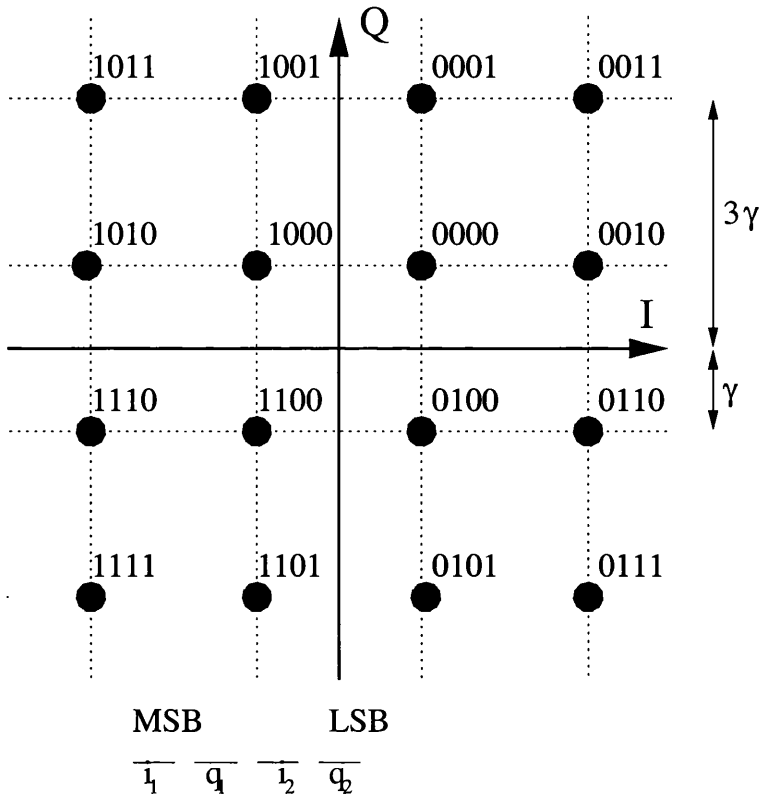

Figure 4.22: Four level (16 symbol) QAM constellation with Gray coding

The use of Gray coding alters the calculation of the error, as the distance between the symbol and the decision threshold is now symbol dependent. For instance, consider the two most significant bits (MSBs) of the 4 bit signal of 16 QAM constellation shown in figure 4.22. Due to the Gray coding scheme the decision state for these two bits is as follows.

$$\begin{aligned} &\text{if } I, Q \geq 0 \quad \text{then} \quad i_1, q_1 = 0 \\ &\text{if } I, Q < 0 \quad \text{then} \quad i_1, q_1 = 1 \end{aligned} \tag{4.80}$$

Therefore if the transmitted code is any of the following codes (1011, 1010, 1110, 1111, 0011, 0010, 0110, 0111) then the 'margin of error' on the MSB i_1 is 3γ. Whereas if any of the remaining codes are transmitted the 'margin of error' is only γ. Following the same rationale the same result can be seen for the 2nd MSB, q_1.

The boundaries for the two least significant bits (LSBs) are defined as:

$$\begin{aligned} &\text{if} \quad I, Q \geq 2\gamma && \text{then} \quad i_2, q_2 = 1 \\ &\text{if} \quad -2\gamma < I, Q < 2\gamma && \text{then} \quad i_2, q_2 = 0 \\ &\text{if} \quad I, Q \leq -2\gamma && \text{then} \quad i_2, q_2 = 1 \end{aligned} \tag{4.81}$$

These two bits will always be at a distance γ from the decision threshold. We can therefore formulate a Gaussian approximation for the error probability, assuming that the channel noise is of variance σ_n.

$$P_e = \frac{3}{4} Q\left(\frac{\gamma}{\sigma_n}\right) + \frac{1}{4} Q\left(\frac{3\gamma}{\sigma_n}\right) \tag{4.82}$$

Extending the signal level to a 6 bit symbol, we produce a 64 QAM signal for

which the decision levels are as follows:

$$\begin{aligned}
I, Q \geq 0 &\Rightarrow i_1, q_1 = 0 \\
I, Q < 0 &\Rightarrow i_1, q_1 = 1 \\
I, Q \geq 4d &\Rightarrow i_2, q_2 = 1 \\
-4d \leq I, Q < 4d &\Rightarrow i_2, q_2 = 0 \\
I, Q < -4d &\Rightarrow i_2, q_2 = 1 \\
I, Q \geq 6d &\Rightarrow i_3, q_3 = 1 \\
2d \leq I, Q < 6d &\Rightarrow i_3, q_3 = 0 \\
-2d \leq I, Q < 2d &\Rightarrow i_3, q_3 = 1 \\
-6d \leq I, Q < -2d &\Rightarrow i_3, q_3 = 0 \\
I, Q < -6d &\Rightarrow i_3, q_3 = 1
\end{aligned} \tag{4.83}$$

4.7.5 Symbol Conditioning

In light of the gray coding used, care must be taken in symbol conditioning the MGF of the interferometric noise. We here describe the moment generating function extended to include the decision variable for the modified Chernoff bound.

The unconditioned MGF of equation (4.79) is made up of two terms, the second of which;

$$I_0\left(sP_r\sqrt{\epsilon}\sqrt{a_i^2(t) + b_i^2(t)}\right) \tag{4.84}$$

is conditioned by the signal states on the interfering terms. For 16QAM $a(t), b(t) \in$

$\{-3\gamma, -\gamma, \gamma, 3\gamma\}$, which allows us to average the MGF over all possible symbol states. Due to the squaring of the symbols we only need to consider the positive states, giving the average as:

$$\frac{1}{N^2}\sum_{i=1}^{N}\sum_{j=1}^{N} I_0\Big(sP_r\sqrt{\epsilon}\sqrt{a_i^2(t)+b_j^2(t)}\Big) \tag{4.85}$$

The first term in equation (4.79):

$$I_0\Big(sP_r\sqrt{\epsilon}b(t)\Big) \tag{4.86}$$

is conditioned by the received signal state, which will also condition the level of the decision variable. We consider 16 QAM, looking at each bit of the i channel individually. Due to the gray coding scheme the most significant bits states are as described in (4.80). The decision threshold stays the same, but half of the time the margin of error is γ and half of the time it is 3γ. Negative values of γ are ignored as the modified Bessel function I_0 is an even function.

$$\begin{aligned}\mathrm{BER}_{i1} = \frac{1}{8}\sum_{i=1}^{N}\sum_{j=1}^{N} & I_0\Big[sP_r\sqrt{\epsilon}\sqrt{a_i^2(t)+b_j^2(t)}\Big] \\ \cdot\Big(e^{-3s\gamma} & I_0\Big[sP_o\sqrt{\epsilon}3\gamma\Big] + e^{-s\gamma} I_0\Big[sP_o\sqrt{\epsilon}\gamma\Big]\Big)\end{aligned} \tag{4.87}$$

Using the same rationale for the least significant bit as described in (4.81), we again formulate a modified expression. For the LSB there are now three decision levels

giving:

$$\mathrm{BER}_{i2} = \frac{1}{4}\Big[2e^{-s\gamma}I_0\big[sP_o\sqrt{\epsilon}3\gamma\big] + \big(e^{-s\gamma} + e^{-3s\gamma}\big)I_0\big[sP_o\sqrt{\epsilon}\gamma\big]\Big] \cdot \sum_{i=1}^{N}\sum_{j=1}^{N} I_0\Big[sP_r\sqrt{\epsilon}\sqrt{a_i^2(t) + b_j^2(t)}\Big] \tag{4.88}$$

Equations (4.87) and (4.88) are used to form the MCB as described in section 4.4.3.

$$P_e \leq \mathrm{MCB} = \frac{M_G(s)}{2s\sigma_n\sqrt{2\pi}}\Big[\mathrm{BER}_{i1} + \mathrm{BER}_{i2}\Big] \tag{4.89}$$

This complete MCB formulation is use in the next section to evaluate bit error rates of the transport of QAM.

4.7.6 Results

Using the formulation of the moment generating functions described above, and normalising constant amplitude parameters such as modulation index and demodulation signal amplitude, we produce the graph of figure 4.7.6. This figure shows that QAM transmission offers an improvement in BER over a standard binary channel, for a normalised received amplitude signal, (decision threshold 0.5). This is predominately due to the use of gray coding for QAM transmission, which places certain symbol combinations further from the decision threshold than would normally be the case. We see however that QAM transmission is subject to higher degradation due to interferometric noise than would be the case in standard binary ASK transmission. This conclusion is logical, as interference effects not only the amplitude, but also the phase of the received signal, which is a major factor in the performance

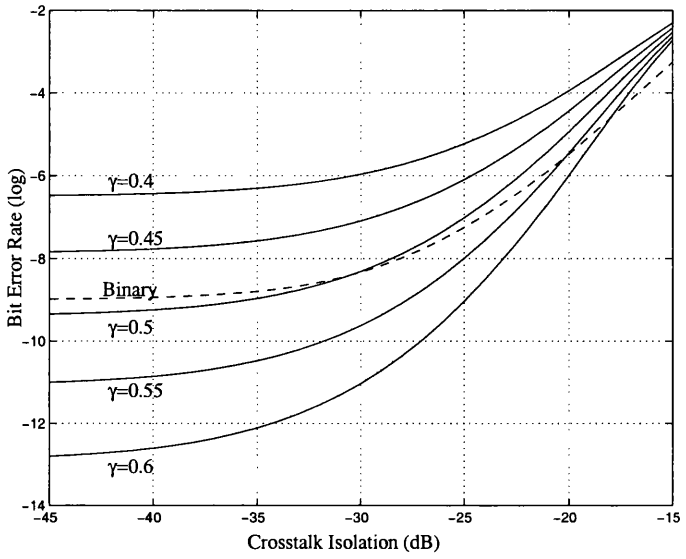

Figure 4.23: Crosstalk isolation against Bit Error Rate for 16QAM transmission

of coherently demodulated signals.

4.8 Summary

In this chapter we have considered various aspects of interferometric beat noise encountered in optical systems. We have examined a number of evaluation methods and extended the use of moment based analysis to include previously unreported systems parameters such as extinction ratio and crosstalk-crosstalk beating. Using these accurate methods we have shown conclusively the limitations of the Gaussian approximation, and offer a prescription of when to use these approximate results. These tools were then used to perform case studies on two very different network examples. The first considers the MWTN node [12] and investigates the effects of differing isolation levels in the components of the node. The second evaluates the impact of interferometric noise in the transport of QAM signals, first as simple

IM-DD systems, and then extended to HFR transport systems.

Chapter 5

Optical Beamforming Networks

5.1 Introduction

In this chapter we detail simulation, analytic and experimental evaluation of optical beamforming networks for application in phased array antenna systems. The main objective is to consider some of the problems likely to be encountered when designing multi-wavelength optical beamforming networks which use wavelength division multiplexing (WDM) technology to reduce the number of components and interconnects involved. In recent years the use of optical methods of beam-steering for phased array antennas has created great interest due to the possibility of squint-free operation and remote delivery without the loss and weight burdens of electrical techniques [54]. In such systems, discrete Bragg fibre gratings are being suggested to provide the time delays necessary to control the beam direction [55].

The specifics of the system investigated will be reviewed in section 5.2. Section 5.3 investigates the network benefits that suppression of the optical carrier may bring if included in such networks. Section 5.4 evaluates the effect of multiple wavelength

beating in these beamforming networks with the results of simulation, analysis and experimentation presented in 5.4.4. Section 5.5 discusses other system related issues that should be considered and may warrant further attention. The contributions of this chapter are summarised in section 5.6

5.2 Details of system operation

The system under investigation is a fiber optic transport network for beamforming in receive phased array antenna applications. Two system configurations have been proposed.

1. The system indicated in figure 5.1 forms the beams by each wavelength falling on its own photo detector via a length of fiber used to create the time delays required for beamforming. This method was the first use of optical steering suggested in 1991 [54] and has since been well researched. However, using this conventional method an N beam network of M elements could require up to $N \times M$ interconnects [56], which for 256 elements forming 256 beams means 65536 interconnects and photodiodes.

2. The second method investigated makes use of wavelength division multiplexing (WDM) technology to reduce the number of components and interconnects required as shown in figure 5.2. However, this results in much tighter component tolerances compared with the previous system. Since being suggested for this application in 1995 [57] Bragg fiber gratings have attracted a great deal of attention. A number of authors have demonstrated the principles of using such gratings and have shown that it is possible to write gratings that will

produce the necessary scan angle [10, 55, 58].

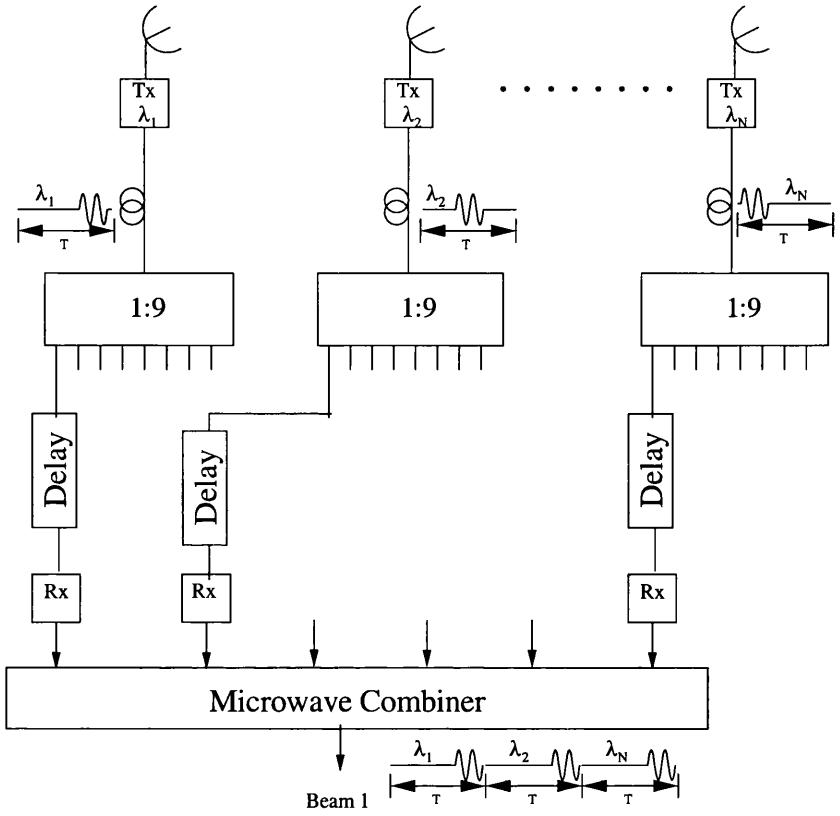

Figure 5.1: Multiple Fixed Beam Optical Fiber TTD Beamforming

The desire for a system that produces true time delay (TTD) derives from the fact that if a phase shift is induced on to the signals to steer the beam then the angle of propagation is dependent on the signal frequency, which for wide bandwidth signals produces a phenomenon called *beam squinting.* This squint can be compensated for if time delays are used instead of phase shifting to form the beams. A review of optical beamforming methods is given in section 3.4.

In the WDM system shown in figure 5.2, each receiver has N wavelengths incident upon it, where N is the number of array elements in the antenna. The most concerning issue is that all the wavelengths received will beat with each other, generating beat noise terms at the frequency of optical separation. Normally, if there

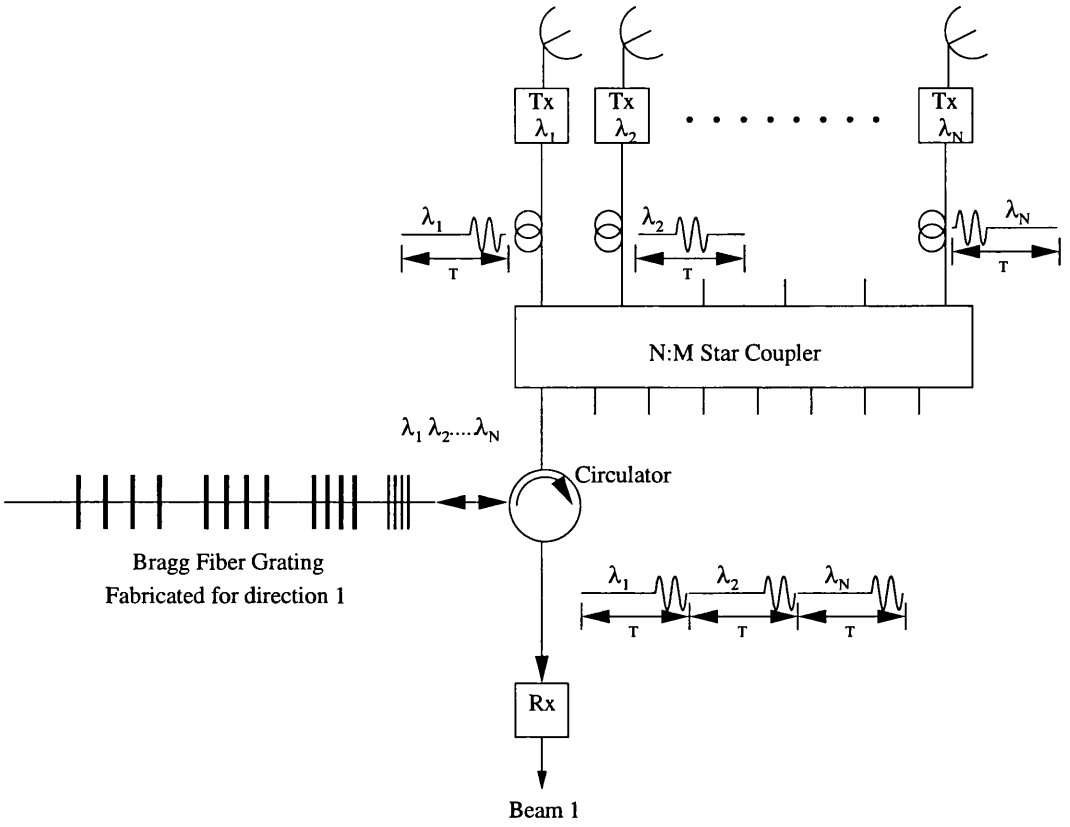

Figure 5.2: Bragg fiber grating Multiple Fixed Beam TTD Beamforming

is sufficient wavelength separation between the lasers, this beat term falls out of the received band, but as the number of channels increases, the separation between them must decrease if all channels are still to fit within the standard EDFA bandwidth ($\approx$ 35nm). This may lead to harmonics caused by the external modulation beating with one another or with the signals themselves to produce in-band beat terms. There is always going to be a trade-off between the desired number of wavelengths and the bandwidth of the information carried, and it is quite possible in broadband applications that the bandwidth required will extend over a number of octaves creating large sidebands. However, for a narrow antenna beamwidth it is also desirable to have a large number of array elements, which in an unpartitioned system would require the same large number of wavelengths.

5.3 Carrier Suppression

One concern in a system such as figure 5.2 is the total optical power level at the photodiode. Saturation levels of most modern photo diodes is of the order of 3-5mW, although research is continuing into higher power devices. It can be shown that in most applications when a modulator is used at quadrature bias, the modulated sidebands contribute very little to the total optical power, even at comparatively high modulation depths. For a working system the level of crosstalk power will also be negligible if a reasonable SNR is to be maintained. We therefore conclude that the optical power level can be reasonably approximated as:

$$P_o = \sum_{k=1}^{N} [P_{INk} - L_{sys}] \tag{5.1}$$

where P_{IN} is the laser input power, and L_{sys} is the total optical power loss incurred in the process of beamforming, for an N element array.

Therefore if the power of the optical carrier can be reduced without reduction of the modulated sidebands the optical power constraints will also be reduced. A number of methods have been suggest in the literature to achieve this power reduction.

1. Optical filtering of the carrier has been investigated [59]. This option is better suited to this RF application than to digital transmission, but is still relatively intolerant to laser wavelength wander. The requirement for very closely matched filters and high stability lasers detracts from the advantages offered.

2. Optical filtering using a laser resonator to lock the filter and laser frequencies

together has been demonstrated in [60]. Again this technique increases the complexity greatly.

3. Biasing the modulator away from quadrature will lower the relative level of the optical carrier, however it will also produce an increase in intermodulation distortion.

We detail experiments to investigate biasing the MZI modulator away from quadrature to achieve this suppression.

5.3.1 Mach-Zehnder Modulator

Consider a continuous wave (CW) signal from a laser source of amplitude E_{in} and optical frequency ω_c, externally modulated using a Mach-Zehnder type modulator by an RF signal of frequency ω_{rf} and peak to peak amplitude $2V_{rf}$. We assume that the arms of the modulator are fed with equal amplitude but opposite phase signals, and that it has a d.c. bias voltage V_b. We define V_π as the voltage necessary to induce a phase shift of π. The transfer response of the MZI modulator is described as:

$$E_{out}(t) = \frac{E_{in}}{2} \cdot [\cos(\omega_c t + \alpha\pi + \beta\pi \cos\omega_{rf} t) + \cos(\omega_c t - \beta\pi \cos\omega_{rf} t)] \tag{5.2}$$

We define:

$$\alpha = \frac{\pi V_b}{V_\pi} \tag{5.3}$$

$$\beta = \frac{\pi V_{rf}}{V_\pi} \tag{5.4}$$

Bessel function expansion of all terms produces:

$$\begin{aligned} E_{out} = E_{in}\Big\{ &+ J_0(\beta)\cdot\cos(\alpha)\cdot e^{j[\omega_t+\phi(t)]} \\ &- J_1(\beta)\cdot\sin(\alpha)\cdot e^{j[\omega_t\pm 2\pi f_{RF}t+\phi(t)]} \\ &+ J_2(\beta)\cdot\cos(\alpha)\cdot e^{j[\omega_t\pm 4\pi f_{RF}t+\phi(t)]} + \ldots \Big\} \end{aligned} \tag{5.5}$$

describing the electric field output of the modulator for a single tone, where J_n is the Bessel function of first kind, nth order. We see a number of components; first the unmodulated centre component at the input optical frequency, second the modulated sidebands, followed by an infinite number of harmonic terms. Therefore the optical power in the carrier at the receiver is:

$$P_{rx}(t) = \frac{E_{in}(t)}{4} J_0^2(\beta)\left[[\cos(\alpha)+1]^2 + \sin^2(\alpha)\right] \tag{5.6}$$

This formulation can be expanded for two tones. We now define the modulating signal as:

$$V_m(t) = V_1\cos[\omega_{e1}(t)] + V_2\cos[\omega_{e2}(t)] \tag{5.7}$$

Again we define the parameters:

$$\alpha = \frac{\pi V_b}{V_\pi} \tag{5.8}$$

$$\beta = \frac{\pi(V_1+V_2)}{V_\pi} \tag{5.9}$$

Therefore the electric field in the fibre after modulation by $V_m(t)$ is:

$$E_o(t) = E_{in}\cos(\omega_o t)\cos\left[\frac{\alpha}{2} + \frac{\beta}{2}[\cos(\omega_{e1}t) + \cos(\omega_{e2}t)]\right] \tag{5.10}$$

Expansion of (5.10) again produces an infinite series of terms. To investigate the effect of carrier suppression on intermodulation distortion we must first find the received electrical signal and then identify the individual spectral components. The received signal is given by substituting (5.7) into (5.10):

$$i_t(t) = |E_o(t)|^2 \tag{5.11}$$

$$\begin{aligned}
&= \frac{E_{in}^2}{2}\Bigg[1 + \frac{1}{2}\cos(\alpha)J_0^2(\beta) \\
&+ J_0(\beta)\sum_{k=1}^{\infty}(-1)^k J_{2k}(\beta)\cos(2k\omega_{e1}t)\cos(\alpha) \\
&+ J_0(\beta)\sum_{k=1}^{\infty}(-1)^k J_{2k}(\beta)\cos(2k\omega_{e2}t)\cos(\alpha) \\
&- J_0(\beta)\sum_{k=0}^{\infty}(-1)^k J_{2k+1}(\beta)\cos([2k+1]\omega_{e1}t)\sin(\alpha) \\
&- J_0(\beta)\sum_{k=0}^{\infty}(-1)^k J_{2k+1}(\beta)\cos([2k+1]\omega_{e2}t)\sin(\alpha) \\
&+ 2\sum_{k=1}^{\infty}\sum_{i=1}^{\infty}(-1)^k(-1)^i J_{2k}(\beta)J_{2i}(\beta)\cos\left[(2k\omega_{e1} \pm 2i\omega_{e2})t\right]\cos(\alpha) \\
&- 2\sum_{k=0}^{\infty}\sum_{i=0}^{\infty}(-1)^k(-1)^i J_{2k+1}(\beta)J_{2i+1}(\beta)\cos\left[([2k+1]\omega_{e1} \pm [2i+1]\omega_{e2})t\right]\cos(\alpha) \\
&- 2\sum_{k=0}^{\infty}\sum_{i=1}^{\infty}(-1)^k(-1)^i J_{2k+1}(\beta)J_{2i}(\beta)\cos\left[([2k+1]\omega_{e1} \pm 2i\omega_{e2})t\right]\sin(\alpha) \\
&- 2\sum_{k=1}^{\infty}\sum_{i=0}^{\infty}(-1)^k(-1)^i J_{2k}(\beta)J_{2i+1}(\beta)\cos\left[(2k\omega_{e1} \pm [2i+1]\omega_{e2})t\right]\sin(\alpha)
\end{aligned} \tag{5.12}$$

which can now be broken down into individual components. The received signals are given by:

$$i_{rf} = \frac{E_{in}^2}{2} \sin(\alpha) J_0(\beta) J_1(\beta) \tag{5.13}$$

$$i_{2nd} = \frac{E_{in}^2}{2} \cos(\alpha) J_0(\beta) J_2(\beta) \tag{5.14}$$

$$i_{IM2} = \frac{E_{in}^2}{2} \cos(\alpha) J_1^2(\beta) \tag{5.15}$$

$$i_{IM3} = \frac{E_{in}^2}{2} \sin(\alpha) J_1(\beta) J_2(\beta) \tag{5.16}$$

where i_{rf} is the photocurrent due to each of the modulating RF signals, i_{2nd} represents each second harmonic (at $2\omega_{e1}$ and $2\omega_{e2}$), i_{IM2} the 2nd order intermodulation term (at $|\omega_{e1} - \omega_{e2}|$) and i_{IM3}, the 3rd order intermodulation term (at $|\omega_{e1} - 2\omega_{e2}|$ and $|2\omega_{e1} - \omega_{e2}|$). The important point to note from these four equations is the term in α. From the definition of equation (5.8) we can see that when the modulator is biased at $V_\pi/2$, which is the normal quadrature bias point, the value of α is $\pi/2$. Therefore, all even order distortion products are, in theory, eliminated (for practical devices they are minimal).

We now consider this scenario experimentally and compare the results.

5.3.2 Carrier Suppression Experiment

The set up devised to experimentally measure the level of carrier suppression for various bias levels is shown in figure 5.3. A DFB laser source was externally modulated by a two tone RF signal source, with tones at 4.5GHz and 6GHz, and the bias level of the modulator was carefully controlled using a stabilised voltage supply. The output of the modulator was photodetected and amplified using a low

noise RF amplifier, with the output viewed on an electrical spectrum analyser.

The purpose of this experiment was to examine the increase in intermodulation and harmonic terms and the reduction in optical carrier power produced when biasing the modulator away from quadrature. The modulator used in this experiment has a V_π specified as 6-8v, and as can be seen from the results, has a built in π phase differential between the arms.

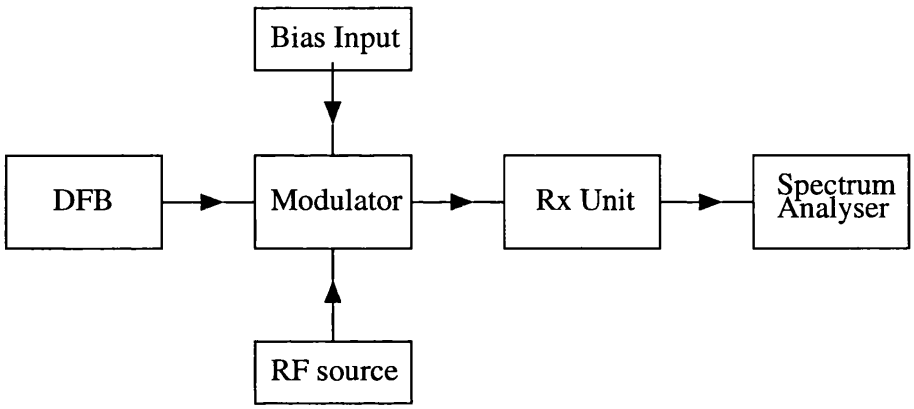

Figure 5.3: Experimental setup for carrier suppression

The results in figure 5.4 show that lowering the biasing point of this modulator gives a noticeable drop in the optical power, indicating a drop in the power ratio between the carrier and sidebands. However as a side effect of biasing away from quadrature, the signal to 2nd order intermodulation ratio decreases by 10dB over a range of 2 volts. In line with the prediction of section 5.3.1 we show that lowering the bias point of the Mach-Zehnder modulator does not significantly increase the third order nonlinearity of the modulator, only the second order nonlinearity and the second harmonic term. It should be noted that in most schemes considered only the third order intermodulation term is important as the other terms will fall outside the receiver bandwidth. Figure 5.4 also shows a theoretical evaluation of the optical

power at the original carrier wavelength. We see that as the suppression increases, the optical power predicted starts to drop faster than the experimentally recorded total optical power, demonstrating that the side bands become the dominant power.

This approach allows the total optical power carried in the system to be reduced while the RF to RF link loss remains approximately constant. This can yield a number of advantages in a system:

1. less optical power allowing more gain from EDFAs before saturation;
2. improved tolerance to nonlinear fibre effects such as SRS and XPM/GVD, the contribution reducing by the square of the optical power reduction;
3. reduction in the saturation and power requirements of the photodiodes, (this may also have the effect of reducing non-linearities in the photodiode);
4. noise improvement in shot noise limited systems.

5.3.3 Carrier Suppression with Saturated Amplification

If the received optical power is not a concern then it has been suggested that this use of off-quadrature biasing can lead to an increase in the linear dynamic range of a link if the optical power at the receiver is kept constant as the bias level is lowered [61]. This can be achieved by either controlling the laser bias level or, as we demonstrate here, by the use of optical amplification. The system was set up with two RF tones at 4.5GHz and 6GHz combined to give 13dBm/tone at the input of the modulator. The optical amplifier was pumped such that the optical output was in the saturation regime when the modulator was biased at quadrature. The pump

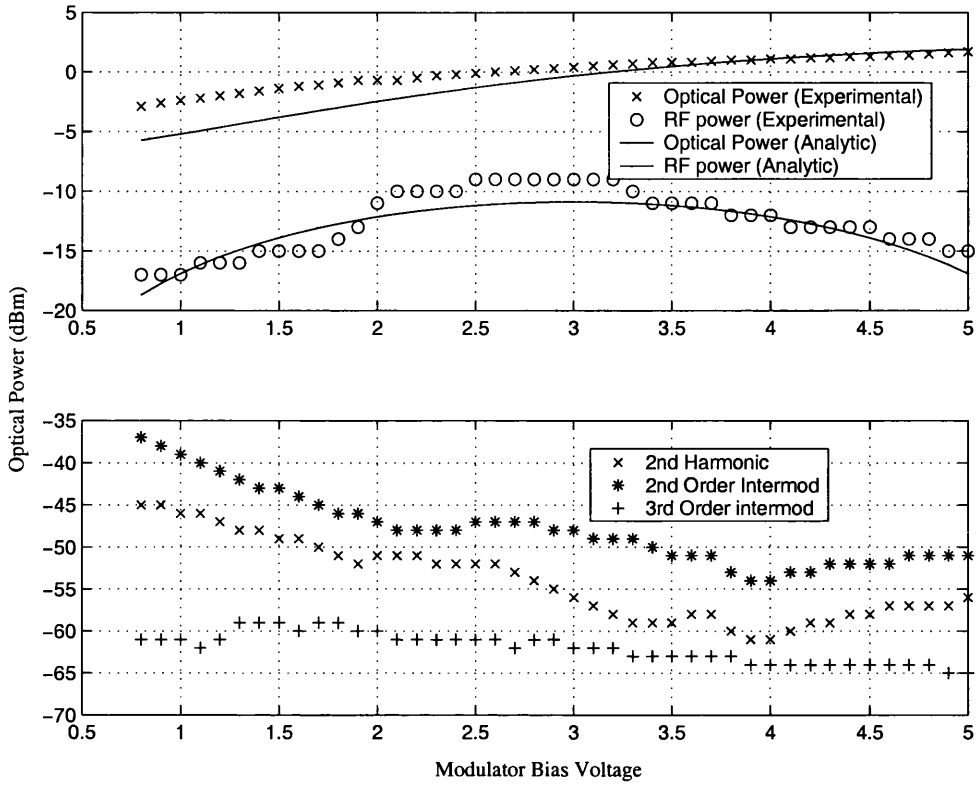

Figure 5.4: Optical Power vs modulator bias

power was also set to such a level that the ASE noise level at the receiver was not dominant in the link, so that the link was thermal noise limited.

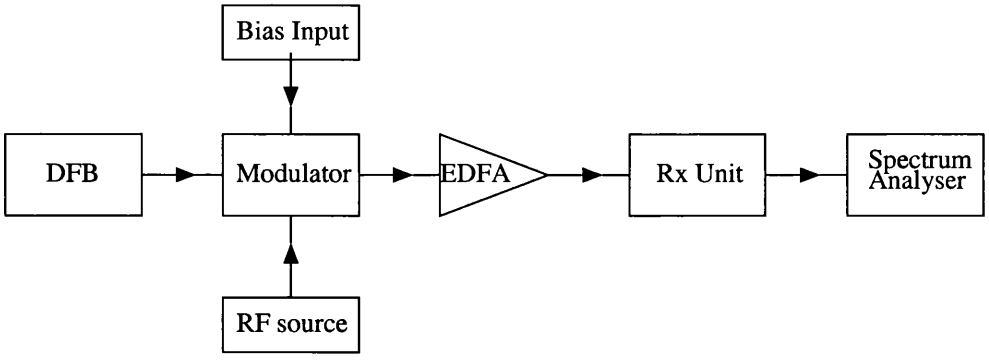

Figure 5.5: Experimental setup for carrier suppression with EDFA

We see from figure 5.6 that as the bias point is lowered the received RF power increases. Because the optical amplifier is in its saturation region, the optical power

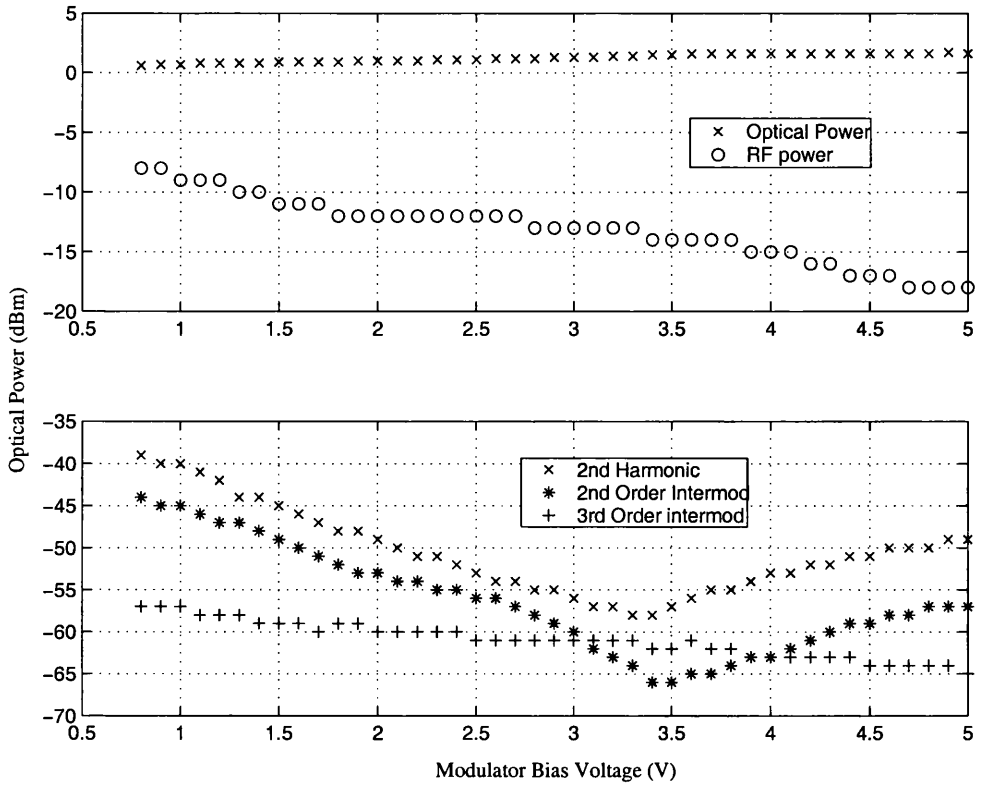

Figure 5.6: Performance of carrier suppression.

output will stay approximately constant. However, as the bias level is lowered the power at the optical carrier frequency will drop allowing the optical sidebands to receive greater amplification. This causes an increase in the effective modulation depth of the signal, resulting in a greater received signal power.

Inherent to this lower bias point as previously discussed are increases in the intermodulation and harmonic levels in the system. The ratio of third order intermodulation terms (at 3GHz and 7.5GHz) to signal level stays roughly constant as expected, however we see a dramatic rise in both the 2nd order intermodulation terms (1.5GHz and 10.5GHz) and the 2nd order harmonic terms (9GHz and 12 GHz). It can be seen again, however, that both of these terms should fall out of band in most practical systems.

5.4 Multiple Wavelength Mixing

Interferometric beat noise in digital transport systems is a well studied phenomenon [29, 31, 38]. However, the majority of these studies consider the bit error rate of the system for interfering signals of much lower power than the data channel. In this analogue scenario we are studying multiple wavelengths of approximately equal power, that have been modulated with an RF signal, being received by a single photodiode.

Let us consider how we describe an optical signal of power P emanating from a DFB laser :

$$E(t) = \vec{\rho}\sqrt{P}\exp j[\omega t + \phi(t)] \tag{5.17}$$

where $\vec{\rho}$ expresses the state of polarization, ω is the optical frequency and $\phi(t)$ the optical phase.

If N of these optical signals fall upon a photodiode, each having been modulated with a signal including bias of $m(t)$, the total field incident on the photo-detector will be :

$$E_{tot}(t) = \sum_{k=1}^{N} \vec{\rho_k}\sqrt{P_{ok}m_k(t)}\exp j[\omega_k t + \phi_k(t)] \tag{5.18}$$

Taking the semi classical approach of optical detection, we define the instantaneous optical power as being proportional to the squared magnitude of the electro-magnetic

field, allowing us to describe the field received at the photo-detector as :

$$i_t = \mathbf{R}|E_{Tot}|^2 \tag{5.19}$$

$$\text{where} \quad \mathbf{R} = \frac{\eta q}{h\nu}$$

where q is the electron charge, h is Planck's constant, η is the quantum efficiency, ν is the frequency of the light, and $\mathbf{R}$ is the responsivity.

Assuming worst case polarisation and using the following equality :

$$\left|\sum_{k=1}^{N} x_k\right|^2 = \sum_{k=1}^{N} |x_n|^2 + 2\text{Re}\left(\sum_{k=1}^{N-1}\sum_{l=k+1}^{N} x_k x_l^*\right) \tag{5.20}$$

we can define the received photocurrent as:

$$i(t) = \mathbf{R}\left[\sum_{k=1}^{N} P_k m_k(t) + 2\text{Re}\left(\sum_{k=1}^{N-1}\sum_{l=k+1}^{N} E_K(t)E_l^*(t)\right)\right] \tag{5.21}$$

The first term of (5.21) is the sum of the received signals which is intrinsically the same as if each optical signal were received by its own photodiode and then summed by an ideal microwave combiner. The second term is the interferometric beat noise term in which each optical signal beats with all other optical signals. The position in the received spectrum of each beat term is determined by the wavelength separation between the optical signals. Obviously, if the beat frequency is well outside the bandwidth of the filter there is very little impact. It should be noted, though, that the use of a Mach-Zehnder modulator does produce harmonic terms that still may fall in band even though the optical signals are separated by more than three times the filter bandwidth.

5.4.1 Analytic Formulation

Using the description of the optical signal and received photocurrent given in section 4.2 we can form an analytic evaluation of the signal to optical interference noise ratio. This treatment broadly follows the method of Shankaranarayanan [62] which investigated optical beat interference in WDMA/FDMA networks.

Considering first two independent single mode lasers, emitting fields $E_i(t)$ and $E_j(t)$, we assume that if at least one field is stationary the power spectral density (PSD) of the received photocurrent is :

$$\mathbf{S}_i(f) = \mathbf{R}^2 \mathbf{S}_{IT}(f)|H(f)|^2$$

$$\text{where} \quad \mathbf{S}_{IT} = \mathbf{S}_{Ij}(f) + \mathbf{S}_{Ii}(f) + 4\mathbf{S}_{Ei}(f) \otimes \mathbf{S}_{Ej}(f) + d.c \tag{5.22}$$

where $\mathbf{S}_{IT}$ is the total intensity, $H(f)$ is the transfer function of the receiver, $\mathbf{S}_I(f)$ are the PSDs of the individual intensities, $\mathbf{S}_E(f)$ are the PSDs of the optical fields and $\otimes$ denotes convolution; the d.c. terms are ignored. For N independent fields:

$$\mathbf{S}_i(f) = \mathbf{R}^2|H(f)|^2 \left[\sum_{m=1}^{N} \mathbf{S}_{Im}(f) + \sum_{i=1}^{N-1} \sum_{j=1+1}^{N} 4\mathbf{S}_{Ei}(f) \otimes \mathbf{S}_{Ej}(f) \right] \tag{5.23}$$

If the main detector bandwidth is formed by a filter with a bandwidth of $2B$ centred at f_c then assuming the passband to be rectangular (ideal filter characteristic) we define :

$$H(f) = \left\{ \begin{array}{ll} 1 & f_c - B \leq f \leq f_c + B \\ 0 & otherwise \end{array} \right\}$$

Making use of the fact that the two sided power spectrum of real signals is an even function of frequency we can define the signal power as:

$$\begin{aligned} P_{sig} &= \mathbf{R}^2 \int_{-\infty}^{\infty} \sum_{m=1}^{N} \mathbf{S}_{Im}(f)|H(f)|^2 df \\ &= 2\mathbf{R}^2 \int_{f_c-B}^{f_c+B} \sum_{m=1}^{N} \mathbf{S}_{Im}(f) df \end{aligned} \tag{5.24}$$

while the total interference in the same band can be described as :

$$\begin{aligned} P_{beat} &= \mathbf{R}^2 \int_{-\infty}^{\infty} \sum_{m=1}^{N} |H(f)|^2 \sum_{i=1}^{N-1} \sum_{j=1+1}^{N} 4\mathbf{S}_{Ei}(f) \otimes \mathbf{S}_{Ej}(f) df \\ &= 2\mathbf{R}^2 \int_{f_c-B}^{f_c+B} \sum_{i=1}^{N-1} \sum_{j=1+1}^{N} 4\mathbf{S}_{Ei}(f) \otimes \mathbf{S}_{Ej}(f) df \end{aligned} \tag{5.25}$$

We may use (5.24) and (5.25) to give the signal to interference noise ratio:

$$\text{SINR} = \frac{P_{sig}}{P_{beat}} \tag{5.26}$$

To complete this formulation we must define the signal power spectra of the optical signals in our system. Although strictly we need to consider the optical field spectrum of each laser we can consider the linewidth to be negligible when compared to the signal bandwidth. We now require the optical field power spectral density after modulation. Assuming external modulation using a Mach-Zehnder modulator as defined in equation (5.6) and a modulating signal of $x(t) = \sin(2\pi f_{RF} t)$, the power

spectral density of the optical field will be:

$$\mathbf{S}_E(f) = \frac{E_o^2}{8} \sum_{k=-\infty}^{\infty} J_k^2 \left(\frac{\pi\alpha}{2}\right) [\delta(f - f_o - kf_{RF}) + \delta(f + f_o + kf_{RF})] \tag{5.27}$$

where J_n is the Bessel function first kind nth order, $\delta(f)$ is the Dirac delta function, and f_o is the frequency of the optical carrier. The total received beat noise power if N such spectra at optical frequencies f_{ok} $(k = 1 \ldots N)$ beat together is given by substituting in (5.25) as :

$$P_{beat} = 2\mathbf{R}^2 \int_{f_c-B}^{f_c+B} \sum_{i=1}^{N-1} \sum_{j=1+1}^{N} \frac{E_{Oi}^2 E_{Oj}^2}{16} \sum_{k=-\infty}^{\infty} \sum_{l=-\infty}^{\infty} J_k^2 \left(\frac{\pi\alpha}{2}\right) J_l^2 \left(\frac{\pi\alpha}{2}\right) \cdot$$
$$[\delta(f + f_{oi} - f_{oj} + kf_{RFi} - lf_{RFj}) + \delta(f - f_{oi} + f_{oj} - kf_{RFi} + lf_{RFj})]df \tag{5.28}$$

Similarly from (5.24) the signal power is given by:

$$P_{sig} = 2\mathbf{R}^2 \int_{f_c-B}^{f_c+B} \sum_{i=1}^{N} \frac{E_{Oi}^4}{16} J_1^2 (\pi\alpha) [\delta(f - f_{RFi}) + \delta(f + f_{RFi})] \tag{5.29}$$

We also include shot and thermal noise in the SNR formulation as :

$$P_{shot} = 4B\bar{I}q \tag{5.30}$$

$$P_{thermal} = \frac{4BK_BT}{R} \tag{5.31}$$

where $\bar{I}$ is the average photocurrent, q is the electron charge, K_B is Boltzmanns constant, T is the ambient temperature and R is the resistance of the receiver. This

gives the overall SNR as:

$$\text{SNR} = \frac{P_{sig}}{P_{beat} + P_{shot} + P_{thermal}} \tag{5.32}$$

After substitution, equation (5.32) can be solved (e.g. using Mathematica or MATLAB software) using the following parameters.

Symbol	Value	Description
N	2,3,5,7,9	Number of wavelengths
α	0.3	Modulation depth
E_o	20 dBm	Optical field intensity
f_c	4 GHz	Filter centre frequency
$2B$	4 GHz	Filter bandwidth
$\mathbf{R}$	$0.8A/W$	Photo diode responsivity
f_r	4GHz	Radar Signal frequency
k,l	5	Number of Bessel terms considered
k_b	1.38066×10^{-23}	Boltzmanns Constant
T	293	Temperature
R	50Ω	Receiver Resistance
q	1.60218×10^{-19}	Electron Charge
λ	1550nm	Laser Central wavelength

Table 5.1: Evaluation parameters: Analytic

5.4.2 Simulation Model

The SPW photodiode block was built using the expansion of (5.20) by first summing the photocurrent produced by each individual optical signal to form the signal output. The beat term was produced using a custom coded C code block that takes as its input two vectors containing the optical spectra and the wavelength data as specified in 2.3.1. Each term in each spectra is then compared and a frequency and amplitude value calculated relating to its contribution to the beat spectrum. Taking the FFT of the beat spectrum then produces the beat signal.

Firstly we consider the power spectral densities (PSD) produced by simulation. Figure 5.7 shows the PSD of the laser source used in the simulations. We can see that the linewidth is approximately as defined in table 5.2. Figure 5.8 is the baseband optical signal after modulation by a Mach-Zehnder modulator. We can clearly see not only the optical carrier and the two sidebands at the modulating frequency but also the harmonic terms.

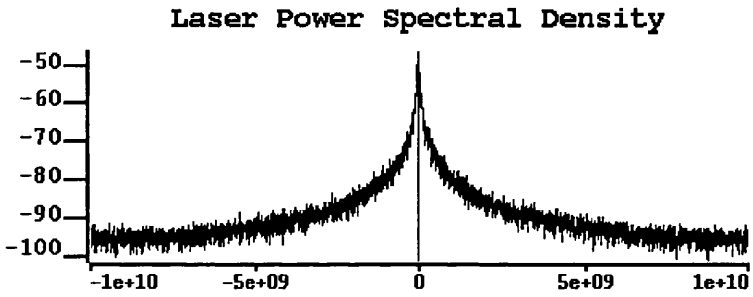

Figure 5.7: Laser power spectral density

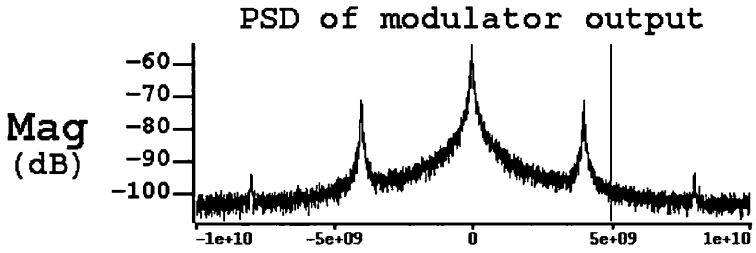

Figure 5.8: Power spectral density of the modulated laser field

5.4.3 Experimental Evaluation

For the experimental validation the configuration shown in figure 5.10 was used, with the signal and noise floor levels measured using an electrical spectrum analyser. It was first demonstrated that the histogram of interferometric beating is

Parameter	Value
System	
Sampling Frequency	20GHz
FFT length	16384
Number of Wavelengths	3,5
Input Signal	
Power	-10,0,10,20 dBm
Frequency	4GHz Sine wave
DFB Laser	
Linewidth	50MHz
Optical Power	0.0 dBm
RIN	-170 dBc/Hz
Wavelength	≈1550nm
MZ modulator	
V_{π}	12 V
V_{bias}	6 V
Optical excess loss	4.5 dB
Input Impedance	20 Ω
Optical Coupler	
Excess loss	0.1 dB
Splitting loss	3 dB
Photodiode	
Insertion loss	0.1 dB
Responsivity	0.8 A/W
Filter	
Type	Bessel Bandpass IIR
Order	4th
Centre Frequency	4 GHz
Passband Width	4 GHz
Electrical Amplifier	
Number of wavelengths	3,5
1dB Compression point	34 dBm
2nd order intercept point	45 dBm
3rd order intercept point	35 dBm
Power Gain	40 dB
Impedance	50 Ω

Table 5.2: Evaluation parameters: Simulation

arc-sinusoidal as has been previously considered, as shown in figure 5.11. Experimentally all spurious terms were recorded to allow comparison with the analytic results of section 5.4.1, which assume that only terms that fall exactly within the

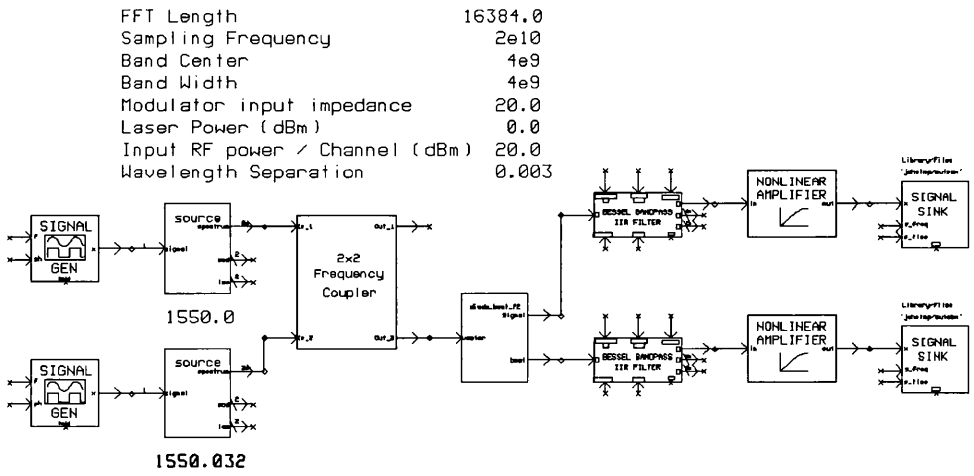

Figure 5.9: SPW block diagram of the experiment to beat two laser sources.

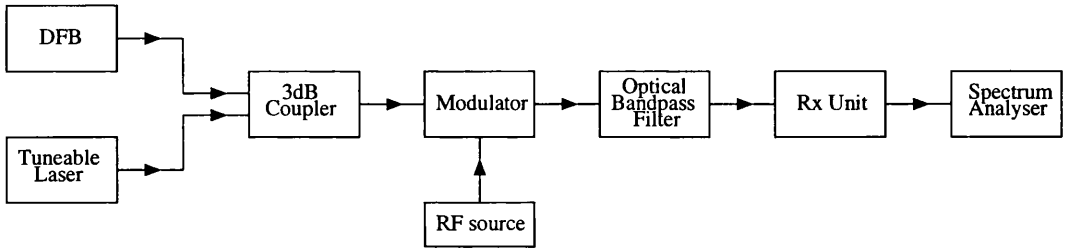

Figure 5.10: Experimental setup

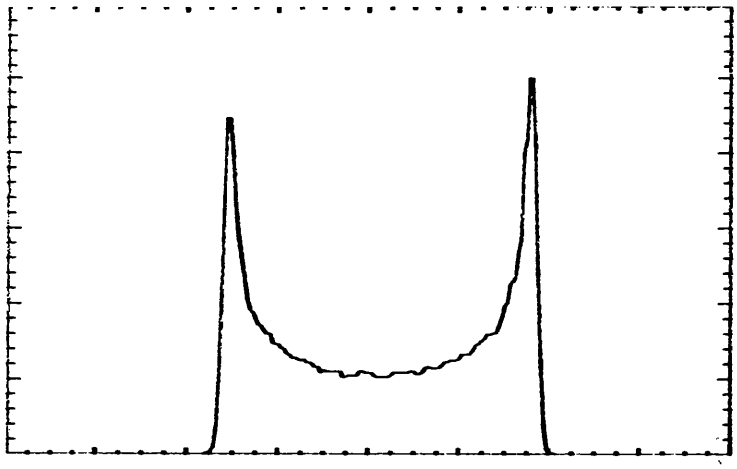

Figure 5.11: Histogram of interferometric beating

3dB pass band of the electrical receiver will contribute to the overall noise level in the system. This leads to sharp steps in the predicted performance as shown in figure 5.12 for a 4GHz signal and a 2-6GHz electrical passband. We see broad agreement between the analytical results and those recorded experimentally, except for the limiting SNR value the system reaches for large frequency separations. The most probable cause of this difference is noise elements within the system that have not been considered by the analysis, such as RIN, photoreceiver amplifier thermal noise, etc.

In practical systems the electrical response of the photoreceiver will not be an ideal bandpass characteristic but will roll off either side of the pass band. A limiting factor to the achievable minimum wavelength separation between sources will be the rate of this roll off, set by the order of the electrical filter used in the receiver. Due to the unavailability of comparable electrical filters, all terms were measured and their contribution scaled depending on the frequency at which they occurred using a Bessel filter response. Figure 5.13 demonstrates how the variation of the order of this Bessel function effects the SNR at higher laser separation frequencies. We see that adding two extra poles to the filter characteristic will increase the achievable signal to noise ratio by as much as 8dB.

5.4.4 Results

The simulation results presented here focus on problems encountered when multiple wavelengths fall on a single photodiode as described analytically in section 4.2. Here we consider 3 and 5 sources being received at a photo detector, using the parameters in table 5.2 for the simulations. The simulations used a system similar

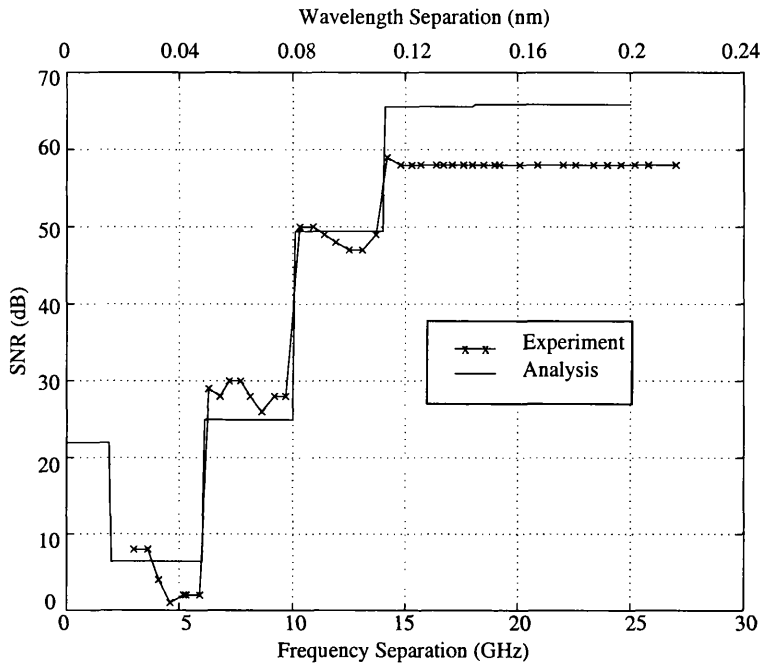

Figure 5.12: Analytic and experimental results of frequency separation against SNR for a 4GHz signal, 2-6GHz filter band.

to that shown in figure 5.9. The results of these simulations, figures 5.14 and 5.15, show as expected that SNR is dependent on the frequency separation between laser sources. This experiment assumes that all sources are separated by exactly the same amount. The PSD created by this beating is shown in figure 5.16 for a system with two sources separated in frequency by 4GHz. We see that the carriers create a beat term at 4GHz, while the sidebands form terms at d.c. and at 8GHz.

Figures 5.17 to 5.20 show the analytic results. Due to the assumption of negligible linewidth and rectangular filter shape the plots are not as smooth as would be expected, instead we see discontinuities between SNR levels resulting in a 'stair case' effect.

Figure 5.17 shows results taken over the same range of values as those adopted for the SPW simulations in figure 5.14. We see that for an SNR greater than

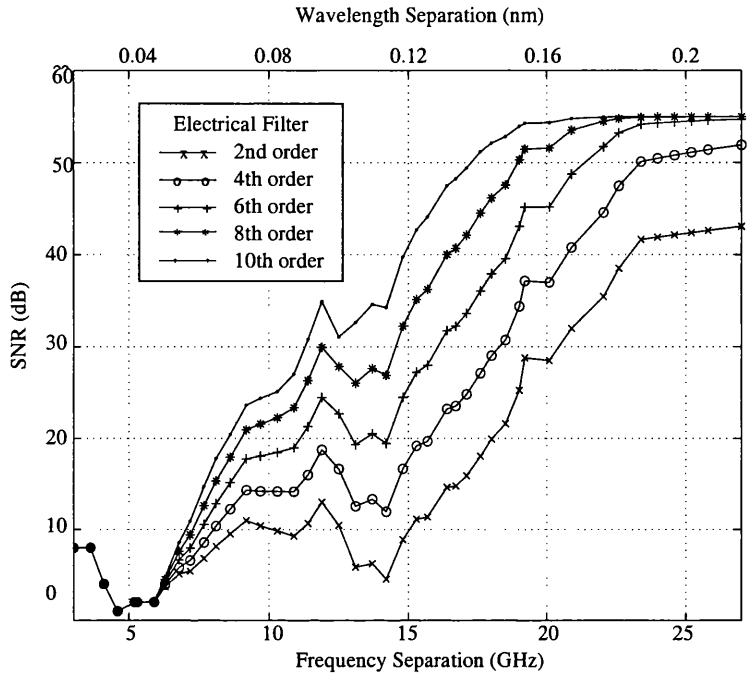

Figure 5.13: Experimental results of frequency separation against SNR for 4GHz signal, 2-6GHz filter band. Adjusted analytically for various electrical filter orders

70dB the spacing between optical carriers must be at least 3 times the electrical bandwidth. These results, formed assuming that all lasers are wavelength stable and equally separated, show as expected that the number of contributing sources is only of importance for very low separation. The closest two sources dominate the interference noise above ≈3GHz until the inherent system noise level is reached. As this level is controlled by the number of sources we can conclude that the system is shot noise limited.

While examining figures 5.17 to 5.18, it was noted that the increase in SNR seen is not as great as would be expected for the increase in channel numbers. Figure 5.19, showing the contributions plotted separately, demonstrates that as more signals are received the signal power does increase as expected but the noise contribution from the interferometric beat increases at a greater rate, with the result that the

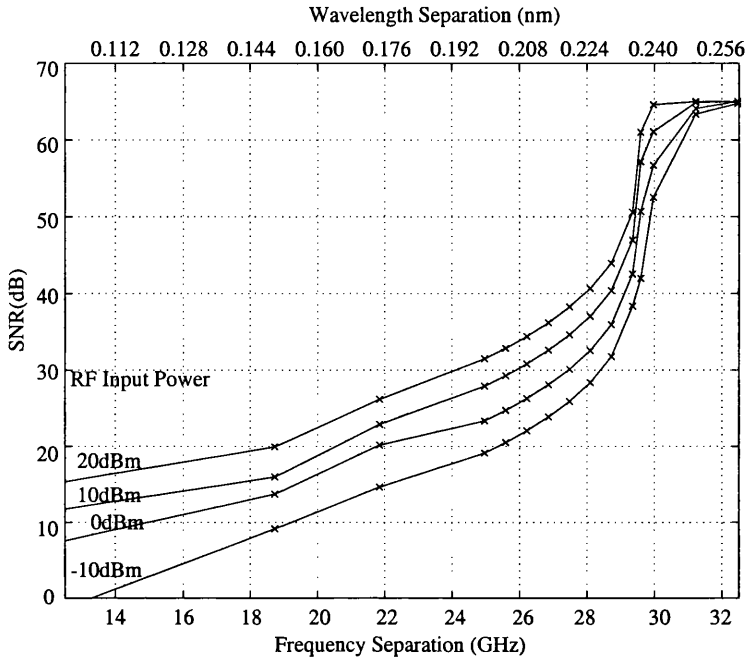

Figure 5.14: Frequency Separation against SNR for a 4GHz signal, filter band 2-6 GHz, with 3 sources.

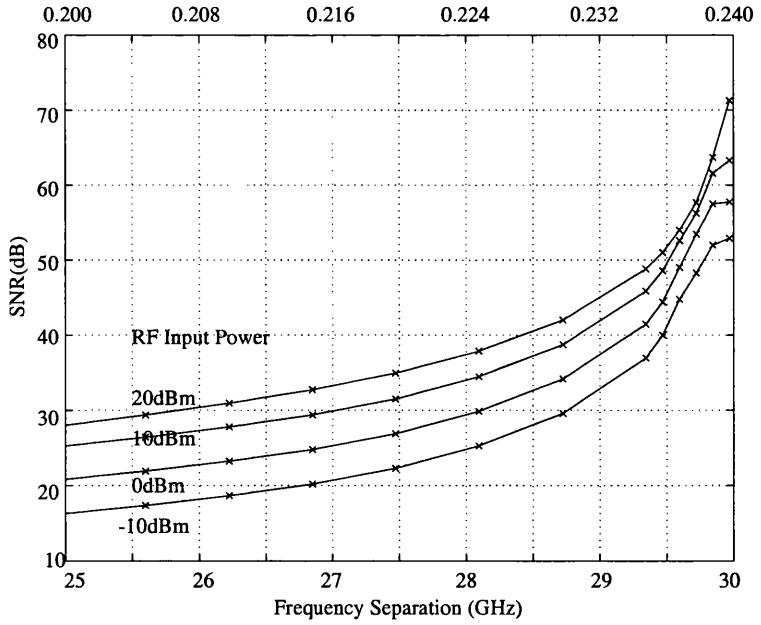

Figure 5.15: Frequency separation against SNR for a 4GHz signal, filter band 2-6 GHz, with 5 sources.

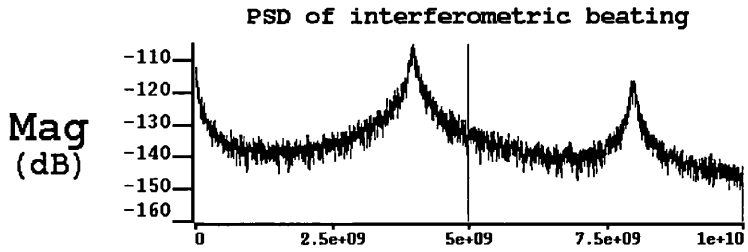

Figure 5.16: Power spectral density of the beat spectra of two laser sources separated by 0.032nm (4GHz).

increase in SNR that would be expected by a simple addition of powers method is not realised. This is shown with expanded vertical scales to enhance clarity in figure 5.20.

5.5 System Issues

As shown in the previous section the acceptable laser separation for a given SNR is determined by the electrical band required to be filtered at the receiver. If the highest frequency is 18GHz then each laser must be separated at all times by more than 54GHz (0.43nm) for acceptable operation. This will allow an absolute maximum of 80 wavelengths in the system (assuming 35nm EDFA bandwidth), although in practice, due to stabilisation factors, no more than 50/60 would be used. One option proposed by Alameh [63], is to down convert signals at higher bands so that they fall into a lower frequency band, thereby increasing the tolerance to laser separation. For a receive channel this does introduce added complexity. Although direct modulation of the Mach-Zehnder with the local oscillator has been proposed [63] there is still the problem of modulating all wavelengths with an accurately co-phased local oscillator to preserve the required phase information. With commercial

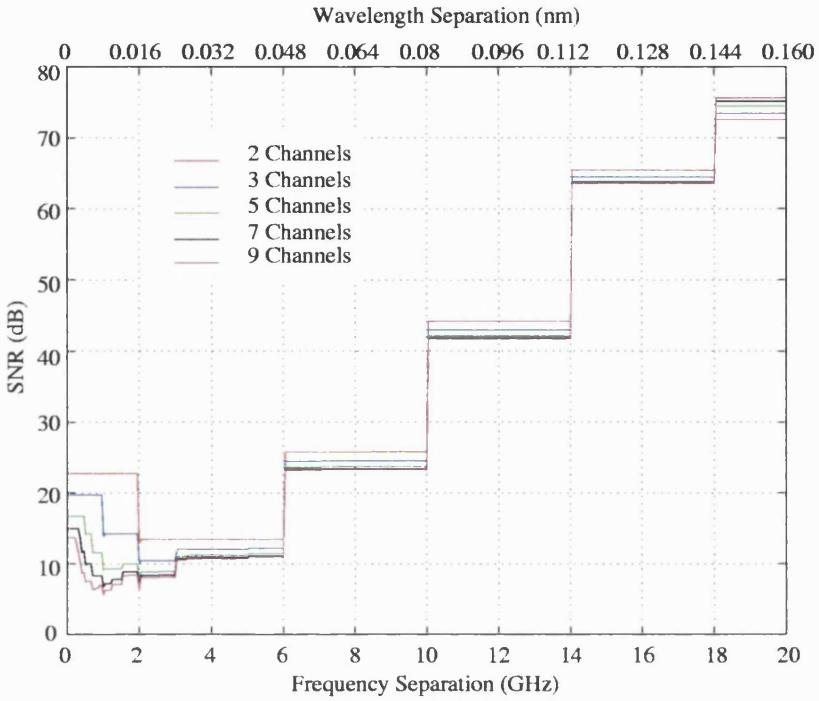

Figure 5.17: Frequency Separation against SNR for a 4GHz signal, filter band 2-6 GHz.

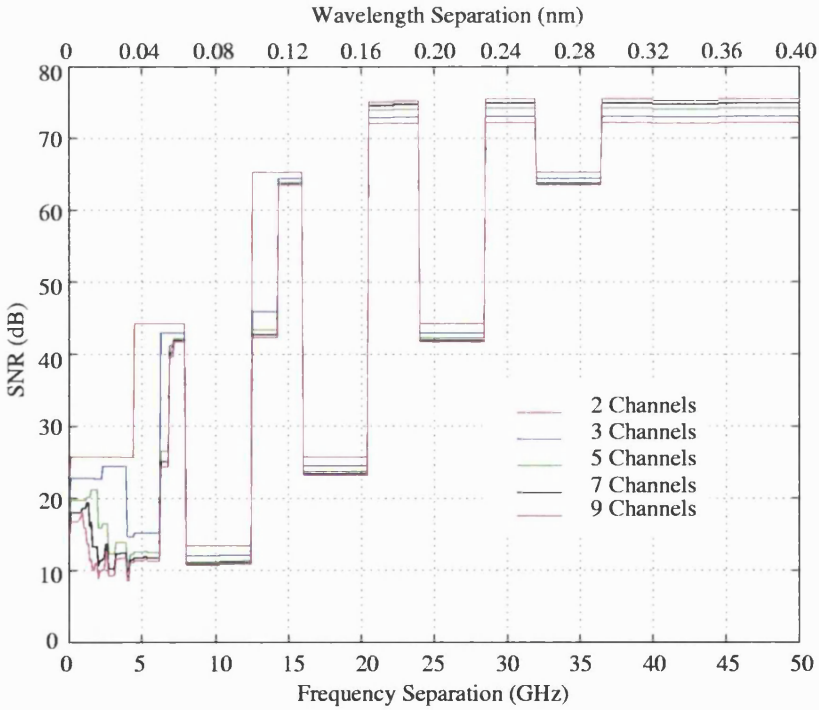

Figure 5.18: Frequency Separation against SNR, filter band 8-12.4 GHz, 8GHz signal

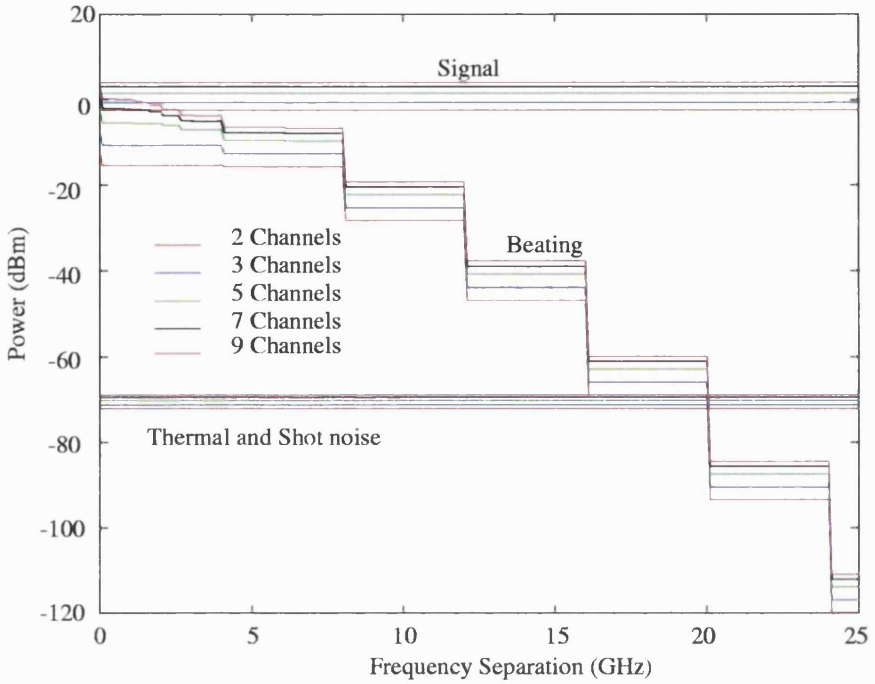

Figure 5.19: Frequency separation against Power for Signal, beating and noise.

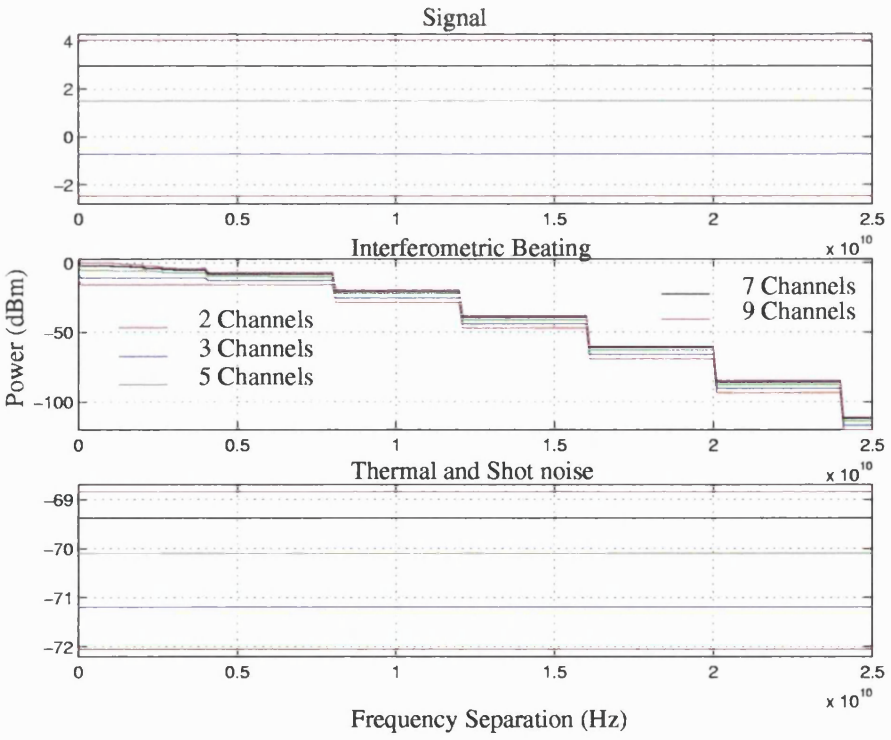

Figure 5.20: Frequency separation against Power for Signal, beating and noise. (Expanded vertical power)

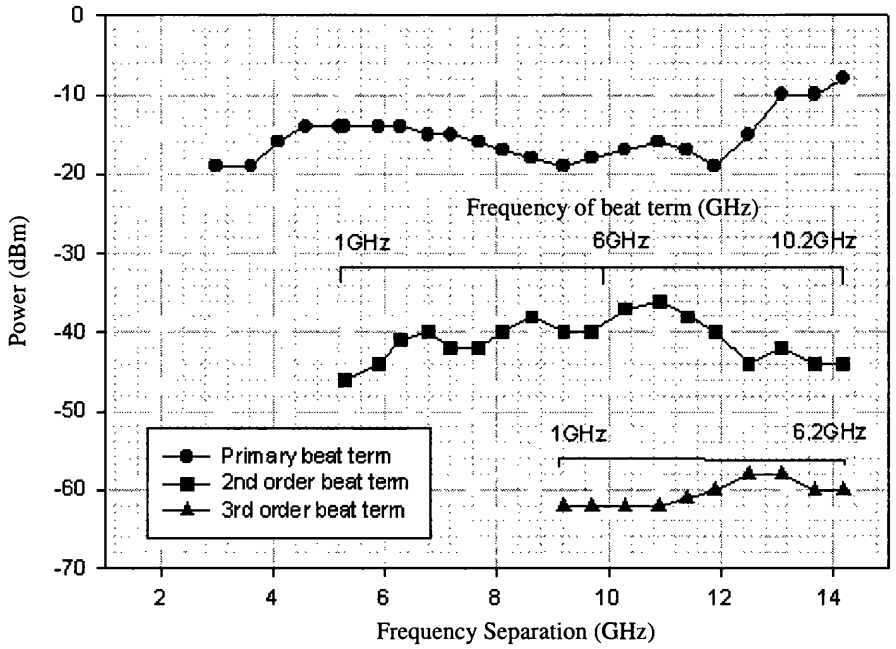

Figure 5.21: Relative power of beating terms

availability of wider band optical amplifiers such constraints would be eased.

5.6 Summary

In this chapter we have validated analytic methods using experimental results and investigated the effect of electrical filtering on the achievable laser wavelength separation. We explored how, in multi-wavelength networks proposed for next generation all optical beamforming networks, the wavelength separation between the laser sources must be carefully controlled if the required high signal to noise ratios are to be achieved. Scaling the results presented here it can be shown that for a system to operate over a 2-18GHz band then the laser separation must be greater than 0.43nm (54GHz@1550nm), allowing a maximum of 80 wavelengths in the 35nm EDFA window. We conclude that until extended band EDFAs become a

mature technology, an all optical beamforming network based on Bragg fibre grating WDM techniques will not provide the size of phase array commonly used without employing partitioning of the system.

Chapter 6

Spectrum Slicing in RF delivery Systems

6.1 Introduction

Since the technique of spectrum slicing was first conceived for local access systems the principle of using broadband light sources to produce a number of WDM channels has been considered for a large number of applications due to the potential cost and size benefits of this technique. A schematic showing the principle of spectrum sliced transmission is shown in figure 6.1. A broadband light source, for instance an LED, is split into a number of channels using a $1 \times N$ WDM demultiplexer. These channels are then individually modulated and multiplexed back into a single mode fibre.

Section 6.2 reviews the history of spectrum sliced systems from the early attempts to provide cheap access network links to today's research lab experiments of gigabits per second over many kilometres of fibre. We then discuss the application of spectrum sliced system to the transmission of RF, which leads to the enhanced

analytical characterisation in section 6.3. The associated experimental evaluation of these results is presented in section 6.4. From the findings of these last two sections we comment in section 6.5 on the applicability of spectrum slicing as a technology for the transport of RF signals in the types of beamforming networks described in chapter 5. Section 6.6 summarises the findings of this chapter.

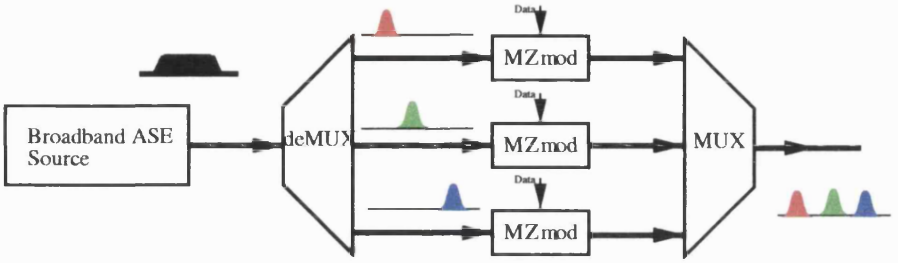

Figure 6.1: Schematic of a spectrum sliced WDM transmitter

6.2 Review of Spectrum Slicing

The first demonstrations of this technique used light-emitting diodes (LEDs), with one of the earliest in 1985 [64] reporting 40 channels at 50Mbit/s using 5 LEDs spread from $0.75\mu m$ to $1.55\mu m$ using a linewidth of 6.5nm. This showed the possibility of such a system but transmission using such a large spectrum prohibits anything more than final drop access network distances due to dispersion and other fibre effects. A taxonomy of several other papers reporting improved systems operating in a single optical window is presented in table 6.2

The use of LEDs for spectrum sliced systems was severely limited due to the low power capabilities of such devices. With the development of high power superluminescent diodes (SLDs) better results were produced, but while SLDs gave much

Capacity	Optical band (μm)	Band-width	Distance (km)	Comments	Ref
LED based systems					
40x50Mb/s	0.75-1.55	50nm	-		[64]
20x384kb/s	1.5	3 Å	9.7		[65]
4x2Mb/s	1.3	3.65nm	2.2		[66]
SLD based systems					
10x150Mb/s	1.280	0.7nm	7		[67]
16x50Mb/s	1.280	0.7nm	7		[67]
3x144Mb/s	1.55	2.4nm	-	SLD & EDFA	[68]
Optical amplifier based systems					
4x622Mb/s	1.55	0.23nm	-	ASE from SOA	[69]
1.7Gb/s	1.55	0.6Å	94		[70]
1.7Gb/s	1.55	1nm	165	DSF	[71]
1.7Gb/s	1.56	0.68nm	-	EDFL	[72]
2.5Gb/s	1.57	1.8nm	200	DSF & EDFL	[73]
2.5Gb/s	1.56	0.23nm	-	Feedforward noise reduction	[74]
30x622Mb/s	1.53-1.562	0.4nm	-		[75]
4x2.5Gb/s	1.55	0.1nm	240	DSF, nonlinear bandwidth expansion	[76]

Table 6.1: Comparison of spectrum slicing systems

improved performance they still suffered from the same launch power problems of LEDs. However, in the early 90's with the advent of the erbium-doped fiber amplifier as a mature technology, rare earth-doped fiber sources were used to produce high power, broadband amplified spontaneous emission (ASE). Fibre sources have a great advantage over LEDs/SLDs as they are already in single mode fibre format such that they can have almost negligible coupling losses. These sources have somewhat changed the view that spectrally sliced systems are only of real use over the small distances encountered in the access network.

However, in such systems there are a number of considerations that are usually neglected in laser based systems. Due to the incoherent nature of the light produced,

excess noise caused by the beating between the constituents of the optical carrier produces severe limitations on the achievable signal to noise ratio. Unlike systems with coherent laser diodes, in spectrum sliced systems the optical bandwidth must be much greater than the bit rate. Because of this larger linewidth, dispersion becomes an important factor for even relatively short distances causing an increase in excess noise [77]. This is because dispersion spreads the pulse over more that the bit period thereby narrowing its spectrum which corresponds to an increase in excess noise.

6.3 Analytic Characterisation

To a first approximation the signal to noise ratio of a spectrum sliced ASE source is given by [78]:

$$\mathrm{SNR}_{ex} = \frac{mB_o}{2B_e} \tag{6.1}$$

For unpolarised light m=2, for polarised light m=1: B_o and B_e are the optical and electrical bandwidths respectively, defined as:

$$B_o = \frac{\left[\int_{-\infty}^{\infty} H_o(f)\mathrm{df}\right]^2}{\int_{-\infty}^{\infty} H_o^2(f)\mathrm{df}} \tag{6.2}$$

$$B_e = \frac{\int_{-\infty}^{\infty} |H_e(f)|^2\mathrm{df}}{H_e^2(0)} \tag{6.3}$$

where $H_o(f)$ and $H_e(f)$ are the optical and electrical filter frequency characteristics.

Following P.S.Henry [79], we examine how the approximation of equation (6.1) is formed and then consider how accurate this is for spectrum sliced systems transporting RF.

The spontaneous emission power in the optical bandwidth B_o is given by:

$$P_{sp} = N_{sp}B_o \tag{6.4}$$

where N_{sp} is the power spectral density of the ASE used. We can write the electric field $E_{sp}(t)$ associated with this power as a sum of cosine terms.

$$E_{sp}(t) = \sum_{k=-B_{ase}/2\delta v}^{B_{ase}/2\delta v} \sqrt{2N_{sp}\delta v}\cos\left[(\omega_o + 2\pi k\delta v)t + \phi_k(t)\right] \tag{6.5}$$

where ϕ_k is the random phase of each component, B_{ase} is the ASE bandwidth, δv is the nominal separation between terms and ω_o is the optical centre frequency of ASE. Photodetection gives:

$$i(t) = \overline{E_{sp}^2(t)}\mathbf{R} \tag{6.6}$$

where $\mathbf{R}$ is the photodiode responsivity. Defining $M = B_o/2\delta v$ gives the received

photocurrent as:

$$i(t) = 2N_{sp}\delta v\mathbf{R}\left[\sum_{k=-M}^{M}\cos\left[(\omega_o + 2\pi k\delta v)t + \phi_k(t)\right]\right]^2$$
$$= 2N_{sp}\delta v\mathbf{R}\left[\sum_{k=-M}^{M}\cos(\beta_k)\sum_{j=-M}^{M}\cos(\beta_j)\right] \quad (6.7)$$

where $\beta_k = (\omega_o + 2\pi k\delta v)t + \phi_k(t)$

$$\beta_j = (\omega_o + 2\pi j\delta v)t + \phi_j(t) \quad (6.8)$$

Ignoring frequencies at $\sim 2\omega_o$ we can reduce equation (6.7) to :

$$i_{sp-sp}(t) = N_{sp}\delta v\mathbf{R}\sum_{k=0}^{2M}\sum_{j=0}^{2M}\cos[(k-j)2\pi\delta vt + \phi_k(t) - \phi_j(t)] \quad (6.9)$$

To find a signal to noise ratio we must now split equation (6.9) into signal and noise components. However, there is no signal in equation (6.9), the assumption is made in [77] that any signal carried would be formed by the dc part while the time-varying ac part contributes the noise. The dc term is formed when $k = j$, and as there are $2M$ such terms the photo current is:

$$i_{dc} = 2M\delta vN_{sp}\mathbf{R} \quad (6.10)$$

giving a single sided electrical power density of:

$$P_{dc} = [\mathbf{R}N_{sp}B_o]^2 \quad (6.11)$$

Due to the nature of the summation the noise component can be shown to produce

a triangular shaped power density, which near to dc is approximated as:

$$P_{ac} = \frac{2^2 N_{sp}^2 \delta v \mathbf{R}^2}{2} \left(\frac{B_o}{\delta v} - 1 \right) \tag{6.12}$$

$$\approx 2 N_{sp}^2 B_o B_e \mathbf{R}^2 \tag{6.13}$$

From (6.11) and (6.13) we form for a single polarisation a signal to noise ratio of:

$$\text{SNR} = \frac{\mathbf{R}^2 N_{sp}^2 B_o^2}{2\mathbf{R}^2 N_{sp}^2 B_o B_e} = \frac{B_o}{2B_e} \tag{6.14}$$

The process of deriving equation (6.1) in this fashion demonstrates the assumptions made (quantum laws give the same answer). We now investigate the noise power spectrum if an RF signal is modulated onto the optical slice. We take as a starting point equation (6.5) this time modulated by a signal $m(t)$:

$$E(t) = \Big(1 + m(t)\Big) \sum_{k=-M}^{M} \sqrt{2 N_{sp} \delta v} \cos \Big[(\omega_o + 2\pi k \delta v)t + \phi_k(t) \Big] \tag{6.15}$$

where $m(t)$ is defined to be:

$$m(t) = \alpha \cos(\omega_{rf} t) \tag{6.16}$$

Photodetection using the relationship of equation (6.6) produces:

$$i(t) = 2 N_{sp} \delta v \mathbf{R} (1 + m(t))^2 \sum_{k=-M}^{M} \sum_{j=-M}^{M} \cos[(k-j)2\pi \delta v t + \phi_k(t) - \phi_i(t)] \tag{6.17}$$

Substituting (6.16) into (6.17) and expanding terms gives:

$$
\begin{aligned}
i(t) = N_{sp}\delta v\mathbf{R}\Bigg\{ & 3\sum_{k=0}^{2M}\sum_{j=0}^{2M}\cos[(k-j)2\pi\delta v t + \phi_k(t) - \phi_j(t)] \\
& +\alpha^2\sum_{k=0}^{2M}\sum_{j=0}^{2M}\Bigg[\cos\left[\left((k-j)2\pi\delta v - 2\omega_{rf}\right)t + \phi_k(t) - \phi_j(t)\right] + \\
& \qquad \cos\left[\left((k-j)2\pi\delta v + 2\omega_{rf}\right)t + \phi_k(t) - \phi_j(t)\right]\Bigg] \\
& +\alpha\sum_{k=0}^{2M}\sum_{j=0}^{2M}\Bigg[\cos\left[\left((k-j)2\pi\delta v - \omega_{rf}\right)t + \phi_k(t) - \phi_j(t)\right] + \\
& \qquad \cos\left[\left((k-j)2\pi\delta v + \omega_{rf}\right)t + \phi_k(t) - \phi_j(t)\right]\Bigg]\Bigg\}
\end{aligned}
\tag{6.18}
$$

If a DFB laser were employed in this system the linewidth would be small enough so that the terms at dc and $2\omega_{rf}$ would not extend into the passband. However, with the optical source bandwidth much greater that the electrical bandwidth there are now three noise components, each with triangular single sided distributions, contributing as demonstrated pictorially in figure 6.2.

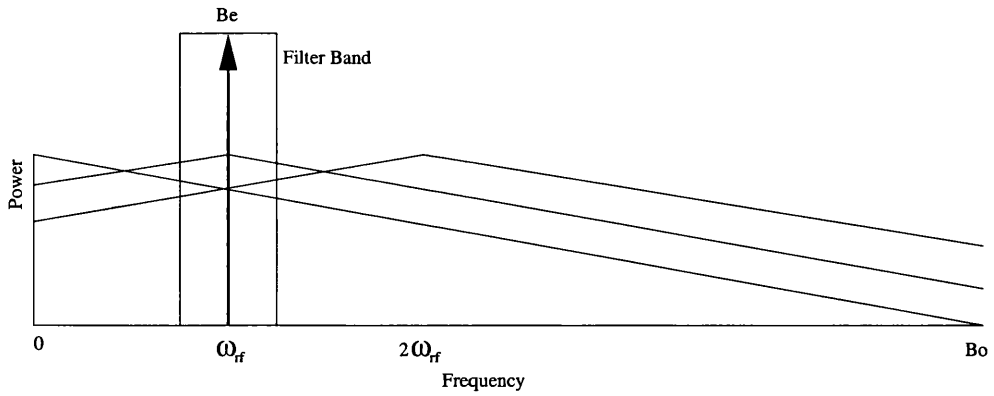

Figure 6.2: Example of noise spectra in spectrum sliced system with RF modulation

The signal is again:

$$P_{sig} = [\mathbf{R}N_{sp}B_o]^2 \tag{6.19}$$

However the noise current is:

$$\begin{aligned} i_{noise}(t) = N_{sp}\delta v\mathbf{R}\Bigg\{ & 3\sum_{k=0}^{2M}\sum_{j=0}^{2M}\cos[(k-j)2\pi\delta vt + \phi_k(t) - \phi_j(t)] \\ & +\alpha^2\sum_{k=0}^{2M}\sum_{j=0}^{2M}\Big[\cos\big[\big((k-j)2\pi\delta v - 2\omega_{rf}\big)t + \phi_k(t) - \phi_j(t)\big] + \\ & \cos\big[\big((k-j)2\pi\delta v + 2\omega_{rf}\big)t + \phi_k(t) - \phi_j(t)\big]\Big] \\ & +2\alpha\sum_{k=0}^{2M-1}\sum_{j=k+1}^{2M}\Big[\cos\big[\big((k-j)2\pi\delta v - \omega_{rf}\big)t + \phi_k(t) - \phi_j(t)\big] + \\ & \cos\big[\big((k-j)2\pi\delta v + \omega_{rf}\big)t + \phi_k(t) - \phi_j(t)\big]\Big]\Bigg\} \end{aligned} \tag{6.20}$$

For the excess noise centred at dc and $2\omega_{rf}$, near ω_{rf} there will be $(2M - \omega_{rf}/\mathrm{dv})$ terms while the component at ω_{rf} will create $(2M-1)$ terms. Therefore the noise power spectral density can be approximated by the same rationale used to form (6.13), whence:

$$P_{noise} = \mathbf{R}^2N_{sp}^2(11B_o - 7\omega_{rf})B_e \tag{6.21}$$

giving an SNR of:

$$\mathrm{SNR} = \frac{\mathbf{R}^2N_{sp}^2B_o^2}{\mathbf{R}^2N_{sp}^2(11B_o - 7\omega_{rf})B_e} \tag{6.22}$$

$$= \frac{B_o^2}{(11B_o - 7\omega_{rf})B_e} \tag{6.23}$$

This analytic result is compared to the results given by experimental evaluations in the next section.

6.4 Experimental Evaluation

To examine the validity of the models presented thus far experiments were conducted, the experimental configuration indicated in figure 6.3 used to measure the performance of transmitting a RF signal using a slice of light from an amplified EELED source. Preliminary experiments were carried out to characterise the optical and electrical filters. Figure 6.4 shows the ASE spectrum produced by the optical amplification of the EELED. The optical power output was measured to be a maximum of +3dBm before saturation of the EDFA occurred. Figure 6.5 shows the ASE spectrum after filtering by a 3.65nm filter and a 0.89nm Fabry Perot filter respectively. To confirm the previous assertions we examined the probability

Figure 6.3: Experimental setup for spectrum slicing of incoherent light.

density function of this slice of ASE, as shown in figure 6.6. we see that it is of approximately Gaussian form as expected. This justifies the widely used assumption that amplified spontaneous emission can be approximately modelled as band limited white thermal noise.

The experiment was set up initially as shown in figure 6.3 allowing examination of the excess noise in the RF band without any external RF noise being introduced. In this configuration the EELED has an optical output of -16.6dBm, the EDFA in-

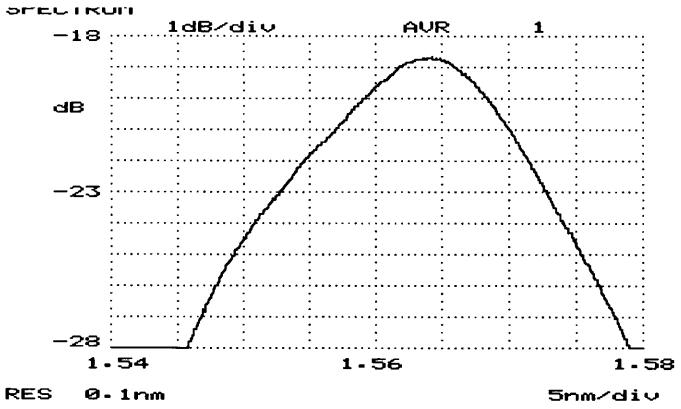

Figure 6.4: Amplified ASE spectrum.

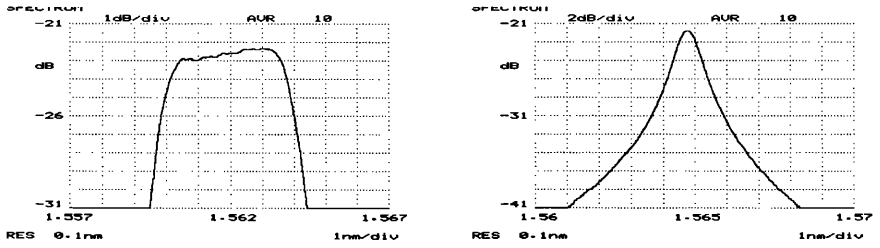

(a) 3.65nm Filter (b) 0.89nm Fabry Perot filter

Figure 6.5: Spectrum sliced ASE

troduces an optical gain of 19.6 dB before saturation occurs. The slicing at 3.65nm and 0.89nm incurs losses of 9.3dB and 14.1dB respectively. Of these losses approximately 1.5dB is due to the insertion loss inherent in the filters, the remainder being slicing loss, due to the band limiting of the wide band ASE spectrum.

Examining the noise floor observed we find, as expected, that the noise power is conditioned by the bandwidth of the spectrum analyser and not by any electrical filters in the RF path. Using this set up with an electrical filter of bandwidth 630MHz centred at 7.5GHz, the combined effect of excess, thermal and shot noise was measured. Removing the optical signal completely gives the noise floor due to

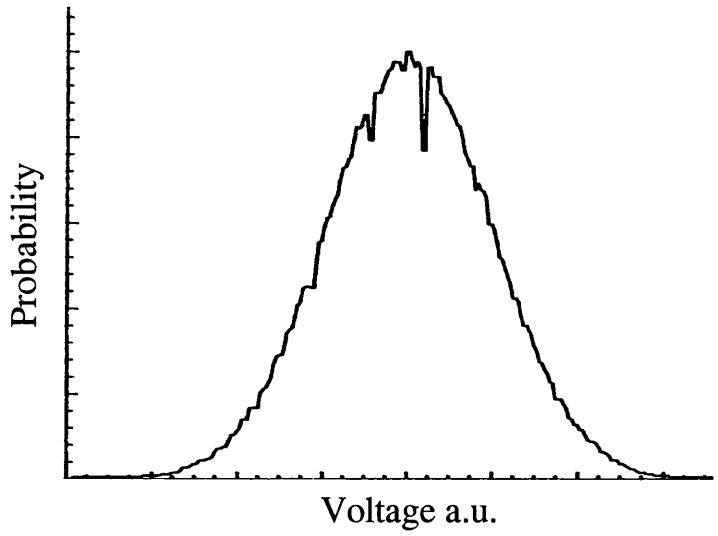

Figure 6.6: Probability Density of ASE noise.

thermal noise. To find the noise floor due to thermal and shot noise an unmodulated laser source was used set to the same optical power as the measured power in the optical slice at the receiver. The noise floors caused by both the excess noise and the thermal noise are shown in figure 6.7 for an optical input of -1dBm. The noise floor due to excess noise is -55dBm while the thermal noise creates a floor of -68dBm. The noise level below that is inherent to the electrical spectrum analyser at -73dBm.

Inserting a modulator to create the configuration of figure 6.8 we investigate the effect of having an RF signal of 20dBm modulated onto the optical carrier. The signal of figure 6.9 was observed for a received optical power of -4.7dBm, with the excess noise floor clearly visible with the RF signal at 7.5GHz in the centre of the band. The excess noise floor can be seen to have lowered slightly for the modulated case due to the received optical power being 4dB lower. Reducing the unmodulated optical power to a similar level produced identical excess noise floor levels.

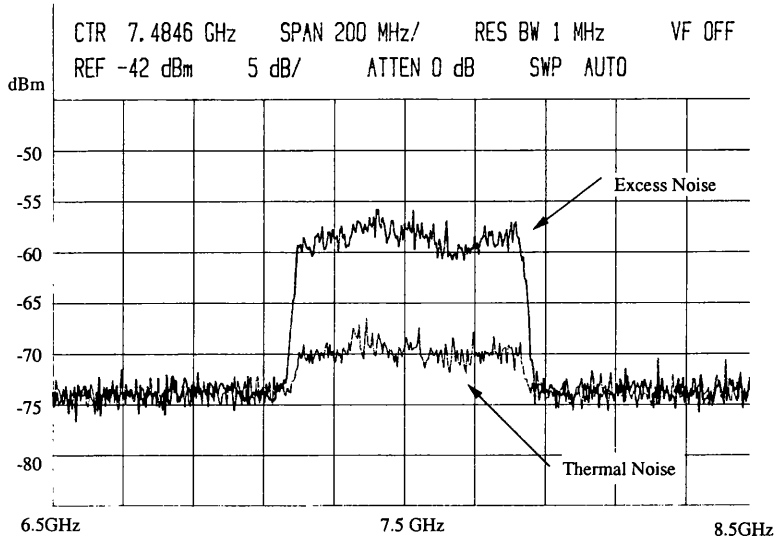

Figure 6.7: Noise floor due to excess and thermal noise.

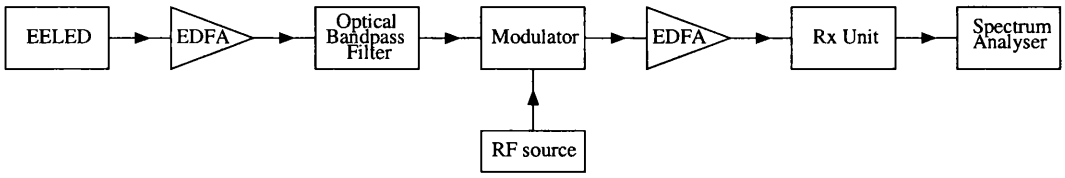

Figure 6.8: Experimental setup for transmission of RF using incoherent light.

With this set up the signal to noise ratio due to the optical excess noise in the system was measured. Although the results of the analytic evaluation suggest that the noise level is independent of signal power this is obvious only true over a limited range of values, a view which is reinforced by the results presented in figure 6.10. This shows that for received power levels above -6dBm the signal to noise level is power independent, while below this level the other noise sources present at the detector begin to dominate, resulting in a drop in SNR.

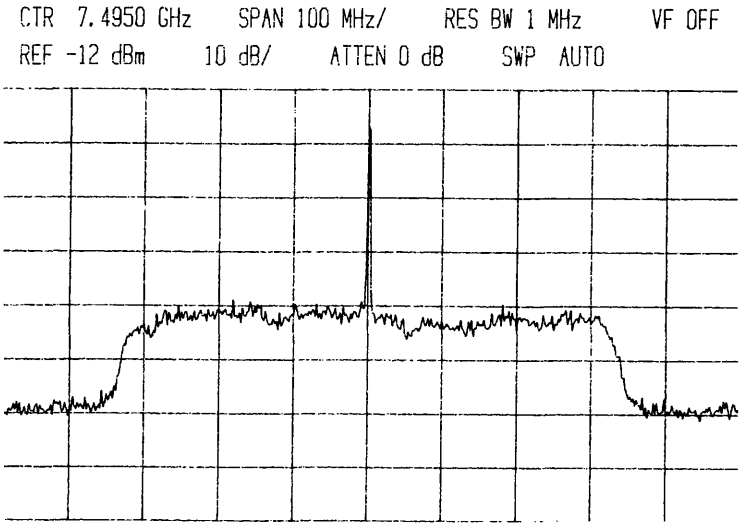

Figure 6.9: Noise floor and RF signal.

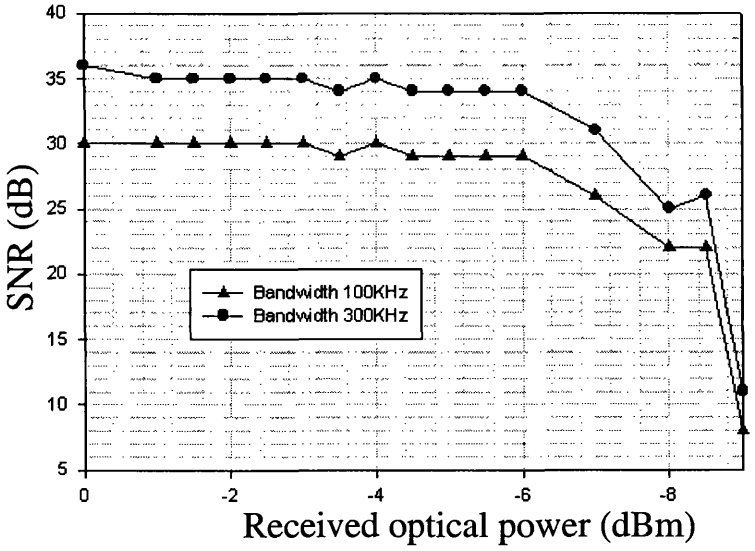

Figure 6.10: Optical power received against SNR for 3.65nm slice.

6.5 Application of Spectrum Slicing

It has been documented that 'a basic limitation of high bit rate transmission using ASE is that the detected signal-to-excess noise ratio (SNRex) of continuous ASE is independent of signal level and for a given detection bandwidth can only be

increased by increasing the spectral width of the source' [77]. This is due to the nature of excess noise, being spontaneous-spontaneous beating between components of the ASE light source. The first aim was to investigate the applicability of spectrum sliced systems for the beamforming networks detailed in chapter 5. From figure 6.11 we see that if the bandwidth of the electrical signal transmitted is 4GHz as suggested for certain beamforming systems then using the first approximation of (6.1) the best signal to noise ratio we can hope for with an optical bandwidth of less than 3nm is 20dB, allowing at maximum only 8 distinct wavelengths to be used in the system.

It should be noted that calculating the electrical signal bandwidth for radar transmission systems is not necessarily obvious. If we were considering a single radar signal which typically consists of a high frequency oscillation (4GHz), modulated by a sequence of pulses, we can consider the characteristic frequency spectrum to be a sinc function centred at the oscillation frequency f_{RF}. Therefore the majority of the signals power is concentrated in the centre lobe which has a relatively narrow bandwidth of the order of 1/(pulse width), an illustrative representative value being 1MHz. If it were possible to pass only this section of the received spectrum then we can see from figure 6.11 that we may predict that systems with 50dB SNR are possible using this arrangement.

There are a number of considerations that may limit the practical application of spectrum slicing, depending on the specific values involved. For 50dB SNRex at 1MHz the optical bandwidth predicted is 1nm which with the usual guard bands would allow at most 20 distinct wavelength channels within the (≈35nm) EDFA bandwidth, although at such a large bandwidth dispersion would certainly induce penalties and restrict the maximum system reach.

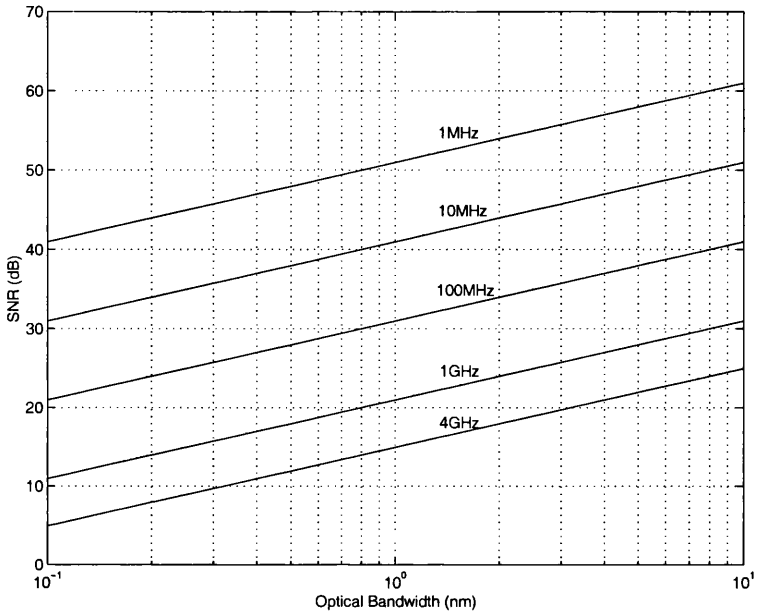

Figure 6.11: Optical Bandwidth against SNR for spectrum sliced systems

Plotting together the results of the detailed analytic and experimental evaluations produce the results of figure 6.12, which can be seen to deviate from the values predicted by the basic theory (6.1) by more than an order of magnitude. As we have noted previously this approximation makes a number of assumptions that are not valid for the case in question. The main deviations for RF systems are:

1. The simple theory considers the electrical passband to be at baseband while we must consider a passband centred at RF for the systems now under examination.

2. The simple theory considers only an unmodulated CW source.

The more rigorous analytic analysis developed here shows that modulation causes other noise terms to be present which can significantly degrade the performance of the system. The results in figure 6.12 show that compared to the basic approxi-

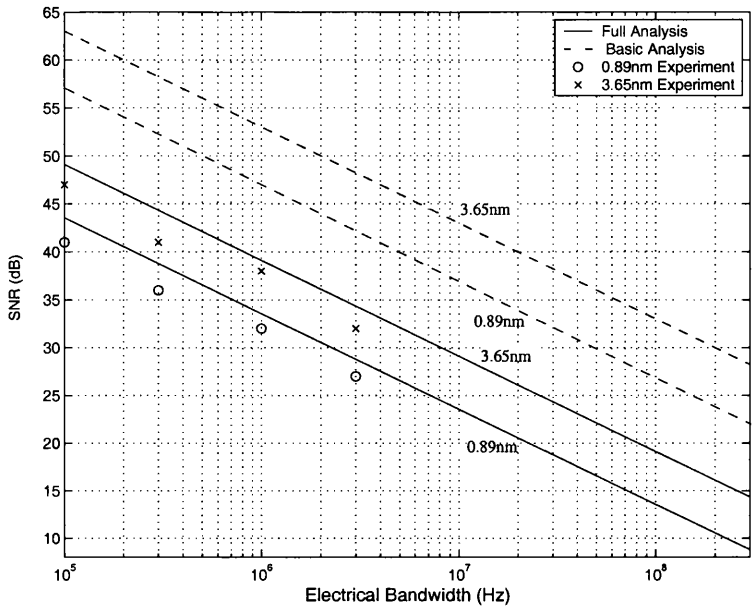

Figure 6.12: SNR against bandwidth measured at 7.5GHz

mation the new, RF system-specific, analysis is closer to the results predicted by experiment for wide bandwidth signals.

With reference to the beamforming networks discussed in chapter 5, unless a method is found to reduce the optical bandwidth to nearer to 0.1nm (comparable to a laser linewidth of 12GHz) by either electrical bandwidth or SNR tolerance reduction then the use of spectrum slicing in the unpartitioned system (figure 5.2) would restrict the system to a very small number of array elements. The hybrid system (figure 5.1) is still a viable option for further research but tolerances could still be prohibitively tight if any large scale system were proposed. Further investigation of this method is still required, especially in regards to the effect very high power broadband optical sources may have on the performance of the system.

6.6 Summary

In this chapter we have considered the application of a technique known as spectrum slicing to the transport of RF signals. We have shown that the approximation often used for spectrum sliced systems is inappropriate for high frequency analogue signals, with this conclusion confirmed by experimentation. From our findings we comment on the applicability of this technology to the beamforming networks of chapter 5, concluding that in its basic form it is not possible to achieve the high signal to noise ratios required.

Chapter 7

Conclusion

7.1 Thesis Summary

In this thesis we have considered aspects of noise in optical systems related to the phenomenon of interferometric beating and the implications for system performance. We have studied the impact of interferometric noise in WDM optical links, considering the effect system parameters such as extinction ratio, crosstalk-crosstalk beating and unequal component isolation have on performance. This investigation was extended beyond simple IM-DD modulation, to consider the benefits of QAM schemes with particular application to hybrid fibre radio systems.

The techniques developed were then applied to optical beamforming networks which have been suggested as a means of achieving the true time delay function required to avoid 'squint' in phased array antenna applications. It was indicated that these networks are also degraded by interferometric beating between the wavelength components summed to give the total beam signal and a qualitative formulation for this was provided for apparently the first time. The system performance was demon-

strated for a network architecture, and possible system refinement were proposed to facilitate the realisation of such networks.

Finally, optical spectrum sliced systems were considered. Although not perhaps an obvious parallel, the inherent noise in spectrum sliced system is in fact due to the interferometric beating between the incoherent components that form the light source and so had close similarities with IN. We derive a new, more accurate analytical representation for the signal to noise ratio of spectrum sliced systems that transport RF signals. From this analysis and experimental evaluation it was possible to comment qualitatively on the possible application of spectrum sliced systems to the beamforming networks investigated in chapter 5.

7.2 Main Contributions of this thesis

The work for this thesis was concerned with evaluating performance of optical systems which are degraded by interferometric noise or related phenomenon. This can be categorised in three main areas:

Interferometric noise in WDM optical networks

- A number of evaluation methods for interferometric noise were compared and contrasted, and the relative strengths and weaknesses of these were demonstrated.

- An extension of the most applicable method, a modified Chernoff bound formulation, was developed to encompass a wide range of important system performance concerns.

- It was shown that the Gaussian approximation predicts a non-existent trend when studying systems with an increasing number of interferers and systems that include non-zero extinction ratio.

- Systems with un-equal interfering powers were considered, including the use of the new extended formulation to demonstrate error bounds and reveal the effect that dominant interferers have on system performance.

- The applicability of the MCB based technique was demonstrated using a case study of the MWTN architecture.

- The effect of interferometric noise on systems designed to transport QAM data was investigated, considering both baseband QAM and radio-over-fibre QAM delivery systems. It was established that QAM has a higher tolerance to the interferometric noise than 'baseband' binary systems.

The evaluation of the performance of optical beamforming networks for phased array antennae systems.

- The beating effects in proposed optical beamforming network architectures were evaluated.

- Simulation and analytic methods, coupled with experimental validation, were presented to described the limits of the particular method with respect to component parameters presently available.

- An appraisal of carrier suppression for application in such systems was conducted.

The applicability of spectrum sliced systems for radar delivery.

- The applicability of the technique of spectrum slicing for the delivery of high frequency signals was explored experimentally, supported by analytical investigation.

- New analytic formulations specific to optical fibre supported RF systems were presented, which show good agreement with experimental results.

- It was shown that the application of spectrum slicing of an incoherent source to transport multi channel signals for beam-steering applications is conditioned by a complex set of constraints involving:

  - required optical bandwidth, constrained in practice by the EDFA window;
  - required electrical signal bandwidth;
  - number of antennae elements and so WDM channels, related to the resolution required;
  - the signal to noise ratio required

  In particular, it was established that for high quality, wide-band radar purposes the demanding resolution and signal to noise ratio requirements cannot be met with the proposed spectrum sliced system.

7.3 Suggestions for further work

A number of further areas for investigation are suggested as a result of the work performed here, including:

- Extend the study of interferometric noise to a wider set of modulation schemes, for example PSK and QPSK.

- Consider impairments of the radio channel in the evaluation of radio-over-fibre QAM systems.

- Consider the applicability of partitioned beamforming networks, specifically with reference to spectrum-sliced transmission networks with a view to evaluating the beat noise performance implications of extended architectures.

- Evaluate more comprehensively the possible use and attainable performance of spectrum slicing for use in radio over fibre systems.

Appendix A

SPW Blocks

This appendix provides a brief summary of the key features of various SPW 'custom-coded' blocks developed to support the simulation of optical fibre networks and systems.

A.1 Optical Coupler

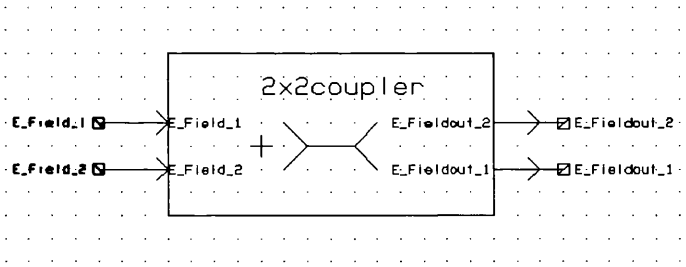

Module names	2x2f
	3x2f
	4x2f
	5x2f
Library	jmgec

These blocks model the action of NxN optical star couplers by combining multiple wavelengths on different fibers onto a single fiber output. In the context of this simulation model this equates to appending together the input vector to create a single of vector from all the inputs.

Operation

This block takes in N vectors containing both FFT and wavelength information and 'butts' them together as discussed in section 2.3.1. If the FFT length is k, then each input will be of length $2k$ and the over all length of the output vector will be $2Nk$.

Parameters

Parameter Name	Description
fft_length	Length of FFT Vector
s_freq	Sampling Frequency
ex_loss	Excess Loss (dB)
sp_loss	Splitting Loss (dB)
c_ratio	Input Coupling ration

Ports

Port Name	Description
in_1	First Input
in_2	Second input
Out_1	Combined Output
Out_2	Combined Output

A.2 Optical Circulator

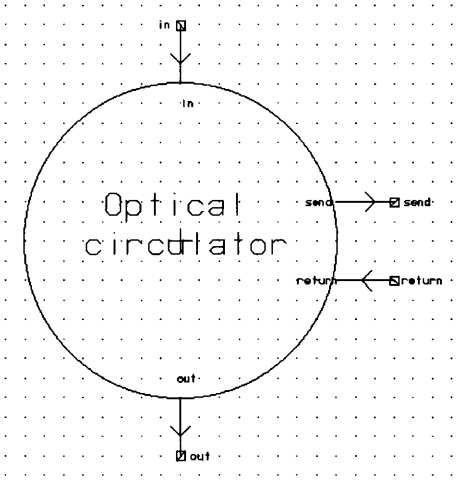

Module names	circulator*n*
Library	jmgec

Optical Circulator: A three or four port non-reciprocal transmission device. We can assume that such a device is wavelength independent over the typical bandwidth of an EDFA. It is characterised by insertion loss, isolation and return loss, with values of 1.63dB, 60dB and 55.6dB respectively having been demonstrated [80]. These terms are defined as: *Insertion Loss*, from input to output port; *Return Loss*, from output (return) port to input; *Isolation* between first input port and second output port.

Operation

This model assumes the parasitic crosstalk between ports to be equal. The input port routes signals to the send port after insertion loss, and also leaks the input signal to the output port as controlled by the crosstalk level. Then return port is also scaled by the insertion loss and fed to the output.

Parameters

Parameter Name	Description
fft_length	Length of FFT Vector
s_freq	Sampling Frequency
in_loss	Insertion Loss (dB)
xtalk	Crosstalk isolation value (negative) (dB)

Ports

Port Name	Description
in	First Input
send	Send terminal of bidirectional fiber port
return	Return terminal of bidirectional fiber port
out	Output terminal.

A.3 Fiber Bragg Grating

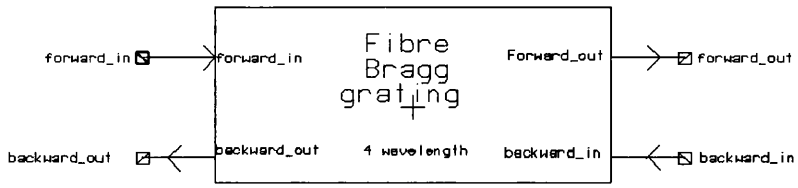

Module names	grating*n*
Library	jmgec

Operation

This block considers the wavelength of each component of the frequency spectra and then forms reflection and transmission components determined by the parameters *reflect_pass, reflect_reflect, trans_pass, trans_reflect.* A variation of this block uses a lookup table to determine the reflection and transmission components, with reference to the separation between the wavelength component and the centre of the grating response. The look up file was created using a detail analysis of the fiber grating in MATLAB.

Parameters

Parameter Name	Description
fft_length	Length of FFT Vector
delay	Grating delay (*ps*) between this grating and the last
bandwidth	Optical bandwidth of the grating (*nm*)
f_cent	Grating centre frequency (*nm*)
reflect_pass	Pass band reflection of grating
reflect_reflect	Out of band reflection of grating
trans_pass	Pass band transmission of grating
trans_reflect	Out of band reflection of grating

Ports

Port Name	Description
forward_in	Forward propagating input (for last grating)
forward_out	Forward propagating output (to next grating)
backward_in	Backwards propagating input (return channel)
backward_out	Backwards propagating output (Towards circulator)

A.4 Mach-Zehnder Modulator

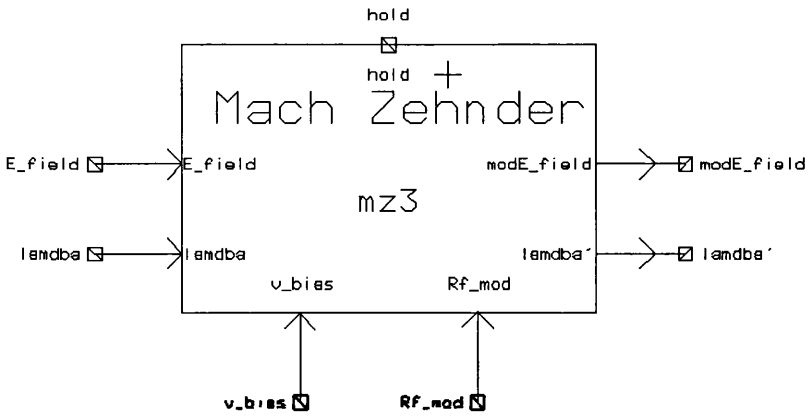

Module names	mz3
Library	jmgec

Operation

This block modulates the laser field with the signal present at the input RF_mod using the transfer characteristic described in section 2.2.4. The MZ modulator is considered as a balanced arm modulator with equal and opposite drive voltages. Modulation excess loss is included in the model, while quadrature loss is inherent in the formulation.

Parameters

Parameter Name	Description
s_freq	Sampling Frequency
v_pi	Voltage required for Π phase shift (v)
excess_loss	Excess loss of the modulator (dB)
R	Input resistance of the modulator (Ω)

Ports

Port Name	Description
E_field	Laser Field Input
lambda	Laser Wavelength
modE_field	Modulated laser field output
v_bias	Modulator bias voltage
Rf_mod	RF modulating signal

A.5 Photo Diode

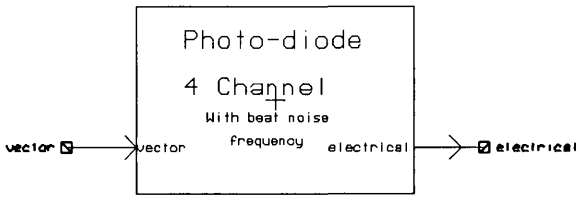

Module names	diode_beat_*fn*
	photodiode_*fn*
Library	jmgec

A photodiode can be approximated using the semi classical approach of optical detection, by assuming that the instantaneous optical power is proportional to the squared magnitude of the electro magnetic field.

Operation

The block photodiode_*fn* considers only the effect of the square law detection without considering the wavelength spacing between the channels that fall on the photo diode, and so should only be used for single wavelength systems. The block diode_beat_*fn* also considers the effect of interferometric beat noise, using the method described in 4.2. The beat components are formed between each pair of inputs to create the beat noise spectrum using the block *beat1*. This spectrum is then convert into the time domain. The outputs of this block are, 1: the signals formed by the detection of each independent signal without any beating, 2: the beating signal itself, allow easy signal to interference ratio calculation, or the total signal can be formed by simple signal addition. The calculation of the beating signal is performed using a custom coded C block.

Parameters

Parameter Name	Description
fft_length	Length of FFT Vector
s_freq	Sampling Frequency
ins_loss	Insertion loss to photodiode (db)
respons	Responsivity (A/W)

Ports

Port Name	Description
vector	Input Vector of multiple wavelengths
signal	Signal Recovered by detection
beat	Signal created by interferometric beating

A.6 Time to frequency domain conversion

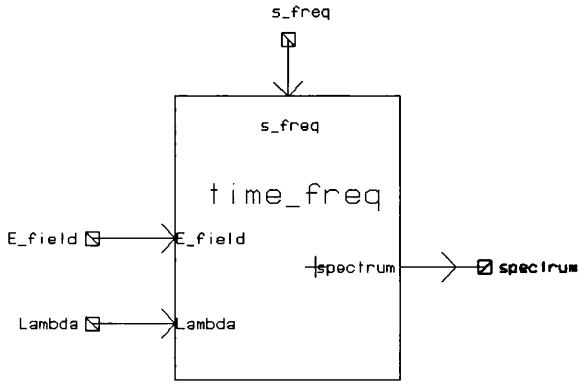

Module names	time_freq
Library	jmgec

The purpose of this block is to convert a baseband time domain signal in a frequency domain vector containing all the information need for processing using the format described in 2.3.1

Operation

This block takes the fast Fourier transform (FFT) of the input time domain signal, which is arranged in order of ascending frequency. A vector of equal length to the FFT is formed using the laser central wavelength and the sampling frequency which describes the exact wavelength of each component. These vectors are then appended to form the output vector which has a length of 2 fft_length.

Parameters

Parameter Name	Description
fft_length	Length of FFT Vector
s_freq	Sampling Frequency

Ports

Port Name	Description
E_field	time domain baseband signal
Lambda	Wavelength of laser (nm)
spectrum	Frequency domain spectrum and wavelength information
s_freq	Sampling Frequency

A.7 Non-linear amplifier

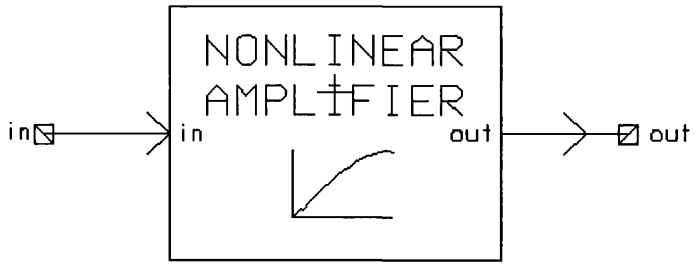

Module names	post_amp
Library	jmgec

Performs non-linear amplification on a photo-current signal to create an output power signal.

Operation

This block convert the photo-current to electrical power and the performs a non-linear amplification function.

Parameters

Parameter Name	Description
s_freq	Sampling Frequency
compres1db	1 dB Compression Point (dBm)
incept2	2nd Order intercept point (dBm)
incept3	3rd Order intercept point (dBm)
thermal	Thermal noise figure (dB)
gain	Power Gain (dB)
R	Input Impedance (Ohms)

Ports

Port Name	Description
in	Input
out	Amplified output

A.8 Optical Fiber

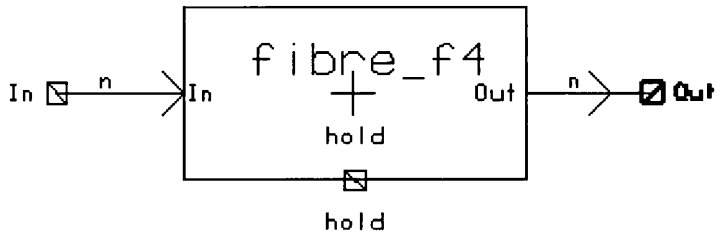

Module names	fiber_f
Library	jmgec

Operation

This block assumes that fiber has a basic linear transfer function, without dispersion of any kind. It includes loss and delay which are both calculated as proportional to fiber length and wavelength independent.

Parameters

Parameter Name	Description
s_freq	Sampling Frequency
fft_length	Length of FFT Vector
f_length	Fibre Length (km)
f_loss	Fibre Loss (dB/km)

Ports

Port Name	Description
In	Fibre Input
Out	Fibre Output

A.9 DFB laser

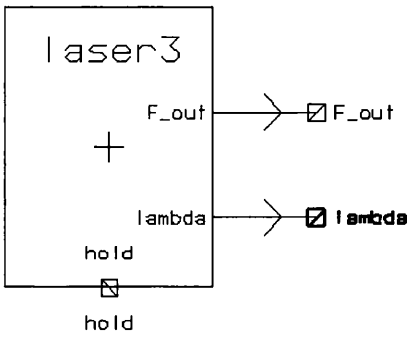

Module names	laser3
Library	jmgec

Due to phase noise with in a laser source the field produced cannot be considered to be a perfect single frequency. An appropriate model for the light produced by a laser is:

$$B(t) = A \quad \exp[j(\omega_0 t + \theta(t) + \phi)] \tag{A.1}$$

Where A is the amplitude, $\theta(t)$ is the random phase, and ϕ is the phase angle, which is independent and equally distributed in $0 \leq \phi \leq 2\pi$. It can be shown that the random phase $\theta(t)$ can be related to the frequency noise $\mu(t)$ by:

$$\theta(t) = 2\pi \int_0^t \mu(x)dx \tag{A.2}$$

The random walk of the phase, called a 'Wiener' process, leads to the laser linewidth having a Lorentzian power spectral density [2]. This process is modelled in this system as a scaled integral of random Gaussian white noise. The variance of which can be calculated by :

$$\sigma_{laser} = \frac{2\pi\Delta\upsilon}{f_s} \tag{A.3}$$

where $\Delta\upsilon$ is the FWHM linewidth of the source, and f_s is the sampling frequency used in the simulation.

Operation

Using the formulation above this block form a baseband complex envelope representation of the laser output. As external modulation is being considered in this system laser chirp has not been considered. The outputs give the time domain laser output and a tag representing the wavelength centre of the signal.

Parameters

Parameter Name	Description
smp_fre	Sampling Frequency
laser_fwhm	The FWHM linewidth of the Laser Source (Hz)
opt_field	Optical Field Amplitude (dBm)
wavelength	Laser Central wavelength (nm)
RIN	Relative intensity noise level (dB/Hz)

Ports

Port Name	Description
F_out	Laser Field Output
Lambda	Laser wavelength

Bibliography

[1] Kawanishi S., Takara H., Shake I., and Mori K. 3Tbit/s (160 Gbit/s x 19 channel) transmission by optical TDM and WDM. *The IEEE Lasers and Electro-Optics Society Newsletter*, 13(5):7–8, October 1999.

[2] Einarsson G. *Principles of lightwave communications.* John Wiley & Sons Ltd, Chichester, England, 1996.

[3] Masuda H. and Kawai S. Ultra wideband raman amplification with a total gain-bandwidth of 132nm of two gain-bands around 1.5um. In *European Conference on Optical Communication*, volume 2 of *ECOC*, pages 146–147, Nice, France, September 1999.

[4] Zhang S.L., Lane P.M., and O'Reilly J.J. Assessment of the nonlinearity tolerance of different modulation schemes for millimeter-wave fiber-radio systems using mz modulators. *IEEE Transactions on Microwave Theory and Techniques*, 25(8):1403–1409, 1997. Pt2.

[5] Takahashi H., Oda K., Toba H., and Inoue Y. Transmission characteristics of arrayed waveguide nxn wavelength multiplexer. *IEEE J. Lightwave Technol.*, LT-13(3):447–455, March 1995.

[6] Antoniades N., Roudas I., Wagner R.E., Jackel J., and Stern T.E. Crosstalk performance of a wavelength selective cross-connect mesh topology. In *IEEE/OSA Optical Fiber Communications Conference*, OFC'98, page paper TuJ4, San Jose, CA, 1998.

[7] Lin L.Y. Micromachined free-space matrix switches with submillisecond switching time for large-scale optical crossconnect. In *IEEE/OSA Optical Fiber Communications Conference*, OFC'98, page paper WH5, San Jose, CA, 1998.

[8] Giles C.R. Lightwave applications of fiber bragg gratings. *IEEE J. Lightwave Technol.*, 15(8):1391–1404, August 1997.

[9] Ennser K., Ibsen M., Durkin M., Zervas M.N., and Laming R.I. Influence of nonideal chirped fibre grating characteristics on dispersion cancellation. *IEEE Photonics Technology Letters*, 10(10):1476–1478, 1998.

[10] Cruz J.L., Ortega B., Andres M.V., Gimeno B., Pastor D., Capamny J., and Dong L. Chirped fibre bragg gratings for phased-array antenna. *IEE Electronic Letters*, 33(7):545–546, March 1997.

[11] Zhao Y. and Palais J.C. Fiber bragg grating coherence spectrum modeling, simulation, and characteristics. *IEEE J. Lightwave Technol.*, 15(1):154–161, 1997.

[12] Hill G.R., Chidgey P.J., Kaufhold F., Lynch T., Sahlen O., Gustavsson M., Janson M., Lagerstrom B., Grasso G., Meli F., Johansson S., Ingers J., Fernandez L., Rotolo S., Antonielli A., Tebaldini S., Vezzoni E., Caddedu R., Caponio N., Testa F., Scavennec A., O'Mahony M.J., Zhou J., Yu A., Sohler W., Rust U., and Herrmann H. A transport network layer based on optical network elements. *IEEE J. Lightwave Technol.*, 11(5/6):667–679, May/June 1993.

[13] Zhang S. L. and O'Reilly J. J. Simulation of fiber supported millimeter-wave communication system. In *The European Simulation Congress EUROSIM'95*, pages 565–570, Vienna, Austria, 11-15 Sept. 1995.

[14] Maclean D.J.H. *Optical Line Systems.* John Wiley and Sons, Chichister: New York., 1996.

[15] O'Reilly J.J. and Lane P.M. Remote delivery of video services using mm-waves and optics. *IEEE J. Lightwave Technol.*, 12(2):369–370, February 1994.

[16] Gliese U., Nielsen T.N., Bruun M., Christensen E.L., and Stubkjaer K.E. A wide-band hetrodyne optical phase-locked loop for generation of 3-16 GHz microwave carriers. *IEEE Photonics Technology Letters*, 4(8):936–938, August 1992.

[17] O'Reilly J.J., Lane P.M., Capstick M.H., Salgado H.M., Heidemann R., Hofstetter R., and Schmuck H. Race R2005 : microwave optical duplex antenna link. *IEE Proceedings, Part J: Optoelectronics*, 140(6):385–391, December 1993.

[18] Ovadia S. The effect of interleaver depth and qam channel frequency offset on the performance of multichannel AM-VSB256-QAM video lightwave transmission systems. *IEEE Photonics Technology Letters*, 10(8):1174–1176, August 1998.

[19] Frigyes I. and Seeds A.J. Optically generated true-time delay in phased-array antennas. *IEEE Transactions on Microwave Theory and Techniques*, 43(9):2378–2386, September 1995.

[20] Parry J.L., de Garis R.M., and Wright P.G. Radar signal path modelling using the signal processing worksystem. In *IEE Colloquium on Radar System Modelling, London.*, page Paper 13, 1998.

[21] Goldstein E.L. and Eskildsen L. Scaling limitations in transparent optical networks due to low-level crosstalk. *IEEE Photonics Technology Letters*, 7(1):93–94, January 1995.

[22] Tur M. and Goldstein E.L. Dependence of error rate on signal-to-noise ratio in fiber-optic communication systems with phase-inducted intensity noise. *IEEE J. Lightwave Technol.*, 7(12):2055–2058, December 1989.

[23] O'Reilly J.J. and Appleton C.J. System performance implications of homodyne beat noise effects in optical fibre network. *IEE Proceedings, Part J: Optoelectronics*, 142(3):143–148, June 1995.

[24] Wood T.H. and Shankaranarayanan N.K. Measurements of the effects of optical beat interference on the bit error rate of a subcarrier-based passive optical network. In *IEEE/OSA Optical Fiber Communications Conference*, OFC'93, page paper ThM3, San Jose, CA, 1993.

[25] Goldstein E.L., Eskildsen L., Lin C., and Silberberg Y. Polarization statistics of crosstalk-inducted noise in transparent lightwave networks. *IEEE Photonics Technology Letters*, 7(11):1345–1347, November 1995.

[26] Monroy I.T. and Tangdiongga E. Performance evaluation of optical crossconnects by saddlepoint approximation. *IEEE J. Lightwave Technol.*, LT-16(3):317–323, March 1998.

[27] Bulow H. System outage probability due to first and second order pmd. *IEEE Photonics Technology Letters*, 10(5):696–698, May 1998.

[28] Papoulis A. *Probability, Random variables and Stochastic processes.* McGraw-Hill, New York, 2nd edition, 1991.

[29] Goldstein E.L., Eskildsen L., and Elrefaie A.F. Performance implications of component crosstalk in transparent lightwave networks. *IEEE Photonics Technology Letters*, 6(5):657–660, May 1994.

[30] Takahashi H., Oda K., and Toba H. Impact of crosstalk in an arrayed-waveguide multiplexer on nxn optical interconnection. *IEEE J. Lightwave Technol.*, 14(6):1097–1105, June 1996.

[31] Legg P.J., Tur M., and Andonovic I. Solution paths to limit interferometric noise induced performance degradation in ASK/direct detection lightwave networks. *IEEE J. Lightwave Technol.*, LT-14(9):1943–1953, September 1996.

[32] Appleton C.J. *Modelling wavelength division multiplexed optical networks.* PhD thesis, University of Wales, Bangor, 1994.

[33] O'Reilly J.J. and Da Rocha J.R.F. Improved error probability evaluation methods for direct detection optical communication systems. *IEEE Transactions on Information Theory*, IT-33(6):839–848, 1987.

[34] Cornwell W.D. and Andonovic I. Interferometric noise for a single interferer: comparison between theory and experiment. *IEE Electronic Letters*, 32(16):1501–1502, August 1996.

[35] Eskildsen L. and Hansen P.B. Interferometric noise in lightwave systems with optical preamplifiers. *IEEE Photonics Technology Letters*, 9(11):1538–1540, November 1997.

[36] Ho K.P., Chan C.K., Tong F.K., and Chen L.K. Exact analysis of homodyne crosstalk induced penalty in WDM netowrks. *IEEE Photonics Technology Letters*, 10(3):457–458, March 1998.

[37] Ho K.P. Analysis of co-channel crosstalk interference in optical networks. *IEE Electronic Letters*, 34(4):383–385, February 1998.

[38] Mitchell J.E., Lane P.M., and O'Reilly J.J. Statistical characterization of interferometric beat noise in optical networks. In *IEEE/OSA Optical Fiber Communications Conference*, OFC'98, page paper WD3, San Jose, CA, 1998.

[39] O'Reilly J.J. and Cattermole K.W. *Problems of randomness in communication engineering*, volume 2. Pentech, London, 1984.

[40] Moura L., Karafolas N., Lane P.M., Hill A., and O'Reilly J.J. Statistical modelling of the interferometric crosstalk in optical networks: The RACE II MUNDI network. In *Proc. European Conference on Networks & optical communications, NOC'96*, volume 3 Technology,Infrastructure,WDM networks, pages 72–79, 1996.

[41] Liu F., Rasmussen C.J., and Pedersen R.J.S. Experimental verification of a new model describing the influence of incomplete signal extinction ratio on the sensitivity degradation due to multiple interferometric crosstalk. *IEEE Photonics Technology Letters*, 11(1):137–139, January 1999.

[42] Ho K-P. Analysis of homodyne crosstalk in optical networks using gram-charlier series. *IEEE J. Lightwave Technol.*, 17(2):149–154, February 1999.

[43] Monroy I.T. and Einarsson G. Bit error evaluation of optically preamplified direct detection receivers with fabry-perot optical filters. *IEEE J. Lightwave Technol.*, 15(8):1546–1553, August 1997.

[44] Moura L., Darby M., Lane P.M., and O'Reilly J.J. Impact of interferometric noise on the remote delivery of optically generated millimeter-wave signals. *IEEE Transactions on Microwave Theory and Techniques*, 45(8):1398–1402, August 1997.

[45] Whittle P. *Probability.* Penguin Books Ltd, Harmondsworth, Middlesex, England, library edition, 1970.

[46] Prabhu V.K. Modified Chernoff bounds for PAM systems with noise and interference. *IEEE Transactions on Information Theory*, IT-28(1):95–100, 1982.

[47] Helstrom C.W. Approximate evaluation of detection probabilities in radar and optical communications. *IEEE Transactions on Aerospace and Electronic Systems*, AES-14(4):630–640, July 1978.

[48] Schumacher K. and O'Reilly J.J. Relationship between the saddlepoint approximation and the modified Chernoff bound. *IEEE Transactions on Communications*, 38(3):270–272, March 1990.

[49] Song J., Chan C.K., Tong F.K., and Chen L.K. Extinction ratio induced crosstalk system penalty in WDM networks. *IEE Electronic Letters*, 32(23):2112–2114, November 1996.

[50] Mestdagh D.J.G. *Fundamentals of multiaccess optical fiber networks.* Artech House inc, 1995.

[51] Gillner L. and Gustavsson M. Scalability of optical multiwavelength switching networks: Power budget analysis. *IEEE Journal on Selected Areas in Communication*, 14(5):952–961, June 1996.

[52] Gustavsson M., Gillner L., and Larsen P. Statistical analysis of interferometric crosstalk: Theory and optical network examples. *IEEE J. Lightwave Technol.*, 15(11):2006–2019, November 1997.

[53] Webb W.T. and Hanzo L. *Modern Quadrature Amplitude Modulation*, chapter 5. IEEE Press and Pentech Press, 1994.

[54] Ng W, Walston A.A., Tongonan G.L., Lee J.J, Newberg I.I., and Bernstein N. The first demonstration of an optically steered microwave phased array antenna using true-time-delay. *IEEE J. Lightwave Technol.*, 9(9):1124–1131, September 1991.

[55] Corral J.L., Marti J., Regidor S., Fuster J.M., Laming R., and Cole M.J. Continuously variable true time-delay optical feeder for phased-array antenna employing chirped fiber gratings. *IEEE Transactions on Microwave Theory and Techniques*, 45(8):1531–1536, August 1997.

[56] Minasian R.A. and Alameh K.E. Optical-fiber grating-based beamforming network for microwave phased arrays. *IEEE Transactions on Microwave Theory and Techniques*, 45(8):1513–1518, August 1997.

[57] Molony A., Edge C., and Bennion I. Fibre grating time delay element for phased array antennas. *IEE Electronic Letters*, 31(17):1485–1486, August 1995.

[58] Molony A., Zhang L., Williams J.A.R., Bennion I., Edge C., and Fells J. Fiber bragg-grating true time-delay systems: Discrete-grating array 3-b delay lines and chirped-grating 6-b delay line. *IEEE Transactions on Microwave Theory and Techniques*, 45(8):1527–1530, August 1997.

[59] LaGrasse M.J., Charczenko W., Hamilton M.C., and Thaniyavarn S. Optical carrier filtering for high dynamic range fibre optic links. *IEE Electronic Letters*, 30(25):2157–2158, December 1994.

[60] Glassner D.S., Frankel M.Y., and Esman R.D. Reduced loss microwave fiber-optic links by intracavity modulation and carrier suppression. *IEEE Microwave and Guided Wave Letters*, 7(3):57–59, March 1997.

[61] Farwell M.L., Chang W.S.C., and Huber D.R. Increased linear dynamic range by low biasing the mach-zehnder modulator. *IEEE Photonics Technology Letters*, 5(7):779–782, 1993.

[62] Elby S.D., Shankaranarayanan N.K., and Lau K.Y. WDMA / subcarrier-FDMA lightwave networks: Limitations due to optical beat interference. *IEEE J. Lightwave Technol.*, 9(7):931–943, July 1991.

[63] Alameh K.E. Frequency downconverter for high-capacity fibre grating based beamformers for phased arrays. *IEE Electronic Letters*, 35(1):"66–67", January 1999.

[64] Pendleton-Hughes S., Weston N., and Carter A.C. Forty channel wavelength multiplexing for short haul wideband communications networks. In *IOOC-ECOC'85*, pages 649–651, 1985.

[65] Wagner S.S., Kobrinski H., Robe T.J., LembergH.L., and Smoot L.S. Experimental demonstration of a passive optical subscriber loop architecture. *IEE Electronic Letters*, 24(6):344–346, March 1988.

[66] Reeve M.H., Hunwicks A.R., Zhao W., Methley S.G., Bickers L., and Hornung S. LED spectral slicing for single mode local loop applications. *IEE Electronic Letters*, 24(7):389–390, March 1988.

[67] Wagner S.S. and Chapuran T.E. Broadband high-density WDM transmission using superluminescent diodes. *IEE Electronic Letters*, 26(11):696–697, May 1990.

[68] Kilkilly P.D.D., P.J.Chidgey P.J., and Hill G. Experimental demonstration of a three channel WDM system over 110km using superluminescent diodes. *IEE Electronic Letters*, 26(20):1671–1673, September 1990.

[69] Sampson D.D. and Holloway W.T. 100mw spectrally-uniform broadband ASE source for spectrum-sliced wdm systems. *IEE Electronic Letters*, 30(19):1611–1612, September 1994.

[70] Chung Y.C., Tkach R.W., and DiGiovanni D.J. SBS limitation on a spectrum-sliced fiber-amplifier light source. In *IEEE/OSA Optical Fiber Communications Conference*, OFC'95, pages 33–34, San Diego, February 1995. TuH6.

[71] Lee J.S., Chung Y.C., Derosier R.M., and DiGiovanni D.J. 1.7Gbit/s transmission over 165km of dispersion-shifted fibre using spectrum-sliced fibre amplifier light source. *IEE Electronic Letters*, 30(17):1427–1428, August 1994.

[72] Lee J.S., Chung Y.C., Wood T.H., Meester J.P., Joyner C.H., Burrus C.A., Stone J., Presby H.M., and DiGiovanni D.J. Spectrum-sliced fiber amplifier light source with a polarization-insensitive electroabsorption modulator. *IEEE Photonics Technology Letters*, 6(8):1035–1038, August 1994.

[73] Han J-H., Lee J-S., Lee S-S., Yun T-Y., Kim H-K., Lee C-H., and Shin S-Y. 2.5Gbit/s transmission of spectrum-sliced fiber amplifier light source channels over 200km of dispersion shifted fibre. *IEE Electronic Letters*, 31(12):989–991, June 1995.

[74] Keating A.J., Holloway W.T., and Sampson D.D. Feedforward noise reduction of incoherent light for spectrum-sliced transmission at 2.5Gbit/s. *IEEE Photonics Technology Letters*, 7(12):1513–1515, December 1995.

[75] Holloway W.T., Keating A.J., and Sampson D.D., Multiwavelength source for spectrum-sliced WDM access networks and LANs *IEEE Photonics Technology Letters*, 9(7):1014–1016, July 1997.

[76] Han J-H, Kim S-J, and Lee J-S. Transmission of 4x2.5-Gb/s spectrum sliced incoherent light channels over 240 km of dispersion shifted fiber with 200 GHz channel spacing. *IEEE Photonics Technology Letters*, 11(7):901–903, July 1999.

[77] Pendock G.J. and Sampson D.D. Transmission performance of high bit rate spectrum-sliced WDM systems. *IEEE J. Lightwave Technol.*, 14(10):2141–2148, October 1996.

[78] Lee J-S. Signal-to-noise ratio of spectrum-sliced incoherent light sources including optical modulation effects. *IEEE J. Lightwave Technol.*, 14(10):2197–2201, October 1996.

[79] Olsson N.A. Lightwave systems with optical amplifiers. *IEEE J. Lightwave Technol.*, 7(7):1071–1082, July 1989.

[80] Wang L.D. High-isolation polarization-independent optical quasi-circulator with a simple structure. *OSA Optics Letters*, 23(7):549–551, April 1998.